

UiO : **University of Oslo**

Johan Blakkisrud

# **Dosimetry in patients treated with [<sup>177</sup>Lu]Lu-lilotomab satetraxetan**

**Thesis submitted for the degree of Philosophiae Doctor**

Department of Physics

The Faculty of Mathematics and Natural Sciences

Department of Diagnostic Physics, Oslo University Hospital,  
Oslo, Norway



**2022**

© **Johan Blakkisrud, 2022**

*Series of dissertations submitted to the  
Faculty of Mathematics and Natural Sciences, University of Oslo  
No. 2484*

ISSN 1501-7710

All rights reserved. No part of this publication may be  
reproduced or transmitted, in any form or by any means, without permission.

Cover: Hanne Baadsgaard Utigard.  
Print production: Reprosentralen, University of Oslo.

*To Leif Harald*



# List of Papers

## I

J. Blakkisrud, JE. Høltedahl A. Løndalen, J. Dahle, T. Bach-Gansmo, H. Holte, S. Nygaard, A. Kolstad and C. Stokke. "Biodistribution and Dosimetry Results from a Phase 1 Trial of Therapy with the Antibody–Radionuclide Conjugate <sup>177</sup>Lu-Lilotomab Satetraxetan". In: *Journal of Nuclear Medicine* **59** (2018), pp. 704–710. DOI: 10.2967/jnumed.117.195347.

## II

J. Blakkisrud, A. Løndalen, J. Dahle, S. Turner, H. Holte, A. Kolstad and C. Stokke. "Red Marrow-Absorbed Dose for Non-Hodgkin Lymphoma Patients Treated with <sup>177</sup>Lu-Lilotomab Satetraxetan, a Novel Anti-CD37 Antibody-Radionuclide Conjugate". In: *Journal of Nuclear Medicine* **58** (2017), pp. 55–61. DOI: 10.2967/jnumed.116.180471.

## III

C. Stokke, J. Blakkisrud, A. Løndalen, J. Dahle, ACT. Martinsen, H. Holte and A. Kolstad "Pre-dosing with lilotomab prior to therapy with <sup>177</sup>Lu-lilotomab satetraxetan significantly increases the ratio of tumor to red marrow absorbed dose in non-Hodgkin lymphoma patients". In: *European Journal of Nuclear Medicine and Molecular Imaging* **45** (2018), pp. 1233–1241. DOI: 10.1007/s00259-018-3964-9.

## IV

J. Blakkisrud, A. Løndalen, J. Dahle, ACT. Martinsen, A. Kolstad and C. Stokke "Myelosuppression in Patients Treated with <sup>177</sup>Lutetium-Lilotomab Satetraxetan can be Predicted with Absorbed Dose to the Red Marrow as the Only Variable". In: *Acta Oncologica* **60** (2021) pp. 1481–1488. DOI: 10.1080/0284186X.2021.1959635.

## Additional papers

J. Blakkisrud, A. Løndalen, ACT. Martinsen, J. Dahle, JE . Høltedahl, T. Bach-Gansmo, H. Holte, A. Kolstad and C. Stokke. "Tumor-Absorbed Dose for Non-Hodgkin Lymphoma Patients Treated with the Anti-CD37 Antibody Radionuclide Conjugate <sup>177</sup>Lu-Lilotomab Satetraxetan". In: *Journal of Nuclear Medicine* **58** (2017), pp. 48–54. DOI: 10.2967/jnumed.116.173922.

A. Kolstad, T. Illidge N. Bolstad, S. Spetalen, U. Madsbu, C. Stokke, J. Blakkisrud, A. Løndalen, N. O'Rourke, M. Beasley, W. Jurczak, UM. Fagerli, M. Kascak, M. Bayne, A. Obr, J. Dahle, L. Rojkjaer, V. Pascal and H. Holte "Phase 1/2a study of <sup>177</sup>Lu-lilotomab satetraxetan in relapsed/refractory indolent non-Hodgkin lymphoma". In: *Blood Advances* **4** (2020), pp. 4091–4101. DOI: 10.1182/bloodadvances.2020002583.

A. Løndalen, J. Blakkisrud, ME. Revheim, UE. Madsbu, J. Dahle, A. Kolstad and C. Stokke "FDG PET/CT parameters and correlations with tumor-absorbed doses in a phase 1 trial of <sup>177</sup>Lu-lilotomab satetraxetan for treatment of relapsed non-Hodgkin lymphoma". In: *European Journal of Nuclear Medicine and Molecular Imaging* **48** (2021), pp. 1901–1914. DOI: 10.1007/s00259-020-05098-x.

The published papers are reprinted with permission from the Society of Nuclear Medicine and Molecular Imaging, Springer and Taylor and Francis. All rights reserved.

# Contents

List of Papers	iii
Contents	v
<b>1 Introduction</b>	<b>5</b>
<b>2 Scientific background</b>	<b>9</b>
2.1 Non-Hodgkins Lymphoma . . . . .	9
2.2 Radioimmunotherapy of lymphoma . . . . .	9
2.3 Dosimetry . . . . .	15
2.4 Biodistribution and dose effect for RIT of Lymphoma . . . . .	20
<b>3 Aims of individual papers</b>	<b>25</b>
<b>4 Materials and Methods</b>	<b>27</b>
4.1 Treatment and patient material . . . . .	27
4.2 Imaging and other radioactivity measurements . . . . .	29
4.3 Dosimetry . . . . .	30
4.4 Statistical methods . . . . .	32
<b>5 Summary of publications</b>	<b>35</b>
<b>6 Discussion</b>	<b>39</b>
6.1 Clinical relevance of dose findings vs/ toxicity . . . . .	39
6.2 Biodistribution . . . . .	43
6.3 Pre-dosing finding . . . . .	44
<b>7 Conclusion and future work</b>	<b>47</b>
7.1 Conclusion . . . . .	47
7.2 Future work . . . . .	47
<b>Bibliography</b>	<b>49</b>
<b>Papers</b>	<b>62</b>
<b>Appendices</b>	<b>107</b>





# Acknowledgement

*The best that most of us can hope to achieve in physics is simply to misunderstand at a deeper level.* - Wolfgang Pauli

I have a tremendous amount of people to thank for making this possible. First and foremost I would like to thank my supervisor, Caroline Stokke. She welcomed me into the exciting world of nuclear medicine physics and I have not looked back since. You are always available for discussions, always encouraging and with a keen eye for details. I could not wish for a better supervisor. I would also like to thank Arne Kolstad for giving me access to your valuable time, your critical eye and strong expertise. Thank you also Anne Catrine Martinsen for your perspectives and highly contagious enthusiasm. A thanks also to Eirik Malinen for being my internal supervisor at the University of Oslo.

Too many to mention, I would like to thank everyone at the Nuclear Medicine Departments at the Oslo University Hospital. An extra special thank you to the great people at the Department of Nuclear Medicine at Ullevål Hospital for letting me into the lab and being a fly on the wall, I hope I was not too intrusive. Thank you also Ayca Løndalen. You are a wonderful colleague who brought life to, and helped me make sense of, the drab gray of CT-images. Your friendly demeanor and knowledge of the field of nuclear medicine and the ability to share this knowledge has been invaluable to me.

Not to go unmentioned are also my colleagues at the Department of Diagnostic Physics. One should not underestimate the value of coffee and conversations, especially in such a nice environment. Thank you for being welcoming and for making it one of the best work places I know of!

Thank you to all co-authors for helping me with the heavy work of writing scientific papers. Your constructive feedback elevated the quality of rough drafts into papers I am proud of. Thank you Jostein Dahle for providing your expertise and insight in the antibody conjugate. Thank you to Nordic Nanovector ASA for supplying much needed  $^{177}\text{Lu}$  for the phantom experiments. Thank you also to Siv Hennem Mohseni for providing valuable language help.

A warm thank you to my family and friends, who despite being explicitly told not to, were constantly asking me if I had finished yet. Thank you Mina for being there for me, and making this world the most enjoyable of all worlds.



# Abbreviations and glossary

- PET** Positron emission tomography
- FDA** Food and Drug administration
- SPECT** Single photon emission computed tomography
- CT** Computed tomography
- ARC** Antibody-radionuclide conjugate
- NHL** Non-Hodgkin lymphoma
- RIT** Radioimmunotherapy
- EBRT** External beam radiation treatment
- VOI** Volume of interest
- RM** Red marrow
- WB** Whole body
- TAC**,  $A(t)$  Time activity curve
- TIAC**,  $\tau$  Time-integrated activity coefficient
- MIRD** Committee on Medical Internal Radiation Dose
- ICRP** International Commission on Radiological Protection
- $r_s, r_t$  Source and target organs
- $\phi$  Absorption fraction
- $\Phi$  Specific absorption fraction
- OLINDA** Organ Level Internal Dose
- R-CHOP** Rituximab-Cyclophosphamide-Doxorubicin-Vincristine-Prednisone
- CVP** Cyclophosphamide-Vincristine-Prednisone
- P.I** Post injection
- CTCAE** Common Terminology Criteria for Adverse Events
- PBN** Percentage at baseline compared to nadir
- TTN** Time to nadir
- CF** Cellularity factor



# Chapter 1

## Introduction

Non-Hodgkin lymphoma (NHL) is a cancer that develops from white blood cells. The majority (85 - 90 %) stem from B-cells. It encompasses subtypes ranging from the aggressive to the indolent. Follicular NHL is a histological subtype, being the most frequent indolent type of lymphoma stemming from the B-cells. Standard treatment includes cytotoxic agents, either with or without immunotherapy with anti CD20 antibodies in patients with systemic disease, and external beam radiation therapy (EBRT) in patients with localized tumours. Follicular NHL is slow growing, but considered to be incurable, calling for an alternative treatment in refractive or relapsing patients [1] [2] [3] [4].

Antibody-radionuclide conjugates (ARCs) are used in radioimmunotherapy, a therapy approach where radioactive nuclei are guided to the cancerous cells with molecular messengers in the form of monoclonal antibodies [5]. The target of the antibodies is specific, complimentary epitopes expressed on the surface of malignant cells. The treatment has the potential to provoke an immunologic response, as well as providing a tumoricidal amount of continuous radiation. If the range of the emitted radiation particles is in the order of multiple cell lengths, this radiation energy is also deposited in neighboring cells not expressing the epitope, thus providing extended therapeutic coverage. The therapy is most applicable in cancers with radiosensitive, well differentiated and systemic tumours.

Initial experience with radioimmunotherapy of NHL set a high bar for survival, with remarkable efficacy results with moderate toxicity, primarily hematological [6] [7] [8] [9] [10] [11]. Several RITs are currently under investigation, both for NHL and other malignancies [12]. Two ARCs targeting the CD20 antigen have received approval from the Food and Drug administration, [<sup>90</sup>Yttrium]Yttrium-ibritumomab tiuxetan (Zevalin®) and [<sup>131</sup>Iodine]Iodine-tositumomab (Bexxar®). These drugs have been approved for relapsed or refractory low grade follicular or transformed B-cell NHL and relapsed or refractory CD20 positive follicular NHL for [<sup>90</sup>Y]Y-ibritumomab tiuxetan and [<sup>131</sup>I]I-tositumomab respectively [13].

Oslo University Hospital is currently treating patients with [<sup>177</sup>Lu]Lu-lilotomab satetraxetan, a novel ARC therapy developed by Oslo University Hospital and Nordic Nanovector ASA that targets the CD37 antigen. The ARC is under investigation in three clinical trials (NCT01796171, NCT02658968 and NCT03806179), enrolling patients with CD37-positive, indolent NHL, the first patient was treated in 2012.

Internal radiation dosimetry is the assessment of absorbed radiation energy (*absorbed dose*) to tissue from unsealed radionuclides. Dosimetry in treatment planning is an ubiquitous part of EBRT [14]. In EBRT, absorbed dose is calculated and can be delivered with error margins within a few percent of

## 1. Introduction

---

this treatment plan [15]. As absorbed dose from internal emitters cannot be calculated in an equal, straight-forward manner, internal dosimetry routines have been lagging those of EBRT. However, there is little reason to believe that radiation therapy with unsealed sources should be exempt from dosimetry, to personalize treatment, optimizing delivery of radiation to target tissue and monitoring absorbed dose to organs at risk. Indeed, the European Council Directive 2013/59 states that

"For all medical exposures of patient for radiotherapeutic purposes, exposure of target volumes shall be individually planned and their delivery appropriately verified..."

where the term "radiotherapeutic" includes nuclear medicine for therapeutic purposes, i.e. radioimmunotherapy.

Proposed reasons for the lag have been the complex spatial and temporal distribution of the sources of radiation, compared to the well defined sources in EBRT, combined with technological challenges for measuring this distribution [16]. Internal dosimetry studies have been limited to studies with few patients, and this has made it challenging to infer a clear connection between absorbed dose and response.

The emergence of quantitative tomographic modalities like PET and SPECT, has made it possible to determine the distribution of the radioactive sources in the patient directly and more accurately, provided that the sources emit radiation suitable for medical imaging. These advances in technology together with standardization and harmonization of methodology in recent years have made accurate dosimetry more feasible and internal dosimetry is gaining momentum. With the evidence of absorbed dose and treatment outcome being "sufficient and constantly increasing", dosimetry is taking the leap from specialised centers to the clinic. [17].

Dosimetry has already been implemented in multiple institutions for a number of treatments. As per a recent European survey, of established treatments where dosimetry is most often applied are iodine treatment for benign thyroid disease, resin or glass microspheres containing  $^{90}\text{Y}$  for treatment of hepatic carcinoma and  $^{131}\text{I}$ I-mIBG for neuroblastoma [18]. Pre-therapeutic dosimetry has also been implemented in treatment of differentiated thyroid cancer with  $^{131}\text{I}$ . [19] [20]. Dosimetry was part of the administration protocol for  $^{131}\text{I}$ I-tositumomab but not  $^{90}\text{Y}$ Y-ibritumomab tiuxetan, most likely due to the latter not being a  $\gamma$ -emitter and challenging to image directly. Clinical trials have shown that hematological toxicity is dependent on calculated absorbed dose to the whole body, assumed to be a proxy for the bone marrow, rather than administered activity in an activity per kilogram body mass dosage regime [21] [22].

The radioactive component of  $^{177}\text{Lu}$ Lu-lilotomab satetraxetan,  $^{177}\text{Lu}$ Lutetium, emits both short ranged  $\beta$ - and long ranged  $\gamma$ -emission. The  $\gamma$ -emission can be directly imaged, making it possible to track the treatment in time after the administration of the drug and allowing for dosimetry. The aim of this thesis was to establish a methodology to use internal dosimetry to compare treatment arms,

---

identify organs at risk and find a way to predict toxicity for patients treated with [ $^{177}\text{Lu}$ ]Lu-lilotomab satetraxetan.





## Chapter 2

# Scientific background

## 2.1 Non-Hodgkins Lymphoma

### 2.1.1 Incidence, prevalence and mortality

Lymphoma is a family of white blood cell-malignancies. The disease is categorized as either Hodgkins lymphoma or Non-Hodgkins lymphoma where the latter accounts for 90 percent of all lymphomas [1]. In the United States there were 74 680 estimated new cases and 19 910 deaths in 2017 from NHL [23]. In Norway there were 519 and 408 new cases of NHL in 2017. The accumulated risk for developing the disease by the age of 75 in the years 2013 to 2017 was 1.4 and 1.0 percent for male and female patients respectively [24].

### 2.1.2 Sub-groups - The indolent types

Roughly 85-90 percent of NHL are derived from B-cells. All B-cells originate as naive B-cells, residing in the bone marrow. When they exit the bone marrow, they start a maturation process through encounters with antigens and T-cells to parts of the lymph nodes, the spleen or other secondary lymphatic tissue. To select for B-cells that produce high-affinity antibodies, the lymphatic tissue exhibits so-called germinal centers. These structures support processes that require double strand DNA-breaks and are thus by design unstable. These double-strand-break processes are guarded by transcription factors, and the alteration of these transcription factors leads to disease [1].

Further classification of NHL depends on identification of the histological sub-type with respect to architecture (follicular or diffuse) and morphology (small or large cells), each with different treatment approaches [1]. Subtypes encountered in this thesis, identified based on immunohistochemistry and molecular characterisation, are follicular lymphoma (the majority of included patients), mantle cell lymphoma and marginal zone lymphoma, all being indolent forms of NHL. Standard treatment of these is either single agent rituximab, with or without maintenance therapy, or chemotherapy combined with rituximab with differences depending on the specific subtype [1] [25].

## 2.2 Radioimmunotherapy of lymphoma

Targeted radiotherapy is a treatment modality where radionuclides are guided to malignant cells to deliver continuous radiation. This treatment modality is particularly applicable on systemic cancers, where tumours are multiple and non-localized. If the carrier molecule exploits the immune system and is a monoclonal antibody, the therapy is sometimes referred to as *radioimmunotherapy*

## 2. Scientific background

---

(RIT) with an *antibody-radionuclide conjugate (ARC)*. In RIT with ARCs, the carrier molecule itself can invoke an intrinsic anti-tumour activity via antibody dependent cytotoxicity in addition to the cell killing in the form of radiation [26] [27].

### 2.2.1 Monoclonal antibodies

Monoclonal antibodies are biological molecules with a structure that resembles the letter Y that can be made to have an affinity for a specific antigen [28]. In 1975, in a Nobel-prize-awarded work published by Kohler and Milstein, a technique to mass produce clones of highly specific antibodies was presented [29]. Today, at least 30 different monoclonal antibodies have been granted by the FDA to treat ailments like cancer, chronic inflammatory disease, infectious diseases and cardiovascular diseases [30], [26]. In oncology, antibodies were first linked to potent, plant derived toxins, like ricin to be used as cell killers [27]. In treatment of NHL, monoclonal antibodies have played a considerable part, as introduction of the anti CD20-antibody rituximab has dramatically changed the therapeutic outcome of these patients [31] [32].

#### 2.2.1.1 Previously used antibodies

The ideal target for a specific RIT is an antigen that is highly expressed malignant tissue. Equally important, the ideal carrier molecule must have affinity for said target. The task at hand then becomes identification of suitable pairs of antigen/antibody.

Potential antigen targets for lymphoma include multiple cluster of differentiation (CD) antigens CD19, CD20, CD22, CD37 and CD45 (fig. 2.1) [5]. These antigens are surface-expressed macromolecules which are easily accessible from both the blood stream and the intracellular fluid. The CD-antigens are expressed during maturation of immune cells and are used in immunophenotyping [33].

Early focus was put on CD20 as a target antigen. CD20 is an integral membrane phosphoprotein of 33-35 kDa expressed on multiple neoplasms, first discovered in 1980 [34]. The antigen is expressed on the surface of the majority of mature B-cells, and in 95 % of B-cell lymphomas [35]. It is the target for the established drug rituximab in addition to multiple other monoclonal antibodies, e.g. obinutuzumab, ofatumumab, veltuzumab and ocrelizumab [36] [31]. I<sup>[131I]</sup>I-tositumomab as part of sequential therapy with Rituximab-Cyclophosphamide-Doxorubicin-Vindicristine-Prednisone (R-CHOP), followed by <sup>[131I]</sup>I-tositumomab and further followed by maintenance therapy has been recently explored [37].

An alternative target to CD20 is CD37, expressed on mature B-cells. CD37 is a member of the tetraspanin family of size 40-52 kDa, discovered and first described in 1986 [38]. The gene of CD37 is expressed on Epstein-Barr-virus-transformed lymphocytes, spleen and blood [39]. Cellular processes like cell adhesion, differentiation, proliferation and tumour invasion have all been linked to tetraspanin members. CD37 has been shown to play a role in the regulation of

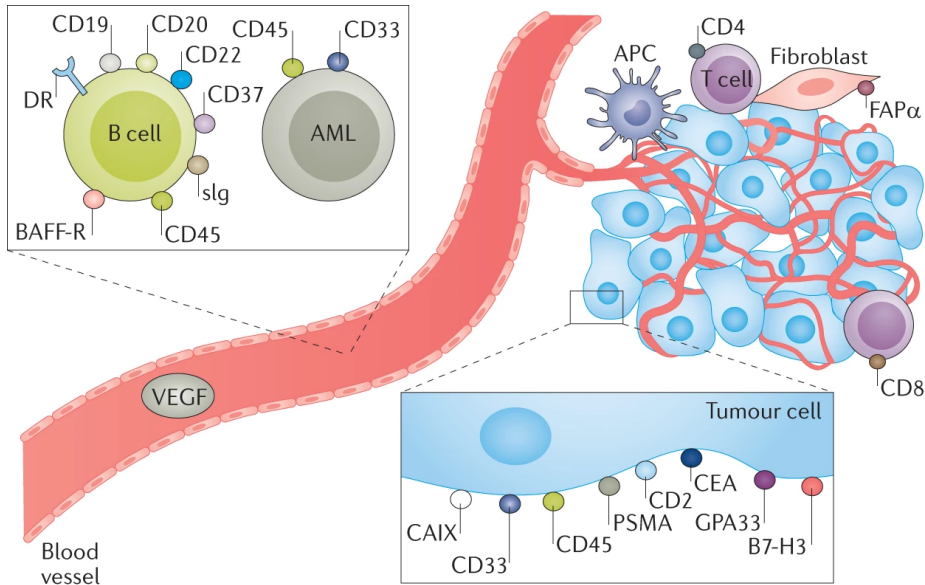


Figure 2.1: Different molecular targets available for RIT for human cancers. B-cell targets like CD37 and CD20 are suitable for treatment of NHL. [5].

immunoglobulin-A-response, anti-fungal immunity and the lack of it is associated with development of B-cell lymphoma [40] [41]. The antigen is also studied as a target for CAR-T-therapy [42]. The details of its functions are currently unknown [43].

### 2.2.1.2 Lilotomab

Lilotomab, previously referred to in the literature as HH1 or tetulomab, is a murine monoclonal antibody developed at The Norwegian Radium Hospital in the 80s. It is a type IgG1 isotype [44]. The antibody has been found to stain 216 out of 217 biopsy samples from patients with different subtypes of B-cell NHL [45].

## 2.2.2 Radioactive nuclei

Ionizing radiation has been used to treat cancer in humans since a case of inoperable breast carcinoma conducted merely four months after the discovery of X-rays [46]. In RIT, the radiation is provided by an unsealed radionuclide.

### 2.2.2.1 Different emitters, gamma and electrons

A radionuclide is an atom that has an unstable nuclear energy state. The nuclide can undergo a spontaneous change in energy state (decay), releasing one or

## 2. Scientific background

---

more radiation particles. The unit for nuclear decay is the Becquerel (Bq) which denotes one decay per second. Currently, eight different modes of “pure” decay have been identified, each with different combinations of emitted particles [47]. As the process is stochastic, it is not possible to predict when a single unstable nuclide decays. The rate of decay is defined by the half life, the time when half of the nuclei have decayed.

When the resulting radiation particles are energetic enough to knock off electrons from other atoms, the radiation is called ionizing radiation. Early discoveries of ionizing radiation grouped the emitted particles into three classes:  $\alpha$ ,  $\beta$  and  $\gamma$ -radiation. Studies of these particles showed that  $\alpha$ -particles were massive and had a positive charge,  $\beta$ -particles were less massive and carried a negative charge, and that  $\gamma$ -particles were mass- and charge-less. Further studies showed that they were helium nuclei, fast electrons and high energy photons respectively. Later, auger-electrons (low-energy electrons, released in a cascade) and characteristic X-rays due to processes where orbital electrons interact with the nucleus have been identified and separated from their  $\beta$  and  $\gamma$ -counterparts. Most radionuclides have multiple decay modes, emitting a mixture of different radiation, although it is common practice to classify radionuclides based on their dominating particle emission.

Most elements present on earth are stable or have half-lives in the order of millions of years, so naturally occurring radioactive materials are rare. However, it was discovered in the 1930s that artificial, unstable radionuclides can be created by bombardment of heavy elements with neutrons. This enabled the creation of new radionuclides, of which some are suitable for medical use [48]. Some 90 years later, a large number of radionuclides have been synthesized, both for therapeutic and diagnostic purposes [49]. Both therapeutic and diagnostic radionuclides should either have an intrinsic affinity for a biological target (like isotopes of iodine), or have the possibility to be chemically linked to a suitable carrier molecule.

Radiation properties of the ideal diagnostic and the ideal therapeutic radionuclide are somewhat conflicted. An ideal diagnostic radionuclide should only emit *penetrative* radiation, meaning radiation that interacts, i.e. gets absorbed or scatters as little as possible before it escapes the patient and is detected. This is achieved by using a radionuclide that primarily emits  $\gamma$ -photons in the range of 100 to 300 keV. An example often used of the *ideal* diagnostic agent is  $^{99}\text{Tc}$ , an isotope of the first man-made element [50]. This is due to its relatively short half-life (6 hours), photon energy of 140 keV and relative ease of production.

In contrast, the ideal therapeutic radionuclide emits radiation with a short particle range, which deposits its energy close to the site of decay. The goal of therapeutic radiation is to make unrepairable damage, i.e. double strand breaks to the DNA. The optimal energy deposition patterns are thus ones that traverse the width of the DNA-helix, without reaching too far to surrounding, normal cells. Emerging and established examples of  $\beta$ -emitters are  $^{177}\text{Lu}$ ,  $^{131}\text{I}$  and  $^{90}\text{Y}$  in increasing order of electron energy, and hence range.

If the radionuclide inhabits properties both suitable for therapy and diagnostic

purposes, the term “theragnostics” has been coined. <sup>1</sup>

### 2.2.2.2 <sup>177</sup>Lu

<sup>177</sup>Lu is a metal in the lanthanide series, with a nucleus containing 71 protons and 106 neutrons. Nuclear decay happens through beta-decay to stable <sup>177</sup>Hafnium, with a max  $\beta$ -energy of 0.49 MeV. The  $\beta$  energy from <sup>177</sup>Lu can be classified as either that of “low” or “moderate” to separate it from  $\beta$ -emitters with comparatively higher  $\beta$ -energy emitters like <sup>90</sup>Y and <sup>131</sup>I. This moderate  $\beta$ -energy means that the  $\beta$ -particles are largely deposited locally. In tissue, the average  $\beta$ -particles range is 0.23 mm in soft tissue. This range allows for cell killing in neighboring cells of the target cell, so-called crossfire effect [52].

The half-life of <sup>177</sup>Lu is approximately 7 days. The current most exact recommended value by the Decay Data Evaluation project from 2004 is 6.647 days which is in accordance with more recent measurements [53] [54] [55].

The  $\gamma$ -spectrum of <sup>177</sup>Lu contains several energy peaks. See fig 2.2 for a current recommended decay-scheme [56].

The two most prominent  $\gamma$ -peaks have energies of 113 and 208 keV. The newest adopted values are 112.94498(6) and 208.3661 keV, with intensities of 10.41(4) and 6.225 per 100 transitions [56]. Additionally, there are four remaining  $\gamma$ -peaks, all below 0.21 per 100 transitions and low-energy specific X-rays and auger-emission.

The dual nature of <sup>177</sup>Lu as both a  $\beta$ - and  $\gamma$ -emitter, makes it a theragnostic radionuclide and it has in recent years gained popularity [12]. It has been established in treatment of metastatic castration-resistant prostate cancer when conjoined with molecules targeting the prostate specific antigen and somatostatin expressing neuroendocrine tumours [57] [58].

## 2.2.3 Clinical radioimmunotherapies

As NHL tumours are both often multi focal and radiosensitive, the malignancy was among the earliest of candidates of RIT [59].

Initial treatment with myeloblative amounts of RIT followed by bone marrow transplant resulted in excellent efficacy-results [5]. However, the high amount of activity was discouraging due to practical reasons. Focus on out-patient regimens with lower, tailored amounts of activity has given rise to numerous trials involving radiolabelled antibodies (see e.g. [5] for a list) Two of these treatments have reached FDA-approval, the first being [<sup>90</sup>Y]Y-ibritumomab tiuxetan and [<sup>131</sup>I]I-tositumomab, which was approved in 2002 and 2003 respectively. Both target the CD20-antigen using two different murine antibodies as carrier molecules. [<sup>90</sup>Y]Y-ibritumomab tiuxetan is based on the antibody ibritumomab [60] and [<sup>131</sup>I]I-tositumomab is based on tositumomab [61]. Bexxar was discontinued in February 2014 [62].

<sup>1</sup>There has been some debate on whether to use the term *theragnostic* or *theranostics*. Due to the latinization of the Greek words *therapia* and *diagnosis* Prof. George Babiniotis has concluded that it should be *theragnostics* with a g, and this word will be used here [51]

## 2. Scientific background

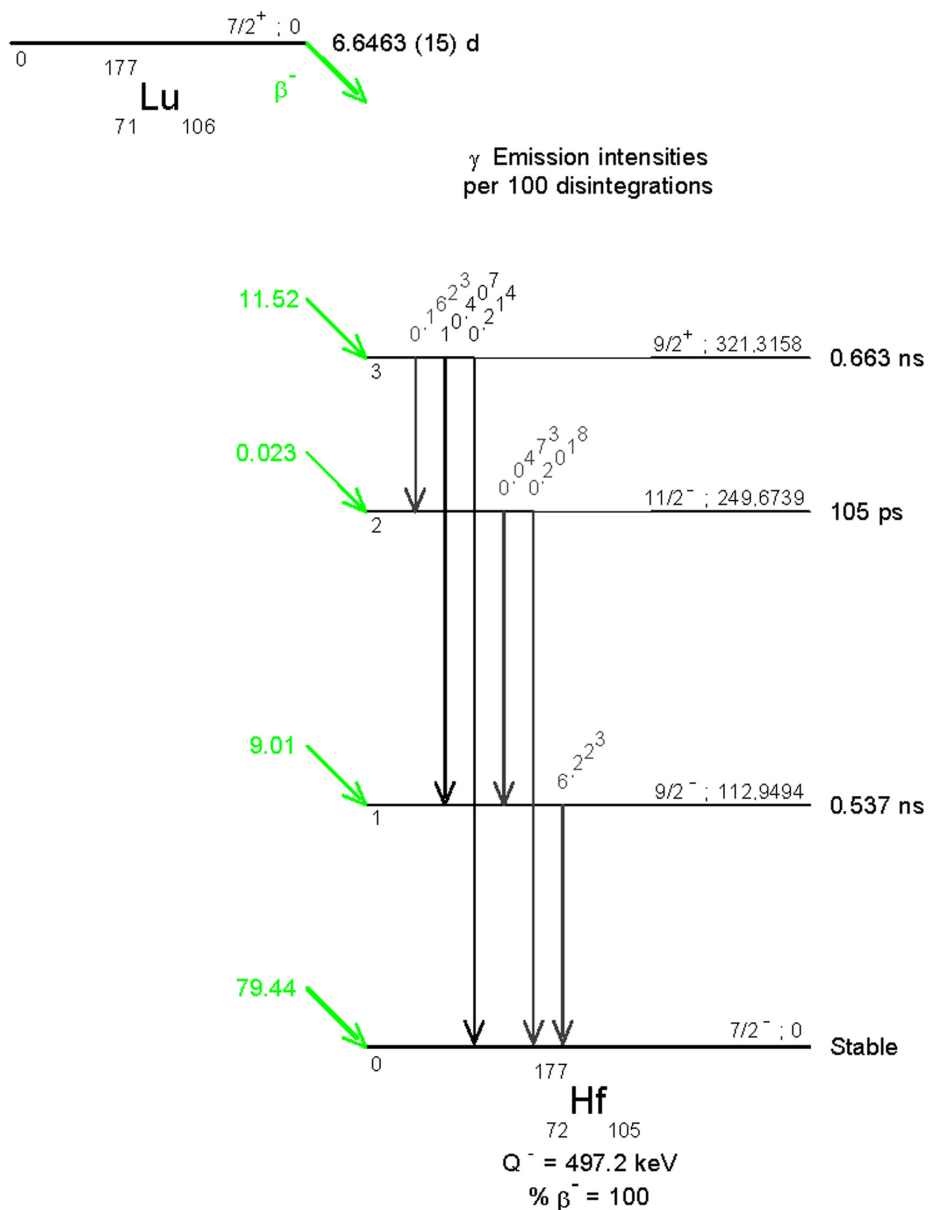


Figure 2.2: Decay-scheme for  $^{177}\text{Lu}$  - from [56].

INN name	Tradename	Radionuclide	Mean $\beta$ -energy (keV)	$\beta$ -range <sup>†</sup> (mm)	Radionuclide half-life
[ <sup>90</sup> Y]Y-ibritumomab tiuxetan	Zevalin	<sup>90</sup> Y	933	1.93	64.1 h
[ <sup>131</sup> I]I-tositumomab	Bexxar	<sup>131</sup> I	182	0.90	8.02 d
[ <sup>177</sup> Lu]Lu-lilotomab satetraxetan	Betalutin	<sup>177</sup> Lu	133	5.53	6.6 d

<sup>†</sup>Defined by the X<sub>90</sub>-value, the diameter of a sphere around the radionuclide where 90 % of the energy have been absorbed in water

Table 2.1: Different physical properties of the two clinically established RITs, compared with [<sup>177</sup>Lu]Lu-lilotomab satetraxetan

Multiple ARCs have been made to target CD20 and as the patent on ibritumomab has expired, generic biosimilars could potentially soon be available, chelated to various radionuclides [63] [64] [65] [66] [67].

CD37 as a target for RIT has been previously explored with a <sup>131</sup>I-labelled antibody MB-1 [68].

### 2.2.3.1 <sup>177</sup>Lu-lilotomab satetraxetan

<sup>177</sup>Lu-lilotomab satetraxetan (Betalutin<sup>TM</sup>) is a novel RIT consisting of <sup>177</sup>Lu, chelated to the murine monoclonal antibody lilotomab via the p-SCN-Bn-DOTA-molecule [45]. It is currently in two clinical trials recruiting patients with relapsed/refractory B-cell lymphoma, the Phase 1/2 LYMRIT 37-01 (NCT01796171) and the Phase 1 LYMRIT 37-07 (NCT03806179) trials [69] [70]. In addition, it is also tested in the LYMRIT-37-05-study, recruiting patients with relapsed or refractory diffuse large B-cell lymphoma (NCT02658968) [71].

The ARC has been shown to inhibit cell growth in B and T-lymphocyte deficient mice injected with Daudi cells. In the same study, the affinity of <sup>177</sup>LuLu-lilotomab satetraxetan to CD37 was found to be comparable to the affinity of <sup>177</sup>Lu-labelled rituximab to CD20. The CD37-lilotomab complex was internalized 10 times faster and to a greater extent than the CD20-rituximab-complex. It was also determined that the drug did not break into free-floating metal and antibody, as shown by the lack of redistribution of activity in the mice [45]. Recent investigations in several murine models have shown <sup>177</sup>LuLu-lilotomab satetraxetan to be more efficient in transformed follicular lymphoma models [72].

## 2.3 Dosimetry

### 2.3.1 Definition of dose

The absorbed dose is defined as the energy imparted in a volume, divided by the mass of said volume. The unit is joule per kilogram mass, called the gray (Gy).

Internal dosimetry (from here on referred to simply as dosimetry) is the process of which the end-point is the absorbed dose. The calculation involves

## 2. Scientific background

---

first measuring or assuming the distribution of radionuclides and then calculating the absorbed energy from the radiation from this distribution.

### 2.3.2 SPECT/CT-based Quantitative imaging

#### 2.3.2.1 The scanner

A SPECT/CT-scanner is a device that is used to map the distribution of activity in the patient body originating from (single) photon-emitters. This is achieved by the detection of emitted  $\gamma$ -photons from multiple angles around the imaged volume, which is subsequently reconstructed into three dimensional images [73]. A full description of the inner workings of the SPECT/CT-scanner is beyond the scope of this work. For a comprehensive introduction to the development of SPECT and SPECT/CT, see Hutton [74]. For an overview of detector technology, see the review article by Peterson and Furenlid, with the main moments outlined here in brief [75]: The detection is done in a step-wise process, to convert the high-energy  $\gamma$ -photons to an electrical signal. The first step is to collimate the photons, excluding the photons that have been scattered on their path to the detector. The  $\gamma$ -photon then interacts with a detection material, the most commonly used is a crystal of sodium-iodide doped with trace amounts of thallium or cerium. Photons in the relevant energy-range of SPECT (30keV - 250keV) interacts with zero to two Compton-scatters followed by a photo-electric absorption. The result is a burst of optical photons, which is then converted into an electrical signal and digitized.

#### 2.3.2.2 Quantitative imaging

If the emission tomography images are to be used as the basis for internal dosimetry, they have to be quantitative, i.e. having a one to one mapping between voxel values and the activity contained in that voxel. Historically, SPECT has not been regarded as a quantitative instrument, due to numerous image degrading artefacts [76]. Important causes of artefacts are, but not limited to, attenuation, scatter and partial volume effect. Attenuation artefacts stem from the SPECT-system not being able to distinguish a low-activity signal from an attenuated high-activity signal (figure 2.3).

The use of hybrid imaging, i.e. a sequential combination of a SPECT and CT-scan integrated in the same scanner, allows the inclusion of a CT-derived attenuation map and hence a correction for attenuation artefacts. Scattered radiation can potentially account for a considerable amount of the detections in the photo peak. Corrections can be made using a variety of strategies, ranging from simple scatter-energy-window-based techniques to sophisticated model-based approaches [76]. A calibration factor, relating the counts in the image to units of activity needs to be found. Current guidelines consist of either imaging a small, point-like source in air or a larger, cylindrical phantom filled with a known amount of activity [77]. The former method is to be done by planar, while the latter by tomographic scans.



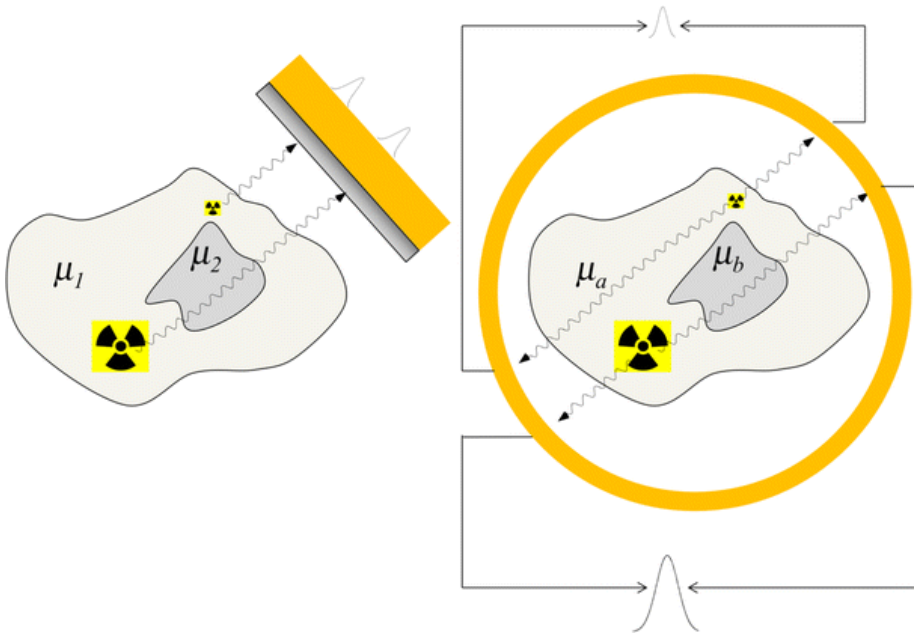


Figure 2.3: In emission tomography, a major image degradation effect is the presence of attenuation of the primary photon flux. On the left, two signals are recorded as equal despite one of them being significantly more intense, and attenuated by a high density material. Figure reproduced from [76]

SPECT/CT-images are the basis for the measurements of the temporal and spatial activity distribution, and should be as accurate as possible. The accuracy depends on numerous factors such as nuclide, target geometry, target definition, scanner, image protocol, etc. and a single accuracy containing all set-ups is not possible to give. A table compiled by Lassmann et al. suggests quantitation accuracies of  $^{177}\text{Lu}$  ranging from -12 to around 7 %, for different geometries and imaging systems [17]. In a recent multi-center inter-comparison study, a cylindrical shell phantom containing a known concentration of  $^{177}\text{Lu}$  was sent to seven European hospitals. Each hospital measured the activity in the inner core, a shell surrounding it and the entire phantom source and the measurements were compared to the true activity, as measured by the National Physical Laboratory. Results showed that all the hospitals over-estimated the activity for the whole source by a mean value of 12 %, but three hospitals had the correct value included in their reported uncertainty ranges, and all hospitals were within 30 % of the true value [78].

### 2.3.3 MIRD-formalism

The Medical Internal Radiation Dose (MIRD)-committee is a group associated with the Society of Nuclear Medicine, and has since the late 1960s published multiple pamphlets, with the aim of developing standardized frameworks and methodology for performing internal dosimetry. The most recent overview of the nomenclature, the one used here, can be found in MIRD Pamphlet No. 21 [79]. There are alternative formalisms (e.g. the ICRP) but the MIRD-formalism will be used here throughout.

Dosimetry is generally a multi-step process, starting as previously mentioned with the measurement of activity through time. The uptake and excretion of the therapeutic drug are governed by metabolic processes, usually over the time scale of several days. This makes continuous monitoring of the activity impractical, and the activity is traced at discrete time points.

$$A_{t_1}, A_{t_2}, A_{t_3}, \dots, A_{t_n} \quad (2.1)$$

These discrete activity time points are used to derive the time-activity-curve (TAC)  $A(t)$ . These TACs have to be defined for each *source organ*.

The integration of these curves yields the time-integrated activity, the total number of disintegration in source region  $r_S$ , previously termed *cumulated activity*:

$$\tilde{A}(r_S, T_D) = \int_0^{T_D} A(t) dt \quad (2.2)$$

Here, the parameter  $T_D$ , the upper integration limit, is often taken to be infinity.

This integration can be done either by fitting the time activity points to an a-priori assumed function and integrated analytically, employ a numerical integration scheme, or a combination of both.

This parameter is important because it is directly proportional to the number of radiation particles, and hence the radiation energy, of the radiating source organ. When normalized by administered activity, the quantity is called a time-integrated activity coefficient (TIAC).

$$\tilde{a}(r_S, T_D) = \frac{\tilde{A}(r_S, T_D)}{A_0} \quad (2.3)$$

In the MIRD-scheme, the quantity to convert time-integrated activity coefficients to absorbed dose is often denoted as  $S(r_T \leftarrow r_S)$ , and the final absorbed dose from source organ  $r_S$  to target organ  $r_T$  is

$$D(r_T, r_S) = \tilde{A} \cdot S(r_T \leftarrow r_S) \quad (2.4)$$

The S-factors result from Monte Carlo-simulations in reference patient geometries. This quantity is dependent on the radionuclide and the mathematical phantom used to represent the patient, which in turn can depend on age, sex and patient size. Development of mathematical phantoms has been a matter of

research interest for over fifty years, from simple models consisting of spheres and cones, to more sophisticated voxel and polygonal-mesh models, see Xu for an overview [80]. The S-factor can be separated into its parts

$$S(r_T \leftarrow r_S) = \frac{1}{M_T} \sum_i E_i Y_i \phi(r_T \leftarrow r_S, E_i) \quad (2.5)$$

here  $i$  denotes different nuclear transitions with energy  $E_i$  and yield  $Y_i$ , these are dependent on the radionuclide and independent of the mathematical phantom.  $\phi$  is the absorbed fraction, a number between 0 and 1 denoting the fraction of energy that is absorbed in the target organ from the source organ. For  $\beta$ -emitters, this number is often assumed to be unity. Finally,  $M_T$  is the mass of the target organ.

To find the final dose of the target organ, contributions from each source organ are summed resulting in the total absorbed dose to target  $r_T$

$$D_T = \sum_{r_S} \dot{A} \cdot S(r_T \leftarrow r_S) \quad (2.6)$$

The S-factors for a large number of nuclei are tabulated in the FDA-approved software Organ Level INTERNAL Dose Assessment (OLINDA/EXM). These S-factors are based on the various phantoms of different relevant patient sizes and sexes, where a series of Monte Carlo-simulations have been performed [81].

Lastly it should be noted that the concepts of *source organ* and *target organ* can be generalized to a more fine-grained calculation, where rather than organs, sub-volumes of organs, single cells or voxels are considered instead of organs.

### 2.3.4 Red marrow dosimetry

The red marrow requires some additional consideration, given that it is both a challenging organ to perform dosimetry on, and also the most common organ at risk in RIT.

The assumption of spatially homogeneous, local deposition of energy cannot be made in the skeletal regions. The reason for this is that the bone marrow is a highly complex structure of tissue, with different structure components having different radiation sensitivity and the details of this structure are in the same order of magnitude as the path length of the  $\beta$ -energies of typical therapeutic radionuclides. The marrow itself is contained in small cavities dispersed throughout the skeleton, in adults mostly in the axial skeleton [82]. These cavities contain islands of hematopoietic (blood-producing, red, marrow) and adipose (fatty, yellow, marrow) cells, interspersed in a honeycomb-like structure by a network of trabecular bone, referred to as the trabecular spongiosa. If a  $\beta$ -particle originating from a radionuclide residing in the red marrow has some of its energy absorbed in fatty marrow, the absorption factor  $\phi(\text{Redmarrow} \leftarrow \text{Redmarrow})$  is no longer unity.

Considerable work has been done in developing models to simulate the trabecular spongiosa, starting from one-dimensional path-length-models developed

## 2. Scientific background

---

by Spiers et al. in the 1970s [83] [84]. These models were later re-evaluated and extended to cover multiple skeletal sites, ages and sex by Eckerman and Stabin [85]. A separate calculation was done by Bouchet et al. who used revised information on regional bone and marrow mass and calculated new absorbed fractions [86]. These two calculations deviates for low and high  $\beta$ -energies, and the two models were resolved in a unified model [87]. An average value of the entire skeleton from this calculation is the basis for the  $S(\text{RM} \leftarrow \text{RM})$  implemented in the OLINDA/EXM-program.

All the aforementioned methodologies and calculations assume that environment of trabecular spongiosa reaches infinitely. In addition to the micro-structure of the marrow, there exists also a macro-structure which potentially can become important. Shah and colleagues developed a *paired image radiation transport* model that incorporated radiation transport in both the micro- and macroscopic domain [88] [89]. The fraction of adipose cells in the marrow-cavities is called the cellularity factor, denoted by the percentage of adipose cells as identified from histological slices. This factor can vary substantially throughout the skeleton, and depends on patient age. This was also explored by Shah et al. using microscopy-imaging and computer simulations [90] [91] [92]. Results of this comprehensive work include two publications, one for a male and one for a female patient, describing mathematical phantoms for electron sources residing in different regions of the marrow space [93] [94] (fig. 2.4) These mathematical phantoms give absorbed fraction-values as a function of  $\beta$ -energy, skeletal site and cellularity factor, and have also been parametrized to account for skeletal size and bone mineral density, being proxy parameters for aging [95]. Combined with a description of the emission data and equation (1.5) these tabulated values can be used to form S-factors for any given radionuclide.

### 2.4 Biodistribution and dose effect for RIT of Lymphoma

The RIT will after administration be eliminated through metabolic processes and bind specifically or non-specifically to antigens. Previous studies of antibody radionuclide conjugate agents, identified uptake in the spleen, liver kidneys and bone marrow [68] [96] [97] ([98], including errata).

The overall toxicity experiences with RIT in the treatment of haematological malignancies have shown that the treatment is well tolerated. This also remains true when high amounts of activity is used in a myeloblative setting [99]. Observed toxicities in non-myoblative have been myelosuppression, fatigue, HAMA formation and in treatments where  $^{131}\text{I}$  has been used, thyroid dysfunction [1]. Secondary myelodysplastic syndrome and acute myelogenous leukemia have been reported, with incidence in the order of 1-3 % [100] [60]. For both of the two FDA-approved drugs  $^{90}\text{Y}$ -ibritumomab tiuxetan and  $^{131}\text{I}$ -tositumomab the hematological toxicities have been transient neutropenia and thrombocytopenia, believed to result from irradiation of the red marrow cells [101]. There has been some interest to correlate the absorbed dose to the myelosuppression, to predict this toxicity. A clear correlation has been proven elusive to find, as there

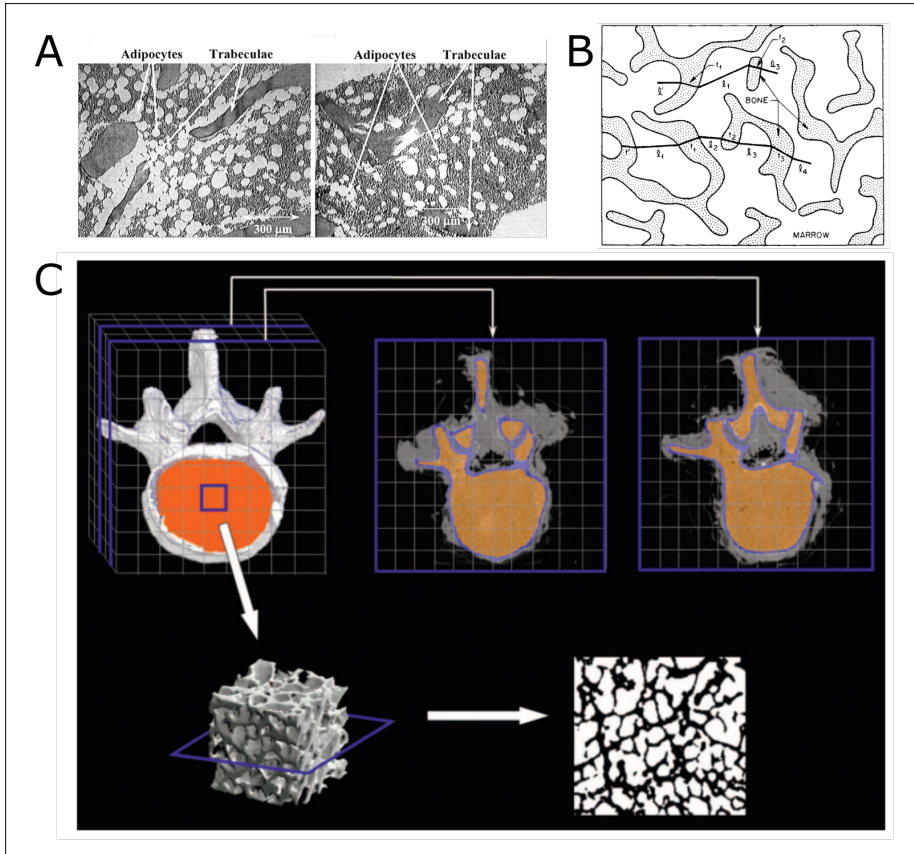


Figure 2.4: The microscopic distribution of the red marrow. Panel A shows images of bone marrow biopsy slides. The fatty marrow cells can be seen indicated in white circular clusters. The panel show two different cellularity factors, 30 percent to the left, and 80 percent to the right. Panel B show electron pathways in across the marrow space and trabecular mesh. Finally panel C show the three-dimensional structure of the trabecular mesh in the lumbar vertebrae. The top left show the a 3D-model of the vertebrae. To the right are two slices, where cortical- and trabecular bone have been color coded as blue and orange respectively. Below is a 3D-model (left) and a slice (right) of the microscopy NMR-images showing the micro-structure of the bone trabeculae. This modelling has been used by the group in the University of Florida to make a comprehensible skeletal phantom that incorporates both macro- and micro-structure of the marrow. Modified from [88] [85] and [90]

## 2. Scientific background

---

are potential confounding factors that affect the bone marrow reserve of each patient.

### 2.4.0.1 [<sup>90</sup>Y]Y-ibritumomab tiuxetan,

Studies of [<sup>90</sup>Y]Y-ibritumomab tiuxetan did not reveal any correlation between absorbed dose and toxicity. Early dosimetry included multiple methods to assess dose, two methods based on planar imaging (lumbar and sacrum) and one blood-surrogate-based. Results did vary across the methods, with a higher estimate of the absorbed dose from the sacrum-based approach (1.0 mGy/MBq), a lowest estimate in the lumbar-approach (0.3 mGy/MBq) and the blood-surrogate method falling in the middle (0.6 mGy/MBq). None of these estimates correlated with the severity of hematological nadir [102]. Later in a larger cohort, no correlation was found, although all calculated absorbed doses to the red marrow were below the protocol-set limit of 3 Gy (the range was 17.5 to 221 cGy) [103]. In the final dosimetry study, including 179 patients and “extensive analyses” no correlation was found between either absorbed dose calculated from sacral imaging or blood-based results and hematologic toxicity. The authors themselves point to methodological challenges [104]. As studies revealed no correlation between absorbed dose and myelosuppression, activity is administered according to a dosage regime, with a maximum dosage level of 14.8 MBq/kg body mass up to 1184 MBq [60].

A later study done by Fisher et al. calculated the absorbed dose in ten patients using quantitative planar imaging, patient specific organ mass and body weight and OLINDA/EXM [96]. An almost two-fold discrepancy compared to the packet insert value for the absorbed dose to RM. Still these estimates have been done by planar imaging, known to be less accurate than tomographic imaging especially when there are significant overlapping structures in the imaging plane [105].

### 2.4.0.2 [<sup>131</sup>I]I-tositumomab

In contrast to [<sup>90</sup>Y]Y-ibritumomab tiuxetan, absorbed dose calculation played a crucial role and was an integrated part of standard clinical practice in the administration of [<sup>131</sup>I]I-tositumomab. Initial studies of [<sup>131</sup>I]I-tositumomab used a dose escalation model where the whole body absorbed dose was measured and used as the dosage step [106]. The standard treatment protocol consists of an initial administration of a tracer amount, 185 MBq, of [<sup>131</sup>I]I-tositumomab. A series of WB images is then performed to verify biodistribution and calculate the WB clearance rate. This is used to calculate the activity to deliver a specified target absorbed dose [21]. A whole body dose of 0.75 cGy believed to reflect the tolerated absorbed dose to the red marrow was found to be a suitable target dose [22]. The therapeutic activity is given seven to 14 days after the tracer administration.

### 2.4.0.3 Other

Stillebroer et al. found a significant correlation between absorbed dose to the red marrow and leukocytic and thrombocytic toxicity, in small patient cohort treated for renal cell carcinoma with the CAIX-targeting  $^{177}\text{Lu}$ Lu-cG250 [107].

The time from the last chemotherapy was found to be the single parameter predicting myelosuppression in a study including patients treated both with I $^{[131\text{I}]}$ I-tositumomab and  $^{90\text{Y}}$ Y-ibritumomab tiuxetan. The absorbed dose to the red marrow was also included as a variable, but the authors suggested that this was due to a too narrow interval of included absorbed doses [101].

Myelosuppression and patient characteristics for patients treated with  $^{131\text{I}}$ -monoclonal antibodies targeting carcino-embryonic antigen were investigated by Juweid et al. They found a correlation between the platelet and white blood cell toxicity grade and red marrow absorbed dose (both), baseline values (both), metastatic disease defined as two or more metastasis found on bone scan or MRI (both) and chemotherapy within three (for platelets) or six (for white blood cells) months of treatment [108]. They concluded on the absorbed dose as the single most important factor, but also that other factors could be crucial to determine toxicity.





## Chapter 3

# Aims of individual papers

The overall aim of this thesis was to establish methods to perform dosimetry on patients treated with [ $^{177}\text{Lu}$ ]Lu-lilotomab satetraxetan with the end goal of investigating the absorbed dose to normal organs in the LYMRIT 37-01-study.

**Aim for Paper I** The LYMRIT-37-01-study is a first in-human trial. In paper I the aim was to investigate the bio-distribution in these initial patients to compare them with the investigations of [ $^{177}\text{Lu}$ ]Lu-lilotomab satetraxetan performed in murine models and with other RITs. Special focus was set on the identification of organs at risk and to explore ways to optimize the initial image protocol.

**Aim for Paper II** In paper I the red marrow was established as the primary organ at risk. In paper II, the aim was to quantify the absorbed dose in the red marrow and establish toxicity correlation. This was primarily to be done with a direct, image based quantitation method, as uptake in the red marrow was visually identifiable on the SPECT/CT-images.

**Aim for Paper III** In the previous papers, it was found that specific pre-dosing with non-radioactive lilotomab had a mitigating effect on absorbed dose to the red marrow. A potential concern is that the blocking effect of the non-radioactive lilotomab could also affect the uptake in tumours. In paper III, patients from additional treatment arms of the LYMRIT-37-01-study and absorbed dose to lesions were included. A therapeutic index, defined as the ratio of the tumour to red marrow absorbed dose was investigated to aid in the selection of an optimal treatment protocol.

**Aim for Paper IV** A correlation between the absorbed dose to the red marrow and myelosuppression was indicated in the previous papers. This correlation was further investigated in paper IV. Correlation could be potentially obscured by confounding factors related to red marrow reserve. The main aim of the paper was to see if inclusion of more patient characteristics could help explain variation in the observed correlation. In this paper, an updated absorbed dose calculation that incorporated the existence of fatty marrow was also included.



# Chapter 4

## Materials and Methods

### 4.1 Treatment and patient material

#### 4.1.1 LYMRIT 37-01 study

Patients included in this work were all included in the LYMRIT 37-01-trial. The trial includes histologically confirmed CD37-positive, relapsed indolent NHL patients. A detailed description of the inclusion and exclusion criteria can be found in [109]. Spanning all papers, four different treatment arms were included. Arms contained different pretreatment and predosing (fig. 4.1). Two arms included a predosing with cold lilotomab, arm 1 (40 mg) and arm 4 (100 mg/m<sup>2</sup>). Patients in arm 2 received 375 mg/m<sup>2</sup> of rituximab, whereas arm 3 did not include any predosing. Treatment arms 2 and 3 were in multiple analyses combined as they both contain no CD37-specific pre-dosing. All patients received a single administration of [<sup>177</sup>Lu]Lu-lilotomab satetraxetan. The amount of activity was given according to a dosage regime based on patient whole body mass (either 10, 15 or 20 MBq/kg) at the day of RIT administration.

#### 4.1.2 Patients

Paper one included seven patients, paper II included eight, paper III nineteen and IV included seventeen patients. A total of 21 different patients were included, of which the majority (18) had follicular histological subtype, two had mantle cell and one had marginal zone NHL. All patients signed a written consent form and the study was approved by the regional ethics committee. All patients throughout this thesis have the same patient identifier (i.e. patient number).

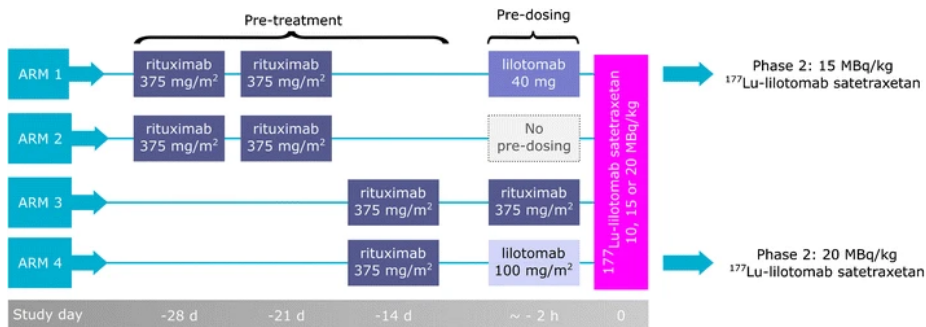


Figure 4.1: An overview of the treatment protocol in the LYMRIT-37-01-study. [110].

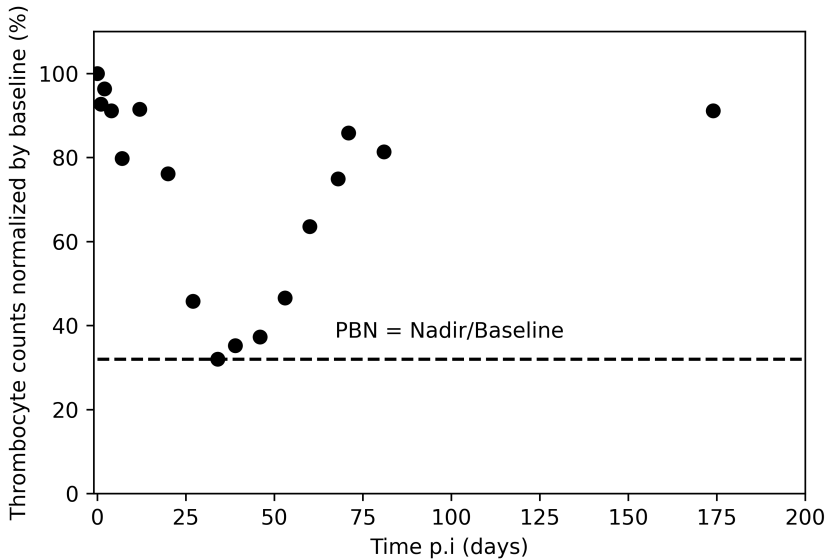


Figure 4.2: Thrombocyte counts normalized by baseline counts p.i. Indicated in the figure is the PBN-value, showed as a dashed line.

Age at treatment, total number of previous chemotherapy treatments, prior history of EBRT and elapsed time since last chemotherapy were also recorded.

### 4.1.3 Toxicity

For papers II, III and IV, blood samples were collected at baseline, multiple times at the day of treatment, once each day 1, 2, 3, 4 and 7, and every week until week 4, and then every 6 months. Thrombocytes and neutrophils were counted. Adverse effects were graded by the Common Terminology Criteria for Adverse Events (CTCAE, version 4.0). For the primary analysis, the patients were split into two groups; one with grade 0, 1, or 2 and one with 3 or 4. In paper IV, the relative value of neutrophils and thrombocytes compared to baseline (PBN) as well as the time to nadir (TTN) was used as indicators of toxicity (fig. 4.2).

Activity concentration was measured in blood samples to be used in pharmacokinetic analyses. The total activity in blood was analysed by noncompartmental analysis in Phoenix WinNonLin 64 using the “linear up log down” method. A detailed description of the pharmacokinetic modelling is found in [109].

## 4.2 Imaging and other radioactivity measurements

All patients were imaged in the same centre, on the same scanner, a Siemens Symbia T16. Both planar and tomographic scans were acquired. The scanner was equipped with a 0.952 inch thick NaI-crystal and a medium energy, low penetration collimator. The scan was performed with 2 x 32 projections, each projection was of 45s length. A non-circular orbit with body contouring was used.

Both the 113 and 208 keV-photopeaks were acquired with a 20 % window width. Both upper and lower scatter windows placed adjacent to the main emission windows were used.

For all planar scans and for the majority of the SPECT/CT-images, a small vial with a known activity of  $^{177}\text{Lu}$  was placed in the field of view as a constancy control.

### 4.2.1 Planar

In paper I, planar WB scans were performed for included patients. These planar scans were done at approximately 2, 4, 8 hours, 96 and 168 hours post injection (p.i.). The planar WB scans were acquired with a matrix size of 256 x 1024 with a 5 cm/min scan speed. For the initial patients, a thin vacuum mattress was used to provide fixation, this was amended for later patients due to practical reason.

### 4.2.2 SPECT/CT

The SPECT/CT imaging protocol consisted of a series of SPECT/CT-images acquired in general 24, 96 and 168 hours p.i. Patients in arm 1 and patient P001 did not have a SPECT/CT-scan at 24 hours p.i.

SPECT/CT-images were reconstructed using the vendor's software. In paper I, the 208 keV-energy window was used whereas in papers II, III and IV, both energy windows were utilised for quantification.

A calibration factor to convert counts to activity was found from reconstructed images of an anthropomorphic torso phantom model (model ECT/TOR/P; Data Spectrum Corp). Volumes of interests were drawn inside the larger "liver"-insert of the phantom, and a conversion factor for both the 208-keV- and 113+208 keV-reconstruction was made.

### 4.2.3 Miscellaneous measurements

Urine samples were collected for two patients, first for each individual micturition during the first 2 h, then the urine from the next 18-22 h was collected together. Whole body measurements of the exterior dose rate of the patient were in general used to calculate the whole body clearance. Measurements were done both anterior and posterior at fixed distances at the height of the sternum. The measured dose rates were background corrected and the geometric means of

## 4. Materials and Methods

---

the anterior and posterior dose rate used to yield the final measurement. The first measurement was performed before the first void, and used as a reference point for total activity in the patient. A time activity curve (TAC) for the whole patient was found by fitting these measuring points to a mono exponential curve.

### 4.3 Dosimetry

#### 4.3.1 Activity quantification

All volume delineations were done using the software tool PMOD version 3.6 (PMOD Technologies Ltd). Volume definitions of the red marrow volume and tumours were done together with a nuclear medicine specialist. A volume of interest (VOI) was drawn around the organ with a 1-2 cm margin, allowing spill-out-activity to be accounted for. Individual TACs were made for each organ and the whole body. In paper I, five-point TACs were made, whereas in papers II, III and IV, a two-point TAC was used. These were integrated and divided by the administered activity  $A_0$  to yield time integrated activity coefficients

$$\tilde{a} = \frac{1}{A_0} \int_0^{\infty} A(t)dt = \frac{\tilde{A}}{A_0} \quad (4.1)$$

Integration was performed by a combination of discrete and analytical techniques. The five-point-curves were integrated by trapezoidal integration between the second and penultimate time-point. The TAC beyond the last time-point was integrated by assuming mono exponential decay from the penultimate time-point to infinity. An effective half life for this mono-exponential washout phase was estimated from the two last time-points. Activity at the first time-point was extrapolated back to time zero. When a two-point TAC was used, mono exponential fitting and integration were used.

#### 4.3.2 Dosimetry

Organ masses were determined by drawing VOIs on CT images. The mass density of organs and tumours except the red marrow in article IV was considered to be 1 g/cm<sup>3</sup>.

For the mass of the red marrow, two approaches were used. In papers II and III a VOI was placed on the interior of the periostenum of the bone of vertebrae L2-L4, denoting the volume  $V_{L2-L4}$ . A trabecular bone volume fraction,  $f_{TB}$ , of 0.135 and 0.148 was subtracted from this volume for male and female patients respectively. Assuming a mass density of the red marrow of 1.0, the mass of the red marrow was then be written as

$$m_{RM} = V_{L2-L4} (1 - f_{TB}) \quad (4.2)$$

The total red marrow activity and mass were then found by assuming that the region of L2-L4 consists of 6.7 percent of the total marrow.

$$m_{RM(patient)} = \frac{V_{L2-L4}(1 - f_{TB})}{0.067} \quad (4.3)$$

$$\tilde{a}_{RM(patient)} = \frac{\tilde{a}_{L2-L4}}{0.067} \quad (4.4)$$

Conversion from TIACs and mass of the source organs liver, spleen, kidneys, red marrow and WB to absorbed dose was done in papers I, II and III with the dose-calculation software tool OLINDA/EXM (version 1.1) [81]. Patient specific organ masses in source-organs (liver, spleen, kidneys and red marrow) and WB-mass were used, reference values from OLINDA/EXM were used for the rest of the organs.

For the tumours, the OLINDA/EXM-sphere module was used. The software program provides a look-up-table with input in the form of TIACs, and the absorbed doses for various sphere sizes are given. A conversion factor,  $\bar{S}$  was made from the 10 g-sphere:

$$\bar{S} = 8.56 \cdot 10^{-5} \text{Gykg/MBqh} \quad (4.5)$$

So the absorbed dose of the tumours could be calculated from

$$D_{\text{tumour}} = \bar{S} \cdot \frac{\tilde{A}_{\text{tumour}}}{m_{\text{tumour}}} \quad (4.6)$$

The contribution from non-specific uptake in the rest of the body was calculated by subtracting the sum of organ TIACs by the cumulative activity of the whole body. This TIAC of the whole body was found either by whole body probe measurements or planar whole body scans, when either was available. In paper II where only the red marrow absorbed doses were calculated, if neither were available, a mean value calculated from the available patients was used.

### 4.3.3 Blood-based method for the red marrow

In paper II, a surrogate method to calculate the absorbed dose to the red marrow was explored [111]. In this method, the cumulative activity concentration in the red marrow was assumed to be equal to that of blood,  $\tilde{A}_{\text{blood}}$ . The total mass of red marrow was found by a scaling factor depending on the whole body mass of the patient

$$m_{RM(patient)} = \frac{m_{RM(ref)}}{m_{WB(ref)}} m_{WB(patient)} \quad (4.7)$$

and the TIAC of the red marrow was then calculated as

$$\tilde{a}_{RM(patient)} = \frac{\tilde{A}_{\text{blood}}}{A_0} m_{RM(patient)} \quad (4.8)$$

### 4.3.4 Red marrow in Paper IV

In paper IV, an improved method to calculate absorbed dose to the red marrow, incorporating different fractions of yellow marrow was used. This method was based on the mathematical phantoms developed at the University of Florida [93] [94]. These two publications tabulate specific energy absorption factors for male and female patients for different skeletal sites, cellularity factors (CFs) and electron energy.

First, CF, energy and skeletal-specific absorbed energy fractions were calculated. This was done by using equations (2) and (4) from [94] to calculate the reference red marrow masses. The absorption fraction  $\phi$  could then be calculated with

$$\phi(\text{RM} \leftarrow \text{RM}, CF, E) = \Phi(\text{RM} \leftarrow \text{RM}, CF, E) \cdot m_{\text{RM-ref}} \quad (4.9)$$

These factors were combined with the electron spectrum of  $^{177}\text{Lu}$ , found from ICRP publication 107 [112] and the mean energy of each emission,  $\Delta_i$  and the corresponding  $\phi$  were summed for all energies  $i$ :

$$S(\text{RM} \leftarrow \text{RM}, CF) = \sum_i \Delta_i \phi(\text{RM} \leftarrow \text{RM}, CF, E_i) \quad (4.10)$$

The absorbed doses for a specific CF could then be calculated from this factor and the corresponding measured skeletal volume  $V$  and cumulative activity  $\tilde{A}$ .

$$D = \tilde{A} \frac{S(\text{RM} \leftarrow \text{RM}, CF)}{V \cdot (1 - f_{\text{TBV}}) \cdot CF \cdot \rho} \quad (4.11)$$

Here  $\rho$  is the mass density used by the University of Florida phantoms,  $1.03 \text{ g/cm}^3$  and  $f_{\text{TBV}}$  is the trabecular volume fractions used in the phantoms. These calculations were done with in-house written software (python, version 3.7.6) where each phantom was implemented as a python-class object with associated class functions to perform absorbed dose calculations. This software is available online <https://github.com/blakkisrud/RedMarrowSFactor>. In paper IV, fractions of 0-90 % fatty marrow in 10 %-intervals and the ICRP-reference-value were calculated for the lumbar vertebrae L2-L4. The ICRP-reference-values were used in the final dose calculations.

## 4.4 Statistical methods

Linear tests were in general utilised. The Shapiro-Wilk-test and visual inspection of quantile-quantile-plots were used to check for normality. Comparisons of groups of patients were performed with the student t-test. A paired t-test was used in paper II to compare the SPECT/CT-derived absorbed doses to those calculated by the blood surrogate method. Correlation between individual absorbed doses and thrombocyte and neutrophil-counts at nadir was investigated with a Pearson test in paper II.



In paper IV, a multivariate analysis was performed based on multiple patient characteristics. All combinations of parameters were tried, and the significant models, defined as all parameters being significant at the 0.05-level, were kept. Multicollinearity was checked with the variance of inflation factor and the Akaike Information criteria was used to identify the best model among significant models. For the final model, a leave-one-out analysis where the predicted and observed CTCAE-grade were compared was performed.

A sigmoid relationship between the absorbed dose and percentage of blood-values at nadir compared to baseline was also performed

$$\text{PBN}(D) = 100 - \frac{100 \cdot D^N}{D^N + D_{50}^N} \quad (4.12)$$

Here  $N$  and  $D_{50}$  are fitting parameters.

For model comparison, the sums of mean squared errors were compared.



## Chapter 5

# Summary of publications

**Paper I** In paper I, the bio-distribution of [ $^{177}\text{Lu}$ ]Lu-lilotomab satetraxetan was explored with the use of serial planar- and tomographic scans. Seven patients in this first-in-human trial were included.

Normal tissue organs with visually distinct uptake were the spleen, liver, red marrow and to a lesser extent the kidneys. The TACs revealed a late mono exponential wash-out phase of [ $^{177}\text{Lu}$ ]Lu-lilotomab satetraxetan in the kidneys and liver after an initial plateau-phase. The plateau phase in the spleen seemed to be somewhat prolonged and to possibly have a later maximum value compared to the other organs.

The spleen was the organ that received the highest absorbed dose overall, with a mean absorbed dose of 3.57 and a maximum absorbed dose of 6.50 Gy. The organ with the second highest uptake was the liver, with a maximum absorbed dose of 2.00 Gy. The kidneys received a lower absorbed dose, a maximum of 0.62 Gy. No adverse renal or hepatic toxicity was observed during the 15 to 50 month follow-up time, which fits well with the dosimetry data as all absorbed doses are below assumed toxic limits.

The whole body half-life of [ $^{177}\text{Lu}$ ]Lu-lilotomab satetraxetan was 82 hours, ranging from 72 to 95 hours. Absorbed dose to the whole body ranged from 0.08 to 0.17 mGy/MBq.

The initial imaging protocol included extensive imaging, with multiple imaging sessions on the day of treatment. Simulations of time activity-curves with fewer time points revealed that removal of the 4 and 8-hour time points did not change the calculated absorbed dose by more than 1 %.

Urine was collected and measured before the first imaging time point for two patients. With less than 2 % secreted in this voiding it was assumed that all activity was retained in the body at the first imaging time point for all patients.

Background-subtraction of the planar images of the kidneys yielded negative values, indicating low uptake in the kidneys compared to surrounding tissue and making it difficult to analyse these organs with planar imaging. Geometric mean planar images were sub-optimal for quantification of activity when compared to SPECT/CT-images, apart from possibly TACs of the liver and spleen.

The study included patients of two different treatment arms. There was no significant difference between absorbed dose per administered activity for pre-dosed and non-pre-dosed patients except for the absorbed dose to the red marrow.

In conclusion, the spleen and liver together with the red marrow accounted for the majority of physiological uptake of [ $^{177}\text{Lu}$ ]Lu-lilotomab satetraxetan.

## 5. Summary of publications

---

**Paper II** Myelosuppression has previously been identified in RIT as being the primary dose limiting toxicity. In paper II, absorbed dose to red marrow and its correlation with myelosuppression was more closely investigated in [ $^{177}\text{Lu}$ ]Lu-lilotomab. As in paper I, the work included two treatment arms, arm 1 that did include pre-dosing with non radioactive lilotomab, and arm 2 that did not. A visually distinct uptake was identified in the skeletal regions of the patients, especially on those that did not receive pre-dosing.

Absorbed dose to the red marrow was calculated by an imaging based approach where the L2-L4 vertebrae were imaged with SPECT/CT and used as a model for the total red marrow. The estimated red marrow absorbed ranged from 67 to 207 cGy. The absorbed dose was mainly from the red marrow itself, with cross dose from the remainder of the body contributing to a maximum value of 17 %.

The majority of patients did experience neutropenia or thrombocytopenia some grade of. Patients were grouped according to either grade 1/2 or grade 3/4 thrombocytopenia and neutropenia. Patients that did experience grade 3/4 thrombocytopenia had a higher red marrow absorbed dose than patients that experienced grade 1/2. For neutropenia, patients with grade 3/4 toxicity had a higher red marrow absorbed dose, but this difference was not statistically significant.

The absolute value of the nadir value, being the value defining the CTCAE-toxicity grade, was also investigated. A significant linear correlation was found between the absolute thrombocyte count at nadir and absorbed dose ( $p = 0.04$ ).

Patients that received pre-dosing with unlabelled lilotomab had a significantly lower absorbed dose to red marrow per administered activity, 0.9 vs 1.6 mGy/MBq.

The activity in blood was also used to calculate pharmacokinetic data. The result of this analysis revealed a significantly larger area under the curve in blood for lilotomab-pre-dosed patients and a lower clearance and volume of distribution.

Both a blood based and an image based methodology for red marrow absorbed dose was performed. Relative difference between the methods ranged from 80 to 638 % with a large underestimation of the absorbed dose calculated by the blood-based methodology. Based on the lack of correlation with toxicity and the visually distinct specific uptake in the red marrow, the blood based methodology was deemed unfit for this therapy.

This work has identified a relationship between absorbed dose to the red marrow and myelosuppression. Also, pre-dosing with unlabelled lilotomab had a mitigating effect on absorbed dose to the red marrow, which leads to a more favourable toxicity profile.

---

**Paper III** Paper III includes patients from four different treatment arms, two without pre-dosing with unlabelled lilotomab (arms 2 and 3), and two with pre-dosing (arms 1 and 4), for a total of 19 patients. The two treatment arms without pre-dosing with unlabelled lilotomab were combined in the primary analysis.

The main focus of paper III was the ratio between the previously identified organ at risk (red marrow) and absorbed dose of the tumours. A higher tumour to organ at risk ratio would suggest the more optimal treatment strategy. The non-pre-dosed group was compared to the arm receiving a fixed amount of unlabelled lilotomab (40 mg, arm 1) and the arm receiving a significantly higher amount (100 mg/m<sup>2</sup> BSA, arm 4).

As seen in arms 1 and 2 patients in paper I, uptake of [<sup>177</sup>Lu]Lu-lilotomab satetraxetan could be most prominently identified in the liver, spleen, and the red marrow in addition to the tumours; this held true for all four arms included in paper III. There was a significantly lower absorbed dose in the spleen in patients in arm 4 compared to the non-pre-dosed group.

A total of 47 lesions were included for dosimetry, with 1 to 5 and a mode of 3 tumours per patient. Absorbed doses to the tumours did vary significantly both inter and intra-patiently. In one patient, the absorbed dose to the tumours ranged from 149 to 859 cGy. Although a higher absorbed dose to tumours was found in arms 1 and 4 compared to the non-pre-dosed group, 1.79, 2.15 and 2.67 mGy/MBq for the non-pre-dosed group, arm 1 and arm 4 respectively, the differences were not statistically significant.

Absorbed dose to the red marrow ranged from 69 to 204 cGy. Patients receiving pre-dosing with cold lilotomab had a lower absorbed dose to the red marrow. This mitigating effect was present both in patients pre-dosed with a fixed amount of 40 mg and 100 mg/m<sup>2</sup>. However, no significant difference between patients of the two different pre-dosing regimens with regards to absorbed dose to the red marrow was observed.

There was a significantly higher ratio of tumour to red marrow absorbed self-dose for both lilotomab-pre-dosing arms. The ratios between the tumour and red marrow absorbed doses were 1.07, 2.16 and 4.62 for non-pre-dosed, arm 1 and arm 4 patients. Some care has to be taken when interpreting this, given the aforementioned inter and intra-patient variation of absorbed dose to the tumours. These results are nonetheless encouraging, and extend those of Paper II that pre-dosing with lilotomab provides a potentially better therapeutic ratio.

**Paper IV** Paper IV includes further investigations of the absorbed dose to the red marrow and its correlation with myelosuppression. Several clinical parameters and new S-factor were included in this work.

The new calculation using the L2-L4-site and the ICRP-CF increased the numerical value of the absorbed dose calculation when compared to previously calculated doses. This difference is systematic except for patient sex and contribution to the red marrow absorbed dose from the whole body.

The PBN and the TTN were used as indicators of myelosuppression, and were the primary dependent variables. PBN ranged from 4 to 56 and 1 to 53 % for thrombocytes and neutrophils. The median time to nadir was 37 and 44 days for thrombocytes and neutrophils respectively. All patients experienced some grade of thrombocytopenia and 14 of the patients experienced neutropenia.

A possible explanation of the variation in response as a function of absorbed dose to the red marrow found in Paper II could be patient heterogeneity in terms of bone marrow reserve. This was tested by including several clinical parameters believed to affect the marrow reserve: age at treatment, baseline cell-count of thrombocytes and neutrophils, prior EBRT, previous chemotherapy treatments and time elapsed since last chemotherapy. Pharmacokinetic parameters activity under the curve and half life in blood were also included in addition to dosage and administered activity. Inclusion of these variables did not contribute to explain the variation within a linear model, and the absorbed dose to the red marrow was identified as the single significant variable. The absorbed dose to red marrow was identified as the single significant parameter, although with low r-squared values, 0.25 and 0.32 for thrombocytes and neutrophils respectively.

The result of the leave-one-out-analysis showed that exact thrombocytopenia and neutropenia grade was predicted in 3/17 and 6/17 for thrombocytopenia and neutropenia respectively. Toxicity grade +/- 1 was predicted in 12/17 (thrombocytopenia) and 15/17 (neutropenia) of the patients.

A sigmoid relationship between absorbed dose to the red marrow and myelosuppression was also investigated. The root mean-square error was comparable to the linear model, and the leave-one-out analysis of the sigmoid curve gave the exact CTCAE-grade of 3/17 and 8/17 for thrombocytes and neutrophils respectively. The CTCAE-grade +/- 1 was predicted in 12/17 and 15/17 for thrombocytes and neutrophils respectively.

## Chapter 6

# Discussion

In this work the biodistribution and absorbed dose to normal organs and tumours for NHL patients treated with [ $^{177}\text{Lu}$ ]Lu-lilotomab satetraxetan were investigated.

The red marrow was identified as the primary organ at risk and a correlation between absorbed dose to the red marrow and myelosuppression was found. Another important finding was that pre-dosing with unlabelled lilotomab prior to RIT had a mitigating effect on the absorbed dose to the red marrow and yielded a favourable biodistribution.

### 6.1 Clinical relevance of dose findings vs/ toxicity

The assessed absorbed doses to the red marrow were in the order of 1-4 Gy depending on dosage and treatment protocol. When compared to suggested toxicity limits, this absorbed dose to the red marrow was the only substantial normal organ absorbed dose. This is in concordance with observed primary toxicities, namely transient thrombocytopenia and neutropenia that reached a nadir approximately 5-7 weeks after therapy [109]. These adverse events are mild when compared to chemotherapy regimens like R-CHOP or CVP and comparable to rituximab monotherapy and other RITs [113] [114].

#### 6.1.1 Tolerance limit

A correlation where an increase in absorbed dose results in increased myelosuppression for patients treated with [ $^{177}\text{Lu}$ ]Lu-lilotomab satetraxetan has been identified. A clear relationship between absorbed dose and toxicity has been difficult to establish, both in RITs and other radionuclide therapies. A contributing factor for this is potentially that internal dosimetry and toxicity studies have currently been limited to studies containing small patient populations and challenges in activity measurements. Notable exceptions are peptide receptor radionuclide therapy, selective internal radiation therapy of liver tumours and radioiodine in treatment for differentiated thyroid cancer [17] [115] [18].

Red marrow dosimetry, given the marrow's distributed nature and microscopic scale complexity represents additional challenges. Although methodology is maturing, there is still a current lack of large scale implementation beyond specialized centers [116]. In treatment of metastatic differentiated thyroid carcinoma, standard operating procedures for performing maximum tolerated activity protocols have been published [117]. A consequence of red marrow dosimetry still being in a state of relative infancy, is that consistent toxicity limits are not readily available for internal emitters. Possible approaches are to

## 6. Discussion

---

either adapt toxicity limits from EBRT, rely on limits found empirically through activity escalation studies or in rare occasions; other radionuclide therapies.

A commonly used toxicity limit for the RM, when radiation is delivered through internal emitters, is 2 Gy, originating from  $^{131}\text{I}$  treatment of metastatic differentiated thyroid carcinoma [118]. Though often used, it is based on a surrogate absorbed dose, as it is 2 Gy to the blood rather than the red marrow itself. In a larger cohort of 200 patients treated with  $^{177}\text{Lu}$ Lu-DOTA-octreotate, a cumulative absorbed dose of 2 Gy to the red marrow was used as a stopping criteria for therapy [119]. In the context of total body irradiation, a typical non-myoblastic regime limit is set to 2 Gy, as higher doses are needed to eradicate blood producing marrow cells [120]. An absorbed dose limit of 3 Gy, adopted from the absorbed dose in EBRT which results in a 5% risk of severe damage within 5 years to the blood forming system, has also been used as a limit for metastatic differentiated carcinoma [121]. The protocol-set limit set in the phase III-studies of  $^{90}\text{Y}$ Y-ibritumomab tiuxetan was also 3 Gy [104].

Even though these limits have been reported and used in the literature, one should be wary of naively comparing them across treatments with different radionuclides and biological vectors. Differing biological effect from the same estimated absorbed dose can arise from different dose-rates, and distribution across several scales, from the whole organism to the sub-cellular scale. When factoring in potential cytotoxicity from the antibodies and other long distance i.e. abscopal effects, the situation quickly grows complex. This stresses the need to compile data for specific radionuclides and treatments. An example is comparison between the  $^{177}\text{Lu}$ Lu-DOTA-octreotate treatment and  $^{177}\text{Lu}$ Lu-lilotomab satetraxetan, even though the radionuclide is identical, the fractionation protocol of the former treatment makes direct comparison unsuitable. Our results indicate that the toxicity limits of a magnitude of 2-3 Gy are appropriate for  $^{177}\text{Lu}$ Lu-lilotomab satetraxetan for adverse events in the form of grade 3/4 neutropenia and thrombocytopenia. Given all the aforementioned restrictions in comparability of absorbed doses, this is still in the same order of magnitude as previously reported and proposed absorbed dose limits to the RM.

Although a statistically significant relationship between absorbed dose and myelosuppression was found, the correlation was weak ( $r^2$ -values of 0.25 and 0.32). There is a possibility that the marrow reserve has been depleted in patients previously treated with myelosuppressive treatments, changing the radiation sensitivity of the RM. We have explored potential confounders assumed to affect the marrow reserve, explaining the variable association between absorbed dose and myelosuppression. None of the investigated patient characteristics contributed to the explanation of this variation. It is important to note that the lack of significant results do not necessarily demonstrate a lack of effect from these confounders, as the patient population is limited and still represents a heterogeneous group with respect to these parameters. Future studies of this patient group should still include these parameters and the analyses should be re-done. As neither of the other variables showed a better correlation than absorbed dose to the RM, this remains the single most important parameter to predict myelosuppression.



### 6.1.2 Prospective dosimetry

As an association between absorbed dose to the red marrow and myelosuppression has been found, the idea of implementing prospective dosimetry, i.e. tailoring the administered activity to plan for a set absorbed dose, is appealing.

This approach to deliver absorbed dose is ubiquitous in EBRT and was routinely done with [ $^{131}\text{I}$ ]I-tositumomab, where clearance rates were found to differ by a factor of five [21]. For [ $^{131}\text{I}$ ]I-tositumomab, a tracer amount of activity, 185 MBq, was administered and a therapeutic amount of activity was set to deliver 0.75 Gy to the whole body [21]. A similar, prospective dosimetry could in principle be implemented in therapy with [ $^{177}\text{Lu}$ ]Lu-lilotomab satetraxetan, however with some additional challenges when compared to [ $^{131}\text{I}$ ]I-tositumomab.

The main issue is the comparatively low  $\gamma$ -yield, as the photopeak of  $^{131}\text{I}$  (364 keV) has an abundance of 82 %, five-fold more than the combined abundance of the 113 and 208-photopeak of  $^{177}\text{Lu}$ . The lower energy of the  $\gamma$ -emission from  $^{177}\text{Lu}$  will result in more photon absorption in the patient and count-statistics are further suppressed, compared to  $^{131}\text{I}$ . This would in sum require longer scan times to allow for comparable count statistics, with the scan times used in the post-therapeutic setting already being of considerable length. Feasibility could potentially be explored by simulating a tracer amount of [ $^{177}\text{Lu}$ ]Lu-lilotomab satetraxetan and decide if the count statistics is sufficient for a reliable quantification. An alternative is to substitute  $^{177}\text{Lu}$  with another, more diagnostically suitable radionuclide that can be detected and accurately quantified also in tracer amounts. It is important to allow time for the red marrow uptake to distinguish itself from the blood pool. Substitute candidates should therefore have a half-life in the order of a few days to study the established kinetics of lilotomab.

Candidates are PET-tracers like  $^{90}\text{Zr}$  (half life 3.3 days) or  $\gamma$ -emitters like  $^{111}\text{In}$  (half life 2.8 days). The latter  $\gamma$ -emitter has been used in prospective dosimetry studies of [ $^{90}\text{Y}$ ]Y-ibritumomab tiuxetan [102]. Pre-therapeutic imaging with a 200 MBq tracer amount of activity with  $^{177}\text{Lu}$  in six patients later treated with 7.4 GBq of [ $^{177}\text{Lu}$ ]Lu-DOTATATE has been presented [122]. There, a long scan-time (60 seconds per view) was used with variable success in predicting normal organ and tumour absorbed doses. The authors commented that a potential improvement in pre-therapeutic image quality could result in better predictions.

When treating with murine monoclonal antibodies there is a possibility of developing a human anti-mouse antibody (HAMA) reaction. This has to be considered if a prospective administration of [ $^{177}\text{Lu}$ ]Lu-lilotomab satetraxetan is to be proposed, as the risk increase with multiple administrations of antibodies [123].

### 6.1.3 Post-therapy dosimetry

This thesis shows that it is feasible to apply imaging dosimetry on patients treated with [ $^{177}\text{Lu}$ ]Lu-lilotomab satetraxetan to acquire an absorbed dose with

a meaningful relationship between absorbed dose and myelosuppression. One can propose that absorbed dose can be used as a prognostic indicator to identify patients that need closer follow-up, as the dose calculation could be done in ample time before the onset of myelosuppression. In the current clinical study, the adverse events are watched by blood sampling, and all patients are thus already carefully monitored.

One can argue that post therapy dosimetry should be performed for all treatment regimens to document the delivered absorbed dose, as required by legislation and routinely performed from EBRT. This would also contribute to increase the evidence on dose-effects for internal emitters. However, an even stronger case for dosimetry can be made in a fractionated treatment setting, or in regimes where re-treatment is an option or as the standard treatment protocol, like peptide receptor radionuclide therapy in the treatment of neuroendocrine tumours [124] [125].

There has been interest for re-treatment with RIT [126]. Fractionated treatment with [ $^{90}\text{Y}$ ]Y-ibritumomab tiuxetan has been explored to treat previously untreated follicular lymphoma patients, where it was found to be an effective initial treatment, especially in patients with high tumour burden [127]. Repeated treatment with [ $^{131}\text{I}$ ]I-rituximab has also been investigated, resulting in increased response rate when compared to a single treatment in patients with relapsed or refractory B cell NHL [128]. In addition, treatment given in multiple weekly administration has been explored with [ $^{177}\text{Lu}$ ]Lu-lilotomab satetraxetan in a murine model, where an increase in tolerated administered activity was discovered [129].

If re-treatment or fractionation is to be considered for [ $^{177}\text{Lu}$ ]Lu-lilotomab satetraxetan in the future, imaging dosimetry can be used to calculate and project cumulative absorbed dose, and potentially aid identification and selection of patients that are best suited for re-treatment. The amount of administered activity or dosage level can also be tailored to the individual patient, based on kinetic information from the post-treatment dosimetry of the initial treatment fraction.

### 6.1.4 Red marrow methodology

The lumbar vertebrae L2-L4 were used as the primary site to measure absorbed dose to the RM. The site is commonly found in the literature, possibly because it is often distinguishable in a planar imaging setting. In the patients treated with [ $^{177}\text{Lu}$ ]Lu-lilotomab satetraxetan, a field of view covering the abdominal area was imaged in the majority of the patients, so the site was often available for dosimetry. It is also a region that contains a reasonable amount of red marrow and conveniently in a geometry that is simple and practical to delineate.

The different assumptions on marrow parameters altered the numerical value of the absorbed dose to the RM. In papers II and III a model where the cellularity, i.e. the fraction of red compared to yellow marrow, was assumed to be unity. This was revised in paper IV, where a marrow to marrow S-factor including different cellularity values, with the ICRP-reference value used for the primary

calculation, was calculated. Regardless of the numerical result, both depend on mathematical phantoms with reference values, the activity concentration in the *marrow space* is in principle the only patient dependent input. The model in paper IV, incorporating a more realistic cellularity factor, albeit a reference value, should theoretically be closer to the actual absorbed dose. A confirmation of the numerical value would require a Monte Carlo-calculation where the patient specific cellularity and intra-marrow morphology were included, and even then the marrow would have to be modelled, as a complete measure of the marrow space in the details needed would be infeasible.

A surrogate method, where the absorbed dose calculated from blood drawn from the patients post-therapy was explored in paper II. This methodology did not result in a correlation with toxicity, indicating that this methodology should not be used for dosimetry with [ $^{177}\text{Lu}$ ]Lu-lilotomab satetraxetan. This could also be inferred by the clearly specific uptake in the red marrow shown by visual inspection of the SPECT/CT-images, well after the blood pool had disappeared from the images.

The imaging of the L2-L4 site, the primary method used across the papers resulted in a linear correlation with toxicity, bolstering its usability and supports its future inclusion in red marrow dosimetry calculations.

## 6.2 Biodistribution

Visual inspection of the SPECT/CT and planar images revealed that [ $^{177}\text{Lu}$ ]Lu-lilotomab satetraxetan accumulated in the liver, spleen and red marrow in addition to the tumours (fig. 2, article I). The treatment evacuated quickly from the blood pool, with the heart not being visible on the SPECT-images after four days. The spleen retained a considerable amount of activity for a prolonged time, as seen on both the time activity curves and visually on the SPECT/CT and planar images.

Pre-clinical work has explored [ $^{177}\text{Lu}$ ]Lu-lilotomab satetraxetan both in nude and SCID mice. This work concluded that the most likely organ at risk was the red marrow [130]. This toxicity was believed to be transient as CD37 is not expressed on stem-cells. When compared with free  $^{177}\text{Lu}$ , [ $^{177}\text{Lu}$ ]Lu-lilotomab satetraxetan had a twofold increase in the spleen and liver. For the kidneys, there was half the amount of uptake of [ $^{177}\text{Lu}$ ]Lu-lilotomab satetraxetan as free  $^{177}\text{Lu}$  [131] This coincides with our clinical findings, as uptake was elevated in both the spleen and liver, whereas the uptake in the kidneys was low.

Previous clinical studies of RIT that included internal dosimetry showed that the spleen, liver, kidneys and bone marrow were primary source organs [68][96][97][132][102]. The findings in this work for [ $^{177}\text{Lu}$ ]Lu-lilotomab satetraxetan suggest a similar overall biodistribution when compared to these previous studies.

For both the liver and kidneys, the absorbed doses were far below the levels believed to induce renal or hepatic toxicity and no such adverse events were observed [133].

### 6.2.1 Practical considerations

The initial image protocol described in publication I was imaging intensive, with three planar imaging time points on the same day as treatment with [ $^{177}\text{Lu}$ ]Lu-lilotomab satetraxetan. As this early phase did not in large part contribute to the integral, the imaging protocol was amended to remove these time points. Planar scans were unreliable for smaller organ volumes, organs with considerable lateral overlap or organs with low activity uptake, precluding reliable kinetic evaluation of smaller tumours and the RM. The planar analysis resulted in negative activity values when using background subtraction on the kidneys. Background subtraction was thus removed from the calculation of these organs. As planar images did not contribute to information not also provided by other modalities (i.e. baseline and follow-up FDG-PET/CT and diagnostic CT-examinations) or was contributing to reliable quantification information, these imaging time points were either removed entirely or substituted for a SPECT/CT-scan. In paper II, the whole body kinetic, used to include contribution to the red marrow absorbed dose, was measured with the planar images. This was later measured with a whole body probe, further removing the need for whole body planar imaging. The conclusion of these experiences is that imaging can be done with fewer tomographic scans, preferable and likely more accurate than a larger number of planar scans, in agreement with the results from others and guidelines [105] [77]. The current imaging protocol as of May 2020 consist of four SPECT/CT-acquisitions, on day 0, 1, 4 and 7, allowing kinetic modelling up to and including two exponentials.

Even though the number of scans has been reduced, the amount and duration of the scans still represent a considerable effort for the patient. For each bed-position, the patient will spend approximately 30 minutes on the SPECT/CT-scanner, followed by the CT-scan. This is uncomfortable for the patient, and can and does result in motion artefacts that degrade the image quality. It could be of interest to explore approaches to reduce the scan-time, either by phantom measurements or simulation studies. Future studies with a focus on motion blurring as a deteriorating factor in quantification and how this could be minimized could possibly be performed, for example with a moving phantom.

In this work the MIRD-formalism combined with tomographic imaging was chosen to calculate the mean absorbed doses. A less simplified alternative to this approach is to use the imaging data directly in a Monte Carlo-simulation, solving the radiation transport in the specific patient geometry and calculate the distribution of the dose in sub-organ level. However, the resolution of the current SPECT/CT imaging system used, although considered state of the art, is insufficient to provide a reasonable input to such a radiation transport code [134].

### 6.3 Pre-dosing finding

Patients from four treatment arms were included in this work, each arm with unique pre-treatment and pre-dosing. Two arms included pre-dosing with unla-

belled lilotomab (arm 1 and 4), one included pre-dosing with rituximab (arm 3) and one included no pre-dosing (arm 2). In most of the analyses, the two arms without pre-dosing with unlabelled lilotomab were combined.

The rationale behind pre-dosing in RIT is to alter the biodistribution to one that favors uptake in target organs, and minimizing uptake in normal organs. Pre-dosing is a part of the standard treatment protocol of [ $^{90}\text{Y}$ ]Y-ibritumomab tiuxetan and was for [ $^{131}\text{I}$ ]I-tositumomab.

In papers II and III, a change in biodistribution with respect to the red marrow absorbed dose and spleen dose was identified. In paper II, a statistically significant difference between arm 1 and arm 2, showing a reduced absorbed dose to the red marrow was found. In paper III, two additional arms were included and patients in the arm including pre-dosing with lilotomab received a significantly lower dose than those that did not.

In early studies of [ $^{131}\text{I}$ ]I-tositumomab, unlabeled antibody was found to prolong the blood and whole body clearance [135]. This is also the experience with [ $^{177}\text{Lu}$ ]Lu-lilotomab satetrexetan, as shown in the pharmacokinetics analysis in paper II. A further elevated blood retention was found in the arm containing the highest amount of lilotomab pre-dosing in a pharmacokinetic study including all four treatment arms [136].

CD20 and CD37 as a synergistic pair have been explored in a drug-antibody conjugate where rituximab enhances the internalization and cytotoxicity [137]. Furthermore, CD20 and CD37 have been found to form hexamers and this has been exploited to induce complement-dependent cytotoxicity [138]. In arm 3, pre-dosing with rituximab was explored. This could potentially also have a mitigating effect on normal organ uptake, as rituximab may also bind to the Fc  $\gamma$  receptors [139]. However, our results do not indicate that pre-dosing with rituximab has a significant mitigating effect, indicating that the blocking is antibody-specific.

The optimal amount of lilotomab pre-dosing is still to be concluded on. Two treatment arms and dosage regimes, arm 1 with 15 MBq/kg and arm 4 with 20 MBq have been continued into a phase IIb as two randomization options. An arm 5, with 60 mg/m<sup>2</sup> BSA has also been initiated. Although increased pre-dosing likely leads to decreased absorbed dose to the RM, there is a possibility that an unnecessary high amount of pre-dosing blocks binding to the tumour tissue. Both treatment arms with lilotomab pre-dosing resulted in a reduced absorbed dose in the RM, albeit there was not a statistically significant difference in absorbed dose to the red marrow between the two pre-dosing-regimens. Our findings do not indicate a considerable blocking of the tumour tissue, leading to favourable tumour to red marrow absorbed dose ratios with pre-dosing.

The mean ratio between tumour and red marrow absorbed dose was doubled between arm 4 and arm 1, suggesting that the higher dosage level of cold lilotomab is the superior dosing regime. Care should be taken when making conclusions based on this parameter as absorbed dose to tumours showed large variations, both inter- and intra-patiently. This variation did also seem to increase for the arm containing the highest amount of lilotomab-pre-dosing. Also, no correlation has been observed between absorbed dose and response evaluation

on FDG-PET/CT-images on the lesion level [140]. The tumour dosimetry precluded smaller and clustered tumours, particularly in the abdominal area that could not be included without compromising accuracy in the calculation. Differences in radio biological parameters like dose rate and biological half life between red marrow and tumour tissue should ideally be incorporated in the analysis. However, if no patient or lesion-specific radio biological parameters are included, the inter-patient numerical value of the ratio is equal and the result is still applicable to discern between treatment protocols. If a parameter that characterizes the total amount of tumour absorbed dose uptake of the ARC in the patient is used, rather than resorting to using index lesions, the tumour to red marrow absorbed dose ratio would become a more reliable parameter, allowing a firmer conclusion. These considerations are currently being investigated.

The absolute mass of pre-dosing in both lilotomab pre-dosing regimens in this work is modest compared to the amounts given as part of RIT treatment with either  $^{90}\text{Y}$ -ibritumomab tiuxetan or  $^{131}\text{I}$ -tositumomab. The therapy protocols for both of the other two RITs include a factor of approximately 2.5 larger mass of cold antibody compared to arm 2 in the current study, assuming  $1.7\text{ m}^2$  body surface area. When the expression of CD37 compared to CD20 (a relative difference of 2 as found *in vitro*) is factored in, the amounts become comparable [45][130].

The spleen represents a large normal-B-cell antigen sink for both CD37 and CD20-expressing cells. Our results indicate that the absorbed dose to the spleen is dependent on lilotomab pre-dosing, with a lower uptake of  $^{177}\text{Lu}$ -lilotomab satetraxetan being associated with lilotomab pre-dosing. Experience from other RITs is similar to our results, with uptake in the spleen being reduced by pre-dosing [135]. Although irradiation of the spleen could induce hematological toxicity, the absorbed dose to the spleen found for  $^{177}\text{Lu}$ -lilotomab satetraxetan (a maximum of 6.5 Gy) is likely too low [141] [142].

Dosimetry plays an important role in phase I-studies and has been included in clinical studies to evaluate tumour uptake, reveal biodistribution and calculate absorbed dose to normal organs. It remains an open question whether dosimetry also can play a key part in the dose-escalation part of a study, or even before activity level escalation. Interestingly, in the first study published on RIT with  $^{131}\text{I}$ -tositumomab, the dose-escalation was given in increments of whole body absorbed dose, rather than amount of activity [135]. In molecular radiotherapy, large variations in individual clinical response have been observed for the same amount of activity, potentially requiring a large number of patients included to reveal statistically sound results [21]. Internal dosimetry can help illuminate these discrepancies more efficiently in escalation studies. In this work, it has been shown that it is possible to differentiate between arms both with imaging based dosimetry and pharmacokinetics. This could potentially allow for earlier selection of optimal pre-treatment and pre-dosing regimens.

As the compiled body of work on internal dosimetry continues to grow, accurate dosimetry can become more widespread and standardized. This could lead to dose escalation based on absorbed dose and not merely on total administered activity or activity dosage level.

## Chapter 7

# Conclusion and future work

### 7.1 Conclusion

In this work, the biodistribution and absorbed dose in patients treated with [ $^{177}\text{Lu}$ ]Lu-lilotomab satetraxetan were investigated with quantitative imaging. The results of this can be summarised in the following three main findings:

The organ at risk as identified by normal organ dosimetry is the RM. This finding is in agreement with clinical observations. When the four treatment arms are compared, the protocols with CD37-specific pre-dosing result in a more favorable biodistribution in the form of a decreased absorbed dose to the red marrow without blocking uptake in the tumours. The last result of this thesis is that absorbed dose to the red marrow is correlated with myelosuppression. This could potentially improve prediction of hematological toxicity.

### 7.2 Future work

There are several interesting directions to continue the work on activity quantification and dosimetry calculations of the [ $^{177}\text{Lu}$ ]Lu-lilotomab satetraxetan patients. A considerable limitation of the calculated absorbed dose to the red marrow is the use of standard CF-factors. It should be possible to include the patient-specific amount of red marrow, either with the use of spectral CT or magnetic resonance imaging.

The absorbed dose can be extended with a calculation of the biologically effective dose. Such calculations would depend on dose rate through time, which can easily be worked out from the time activity-curves presented in this work. The second and less straight-forward dependence is biological parameters like repair capacity and radiosensitivity.

Currently, the long acquisition times and comparatively low amount of imaging photons result in a strain on the patient, ultimately leading to considerable motion artefacts. Interesting work has been conducted to reduce the acquisition times of SPECT/CT-dosimetry protocols using deep learning methods. These methods, which use synthetic intermediate projection data, have been shown to reduce the imaging time with a factor of four, with similar quality as images reconstructed with all projections [143]. These results are from a patient material with  $^{177}\text{Lu}$ -DOTATATE and  $^{111}\text{In}$ -octreotide, with in general a higher count rate. It would be interesting to explore these techniques with the image data of the [ $^{177}\text{Lu}$ ]Lu-lilotomab satetraxetan patients.

Conclusions on the optimal amount of pre-dosing are inconclusive. It could be interesting to use the time activity curve data together with relevant parameters, e.g. association and dissociation constants, to develop a so-called

## 7. Conclusion and future work

---

physiologically based pharmacokinetic (PBPK) model of [ $^{177}\text{Lu}$ ]Lu-lilotomab satetraxetan. This has been performed for patients with acute myeloid leukemia, treated with the CD45-targeting antibody YAML568 [144]. This modelling approach could potentially be used to estimate the amount of optimal pre-dosing.



# Bibliography

- [1] Armitage James, O et al. (2017). “Non-Hodgkin lymphoma”. In: *Lancet* 390(10091), pp. 298–310.
- [2] Huet, Sarah, Pierre Sujobert, and Gilles Salles (2018). “From genetics to the clinic: a translational perspective on follicular lymphoma”. In: *Nat Rev Cancer* 18(4), pp. 224–239.
- [3] Rezvani, Andrew R. and David G. Maloney (2011). “Rituximab resistance”. In: *Best Pract Res Clin Haematol* 24(2), pp. 203–216.
- [4] Batlevi, Connie L. et al. (2020). “Follicular lymphoma in the modern era: survival, treatment outcomes, and identification of high-risk subgroups”. In: *Blood Cancer J* 10(7), p. 74.
- [5] Larson, Steven M. et al. (2015). “Radioimmunotherapy of human tumours”. In: *Nat Rev Cancer* 15(6), pp. 347–360.
- [6] Kaminski Mark, S et al. (2001). “Pivotal Study of Iodine I 131 Tositumomab for Low-Grade B-Cell Non-Hodgkin’s Lymphomas”. In: *J Clin Oncol* 19(19), pp. 3918–3928.
- [7] Sutamtewagul, Grek and Brian K. Link (2019). “Novel treatment approaches and future perspectives in follicular lymphoma”. In: *Ther Adv Hematol* 10.
- [8] Witzig, Thomas E. et al. (2002). “Randomized controlled trial of yttrium-90-labeled ibritumomab tiuxetan radioimmunotherapy versus rituximab immunotherapy for patients with relapsed or refractory low-grade, follicular, or transformed B-cell non-Hodgkin’s lymphoma”. In: *J Clin Oncol* 20(10), pp. 2453–2463.
- [9] Kaminski, Mark S et al. (2005). “131I-Tositumomab Therapy as Initial Treatment for Follicular Lymphoma”. In: *N Engl J Med* 352(5), pp. 441–449.
- [10] Kaminski, Mark. S. et al. (2000). “Radioimmunotherapy with iodine 131 I tositumomab for relapsed or refractory B-cell non-Hodgkin lymphoma: Updated results and long-term follow-up of the University of Michigan experience”. In: *Blood* 96(4), pp. 1259–1266.
- [11] Fisher, Richard I. et al. (2005). “Tositumomab and iodine-131 tositumomab produces durable complete remissions in a subset of heavily pretreated patients with low-grade and transformed non-Hodgkin’s lymphomas”. In: *J Clin Oncol* 23(30), pp. 7565–7573.

- [12] Sgouros, George et al. (2020). “Radiopharmaceutical therapy in cancer: clinical advances and challenges”. In: *Nat Rev Drug Discov* 19(9), pp. 589–608.
- [13] Eskian, Mahsa et al. (2016). “Radioimmunotherapy in non-Hodgkin lymphoma: Prediction and assessment of response”. In: *Crit Rev Oncol Hematol* 107, pp. 182–189.
- [14] Thariat, Juliette et al. (2013). “Past, present and future of radiotherapy for the benefit of patients”. In: *Nat Rev Clin Oncol* 10(1), pp. 52–60.
- [15] Merwe, Debbie van der et al. (2017). “Accuracy requirements and uncertainties in radiotherapy: a report of the International Atomic Energy Agency”. In: *Acta Oncol* 56(1), pp. 1–6.
- [16] Giammarile, Francesco et al. (2017). “Dosimetry in clinical radionuclide therapy: the devil is in the detail”. In: *Eur J Nucl Med Mol Imaging* 44(12), pp. 2136–2139.
- [17] Lassmann, Michael and Uta Eberlein (2018). “The Relevance of Dosimetry in Precision Medicine”. In: *J Nucl Med* 59(10), pp. 1494–1499.
- [18] Sjögreen Gleisner, Katarina et al. (2017). “Variations in the practice of molecular radiotherapy and implementation of dosimetry: results from a European survey”. In: *EJNMMI Phys* 4(1).
- [19] Sgouros, George et al. (2004). “Patient-specific dosimetry for <sup>131</sup>I thyroid cancer therapy using <sup>124</sup>I PET and 3-dimensional-internal dosimetry (3D-ID) Software”. In: *J Nucl Med* 45(8), pp. 1366–1372.
- [20] Wierts, Roel et al. (2016). “Dose-response relationship in differentiated thyroid cancer patients undergoing radioiodine treatment assessed by means of <sup>124</sup>I PET/CT”. In: *J Nucl Med* 57(7), pp. 1027–1032.
- [21] Wahl, Richard L. (2003). “The clinical importance of dosimetry in radioimmunotherapy with tositumomab and iodine I 131 tositumomab”. In: *Semin Oncol* 30(2 SUPPL. 4), pp. 31–38.
- [22] Seldin, David W. (2002). “Techniques for using Bexxar for the treatment of non-Hodgkin’s lymphoma”. In: *J Nucl Med Technol* 30(3), pp. 109–114.
- [23] Siegel, Rebecca L, Kimberly D Miller, and Ahmedin Jemal (2018). “Cancer statistics, 2018”. In: *CA Cancer J Clin* 68(1), pp. 7–30.
- [24] Norway, Cancer Registry of (2017). *Cancer incidence, mortality, survival and prevalence in Norway - Cancer in Norway 2017*. Tech. rep.
- [25] Mohammed, Raihan et al. (2019). “How the discovery of rituximab impacted the treatment of B-cell non-Hodgkin’s lymphomas”. In: *J Blood Med* Volume 10, pp. 71–84.
- [26] Koppe, Manuel J. et al. (2005). “Antibody-guided radiation therapy of cancer”. In: *Cancer Metastasis Rev* 24(4), pp. 539–567.

- [27] Teicher, Beverly A. and Ravi V.J. Chari (2011). “Antibody conjugate therapeutics: Challenges and potential”. In: *Clin Cancer Res* 17(20), pp. 6389–6397.
- [28] Böldicke, Thomas (2016). *Protein Targeting Compounds*. Vol. 917. Advances in Experimental Medicine and Biology. Springer International Publishing.
- [29] Kohler, G. and C. Milstein (1975). “Continuous cultures of fused cells secreting antibody of predefined specificity”. In: *Nature* 256(5517), pp. 495–497.
- [30] Steiner, Martina and Dario Neri (2011). “Antibody-radionuclide conjugates for cancer therapy: Historical considerations and new trends”. In: *Clin Cancer Res* 17(20), pp. 6406–6416.
- [31] Chao, Mark P. (2013). “Treatment challenges in the management of relapsed or refractory non-Hodgkin’s lymphoma - Novel and emerging therapies”. In: *Cancer Manag Res* 5(1), pp. 251–269.
- [32] Casan, J. M. L. et al. (2018). “Anti-CD20 monoclonal antibodies: reviewing a revolution”. In: *Hum Vac Immunother* 14(12), pp. 2820–2841.
- [33] “Cluster of differentiation (CD) antigens” (2004). In: *Immunology Guidebook*. Ed. by Julius M Cruse, Robert E Lewis, and Huan Wang. 2007/05/09. Elsevier, pp. 47–124. URL: <https://doi.org/10.1016/B978-012198382-6/50027-3>.
- [34] P Stashenko, L M Nadler, R Hardy and S F Schlossman (1980). “Characterization of a human B lymphocyte-specific antigen”. In: *J Immunol* 125(4), pp. 1678–1685.
- [35] Einfeld, D A et al. (1988). “Molecular cloning of the human B cell CD20 receptor predicts a hydrophobic protein with multiple transmembrane domains”. In: *EMBO J* 7(3), pp. 711–717.
- [36] Salles, Gilles et al. (2017). “Rituximab in B-Cell Hematologic Malignancies: A Review of 20 Years of Clinical Experience”. In: *Adv Ther* 34(10), pp. 2232–2273.
- [37] Barr, Paul M et al. (2018). “R-CHOP, radioimmunotherapy, and maintenance rituximab in untreated follicular lymphoma (SWOG S0801): a single-arm, phase 2, multicentre study”. In: *Lancet Haematol* 5(3), e102–e108.
- [38] Link, M. P. et al. (1986). “A unique antigen on mature B cells defined by a monoclonal antibody”. In: *J Immunol* 137(9), pp. 3013–3018.
- [39] CD37, Gene expression for (n.d.). *Gene expression for CD37*. URL: <https://www.gtexportal.org/home/gene/CD37> (visited on 09/04/2019).

- [40] Spriël, Annemiek B van et al. (2009). “The tetraspanin protein CD37 regulates IgA responses and anti-fungal immunity.” In: *PLoS Pathog* 5(3), e1000338.
- [41] De Winde, Charlotte M. et al. (2016). “Tetraspanin CD37 protects against the development of B cell lymphoma”. In: *J Clin Invest* 126(2), pp. 653–666.
- [42] Scarfò, Irene et al. (2018). “Anti-CD37 chimeric antigen receptor T cells are active against B- and T-cell lymphomas”. In: *Blood* 132(14), pp. 1495–1506.
- [43] Robak, Tadeusz and Pawel Robak (2014). “Anti-CD37 antibodies for chronic lymphocytic leukemia”. In: *Expert Opin Biol Ther* 14(5), pp. 651–661.
- [44] Smeland, E. et al. (1985). “Characterization of Two Murine Monoclonal Antibodies Reactive with Human B Cells: Their Use in a High-Yield, High-Purity Method for Isolation of B Cells and Utilization of Such Cells in an Assay for B-Cell Stimulating Factor”. In: *Scand J Immunol* 21(3), pp. 205–214.
- [45] Dahle, Jostein et al. (2013). “Evaluating antigen targeting and anti-tumor activity of a new anti-cd37 radioimmunoconjugate against non-hodgkin’s lymphoma”. In: *Anticancer Res* 33(1), pp. 85–96.
- [46] Grubbé, Emil H. (1933). “Priority in the Therapeutic Use of X-rays”. In: *Radiology* 21(2), pp. 156–162.
- [47] Magill, Joseph (2005). *Radioactivity · Radionuclides · Radiation*. Springer.
- [48] Brucer, M. (1978). “Nuclear medicine begins with a boa constrictor”. In: *J Nucl Med* 19, pp. 581–598.
- [49] Cherry, Simon R., James A. Sorenson, and Michael E. Phelps (2012). “Radionuclide and Radiopharmaceutical Production”. In: *Physics in Nuclear Medicine*. Elsevier, pp. 43–61.
- [50] Banerjee, Sharmila, Maroor Raghavan Ambikalmajan Pillai, and Natesan Ramamoorthy (2001). “Evolution of Tc-99m in diagnostic radiopharmaceuticals”. In: *Semin Nucl Med* 31(4), pp. 260–277.
- [51] Frangos, Savvas and John R. Buscombe (2019). “Why should we be concerned about a “g”?” In: *Eur J Nucl Med Mol Imaging* 46(2), p. 519.
- [52] DeNardo, Gerald L. (2005). “Concepts in radioimmunotherapy and immunotherapy: Radioimmunotherapy from a Lym-1 perspective”. In: *Semin Oncol*. Vol. 32. SUPPL. 1. W.B. Saunders, pp. 27–35.
- [53] FG Kondev (2019). “Nuclear Data Sheets for A = 177”. In: *Nucl Data Sheets* 159, pp. 1–412.

- [54] Pommé, S. et al. (2011). “Measurement of the  $^{177}\text{Lu}$  half-life”. In: *Appl Radiat Isot* 69(9), pp. 1267–1273.
- [55] Luca, Aurelian et al. (2016). “Experimental determination of some nuclear decay data in the decays of  $^{177}\text{Lu}$ ,  $^{186}\text{Re}$  and  $^{124}\text{I}$ ”. In: *Appl Radiat Isot* 109, pp. 146–150.
- [56] Kellett, M. A. (2016). “ $^{177}\text{Lu}$ : DDEP Evaluation of the decay scheme for an emerging radiopharmaceutical”. In: *Appl Radiat Isot* 109, pp. 129–132.
- [57] Vallabhajosula, Shankar et al. (2016). “Radioimmunotherapy of Metastatic Prostate Cancer with  $^{177}\text{Lu}$ -DOTAhuJ591 Anti Prostate Specific Membrane Antigen Specific Monoclonal Antibody”. In: *Curr Radiopharm* 9(1), pp. 44–53.
- [58] Zaknun, John J. et al. (2013). “The joint IAEA, EANM, and SNMMI practical guidance on peptide receptor radionuclide therapy (PRRNT) in neuroendocrine tumours”. In: *Eur J Nucl Med Mol Imaging* 40(5), pp. 800–816.
- [59] Green, Damian J and Oliver W Press (2017). “Whither Radioimmunotherapy: To Be or Not To Be?” In: *Cancer Res* 77(9), pp. 2191–2196.
- [60] Rizzieri, David (2016). “Zevalin®(ibritumomab tiuxetan): After more than a decade of treatment experience, what have we learned?” In: *Crit Rev Oncol Hematol* 105, pp. 5–17.
- [61] Goldsmith, Stanley J. (2010). “Radioimmunotherapy of Lymphoma: Bexxar and Zevalin”. In: *Semin Nucl Med* 40(2), pp. 122–135.
- [62] Prasad, Vinay (2014). “The Withdrawal of Drugs for Commercial Reasons”. In: *JAMA Intern Med* 174(12), pp. 1887–1888.
- [63] Turner J, Harvey and J Calais Phillipe (2012). “Standard Operating Procedure for Prospective Individualised Dosimetry for  $^{131}\text{I}$ -rituximab Radioimmunotherapy of Non-Hodgkins Lymphoma”. In: *World J Nucl Med* 11(3), p. 110.
- [64] Kameswaran, Mythili et al. (2015). “Synthesis and preclinical evaluation of  $^{177}\text{Lu}$ -CHX-A-DTPA-rituximab as a radioimmunotherapeutic agent for non-hodgkin’s lymphoma”. In: *Cancer Biother Radiopharm* 30(6), pp. 240–246.
- [65] Melhus, Katrine B. et al. (2007). “Evaluation of the binding of radiolabeled rituximab to CD20-positive lymphoma cells: An in vitro feasibility study concerning low-dose-rate radioimmunotherapy with the  $\alpha$ -emitter  $^{227}\text{Th}$ ”. In: *Cancer Biother Radiopharm* 22(4), pp. 469–479.
- [66] Torres-García, Eugenio et al. (2008). “Biokinetics and Dosimetry of  $^{188}\text{Re}$ -anti-CD20 in Patients with Non-Hodgkin’s Lymphoma: Preliminary Experience”. In: *Arch Med Res* 39(1), pp. 100–109.

- [67] Yadav, Madhav P. et al. (2016). “Dosimetric analysis of  $^{177}\text{Lu}$ -DOTA-rituximab in patients with relapsed/refractory non-Hodgkin’s lymphoma”. In: *Nucl Med Commun* 37(7), pp. 735–742.
- [68] Mark S, Kaminski et al. (1992). “Imaging, dosimetry, and radioimmunotherapy with iodine 131-labeled anti- CD37 antibody in B-cell lymphoma”. In: *J Clin Oncol* 10(11), pp. 1696–1711.
- [69] 37-01, Clinical Trial (n.d.). *Clinical Trial 37-01*. <https://clinicaltrials.gov/ct2/show/NCT01796171>. (Visited on 09/05/2019).
- [70] 37-07, Clinical Trial (n.d.). *Clinical Trial 37-07*. <https://clinicaltrials.gov/ct2/show/NCT03806179>. (Visited on 09/05/2019).
- [71] 37-05, Clinical Trial (n.d.). *Clinical Trial 37-05*. <https://clinicaltrials.gov/ct2/show/NCT02658968>. (Visited on 09/05/2019).
- [72] Pichard, Alexandre et al. (2020). “The therapeutic effectiveness of  $^{177}\text{Lu}$ -lilotomab in B-cell non-Hodgkin lymphoma involves modulation of G2/M cell cycle arrest”. In: *Leukemia* 34(5), pp. 1315–1328.
- [73] Ritt, P., J. Sanders, and T. Kuwert (2014). “SPECT/CT technology”. In: *Clin Trans Imaging* 2(6), pp. 445–457.
- [74] Hutton, Brian F. (2014). “The origins of SPECT and SPECT/CT”. In: *Eur J Nucl Med Mol Imaging* 41 (Suppl 1), S3–16.
- [75] Peterson, Todd E and Lars R Furenlid (2011). “SPECT detectors: the Anger Camera and beyond”. In: *Phys Med Biol* 56(17), R145–R182.
- [76] Bailey, Dale L. and Kathy P. Willowson (2014). “Quantitative SPECT/CT: SPECT joins PET as a quantitative imaging modality”. In: *Eur J Nucl Med Mol Imaging* 41(SUPPL. 1).
- [77] Ljungberg, Michael et al. (2016). “MIRD Pamphlet No. 26: Joint EANM/MIRD Guidelines for Quantitative  $^{177}\text{Lu}$  SPECT Applied for Dosimetry of Radiopharmaceutical Therapy.” In: *J Nucl Med* 57(1), pp. 151–62.
- [78] Wevrett, Jill et al. (2018). “Inter-comparison of quantitative imaging of lutetium-177 ( $^{177}\text{Lu}$ ) in European hospitals”. In: *EJNMMI Phys* 5(1), p. 17.
- [79] Bolch, W. E. et al. (2009). “MIRD Pamphlet No. 21: A Generalized Schema for Radiopharmaceutical Dosimetry–Standardization of Nomenclature”. In: *J Nucl Med* 50(3), pp. 477–484.
- [80] Xu, X. George (2014). “An exponential growth of computational phantom research in radiation protection, imaging, and radiotherapy: A review of the fifty-year history”. In: *Phys Med Biol* 59(18), R233–R302.

- 
- [81] Stabin, Michael G, Richard B Sparks, and Eric Crowe (2005). "OLINDA/EXM: the second-generation personal computer software for internal dose assessment in nuclear medicine." In: *J Nucl Med* 46(6), pp. 1023–7.
- [82] Travlos, Gregory S. (2006). "Normal Structure, Function, and Histology of the Bone Marrow". In: *Toxicol Pathol* 34(5), pp. 548–565.
- [83] Beddoe, A. H., P. J. Darley, and F. W. Spiers (1976). "Measurements of trabecular bone structure in man (for radionuclide dosimetry)". In: *Phys Med Biol* 21(4), pp. 589–607.
- [84] Whitwell, J. R. and F. W. Spiers (1976). "Calculated beta-ray dose factors for trabecular bone". In: *Phys Med Biol* 21(1), pp. 16–38.
- [85] Eckerman, K. F. and M. G. Stabin (2000). "Electron absorbed fractions and dose conversion factors for marrow and bone by skeletal regions". In: *Health Phys* 78(2), pp. 199–214.
- [86] Bouchet, Lionel G et al. (2000). "S Values for Radionuclides Localized Within the Skeleton". In: *J Nucl Med* 41(1), pp. 189–212.
- [87] Stabin, M. G. et al. (2002). "Evolution and Status of Bone and Marrow Dose Models". In: *Cancer Biother Radiopharm* 17(4), pp. 427–433.
- [88] Shah, Amish P. et al. (2005a). "A paired-image radiation transport model for skeletal dosimetry". In: *J Nucl Med* 46(2), pp. 344–353.
- [89] Shah, Amish P. et al. (2005b). "Accounting for beta-particle energy loss to cortical via paired-image radiation transport (PIRT)". In: *Med Phys* 32(5), pp. 1354–1366.
- [90] Shah, Amish P. et al. (2003). "Adipocyte spatial distributions in bone marrow: Implications for skeletal dosimetry models". In: *J Nucl Med* 44(5), pp. 774–783.
- [91] Bolch, Wesley E. et al. (2002b). "Considerations of marrow cellularity in 3-dimensional dosimetric models of the trabecular skeleton". In: *J Nucl Med* 43(1), pp. 97–108.
- [92] Bolch, W. E. et al. (2002a). "Considerations of anthropometric, tissue volume, and tissue mass scaling for improved patient specificity of skeletal S values". In: *Med Phys* 29(6), pp. 1054–1070.
- [93] Hough, Matthew et al. (2011). "An image-based skeletal dosimetry model for the ICRP reference adult male - Internal electron sources". In: *Phys Med Biol* 56(8).
- [94] O'Reilly, Shannon E. et al. (2016). "An image-based skeletal dosimetry model for the ICRP reference adult female - Internal electron sources". In: *Phys Med Biol* 61(24).
- [95] Geyer, Amy M. et al. (2017). "Quantitative impact of changes in marrow cellularity, skeletal size, and bone mineral density on active marrow

- dosimetry based upon a reference model”. In: *Med Phys* 44(1), pp. 272–283.
- [96] Fisher, Darrell R., Sui Shen, and Ruby F. Meredith (2009). “MIRD dose estimate report No. 20: Radiation absorbed-dose estimates for  $^{111}\text{In}$ -And  $^{90}\text{Y}$ -ibritumomab Tiuxetan”. In: *J Nucl Med* 50(4), pp. 644–652.
- [97] Vose, Julie M. et al. (2000). “Multicenter Phase II Study of Iodine-131 Tositumomab for Chemotherapy-Relapsed/Refractory Low-Grade and Transformed Low-Grade B-Cell Non-Hodgkin’s Lymphomas”. In: *J Clin Oncol* 18(6), pp. 1316–1323.
- [98] Forrer, Flavio et al. (2013). “Radioimmunotherapy with  $^{177}\text{Lu}$ -DOTA-Rituximab: Final results of a phase i/ii study in 31 patients with relapsing follicular, mantle cell, and other indolent B-Cell lymphomas”. In: *J Nucl Med* 54(7), pp. 1045–1052.
- [99] Press, O. W. et al. (1995). “Phase II trial of  $^{131}\text{I}$ -B1 (anti-CD20) antibody therapy with autologous stem cell transplantation for relapsed B cell lymphomas”. In: *Lancet* 346(8971), pp. 336–340.
- [100] Hohloch, Karin et al. (2011). “Radioimmunotherapy confers long-term survival to lymphoma patients with acceptable toxicity: Registry analysis by the international Radioimmunotherapy Network”. In: *J Nucl Med* 52(9), pp. 1354–1360.
- [101] Baechler, S. et al. (2010). “Predicting Hematologic Toxicity in Patients Undergoing Radioimmunotherapy with  $^{90}\text{Y}$ -Ibritumomab Tiuxetan or  $^{131}\text{I}$ -Tositumomab”. In: *J Nucl Med* 51(12), pp. 1878–1884.
- [102] Wiseman, Gregory A et al. (2000). “Phase I/II  $^{90}\text{Y}$ -Zevalin (yttrium-90 ibritumomab tiuxetan, IDEC-Y2B8) radioimmunotherapy dosimetry results in relapsed or refractory non-Hodgkin’s lymphoma”. In: *Eur J Nucl Med* 27(7), pp. 766–777.
- [103] Wiseman, Gregory A. et al. (2001). “Biodistribution and dosimetry results from a phase III prospectively randomized controlled trial of Zevalin<sup>TM</sup> radioimmunotherapy for low-grade, follicular, or transformed B-cell non-Hodgkin’s lymphoma”. In: *Crit Rev Oncol Hematol* 39(1-2), pp. 181–194.
- [104] Wiseman G, A et al. (2003). “Radiation dosimetry results and safety correlations from  $^{90}\text{Y}$ -ibritumomab tiuxetan radioimmunotherapy for relapsed or refractory non-Hodgkin’s lymphoma: Combined data from 4 clinical trials”. In: *J Nucl Med* 44(3), pp. 465–474.
- [105] Assié, Karine et al. (2008). “Comparison between 2D and 3D dosimetry protocols in  $^{90}\text{Y}$ - ibritumomab tiuxetan radioimmunotherapy of patients with non-Hodgkin’s lymphoma”. In: *Cancer Biother Radiopharm* 23(1), pp. 53–64.



- [106] Kaminski Mark, S et al. (1996). "Iodine-131-anti-B1 radioimmunotherapy for B-cell lymphoma." In: *J Clin Oncol* 14(7), pp. 1974–1981.
- [107] Stillebroer, Alexander B. et al. (2012). "Dosimetric analysis of  $^{177}\text{Lu}$ -cG250 radioimmunotherapy in renal cell carcinoma patients: Correlation with myelotoxicity and pretherapeutic absorbed dose predictions based on  $^{111}\text{In}$ -cG250 imaging". In: *J Nucl Med* 53(1), pp. 82–89.
- [108] Juweid, M E et al. (1999). "Prediction of hematologic toxicity after radioimmunotherapy with  $(^{131}\text{I})$ -labeled anticarcinoembryonic antigen monoclonal antibodies". In: *J Nucl Med* 40(10), pp. 1609–1616.
- [109] Kolstad, Arne et al. (2020). "Phase 1/2a study of  $^{177}\text{Lu}$ -lilotomab satetraxetan in relapsed/refractory indolent non-Hodgkin lymphoma". In: *Blood Adv* 4(17), pp. 4091–4101.
- [110] Stokke, Caroline et al. (2018). "Pre-dosing with lilotomab prior to therapy with  $^{177}\text{Lu}$ -lilotomab satetraxetan significantly increases the ratio of tumor to red marrow absorbed dose in non-Hodgkin lymphoma patients". In: *Eur J Nucl Med Mol Imaging* 45(7), pp. 1233–1241.
- [111] Sgouros, G. (1993). "Bone marrow dosimetry for radioimmunotherapy: theoretical considerations." In: *J Nucl Med* 34(4), pp. 689–94.
- [112] ICRP (2008). "Nuclear Decay Data for Dosimetric Calculations. ICRP Publication 107". In: *Ann. ICRP* 38(3).
- [113] Flinn, Ian W. et al. (2014). "Randomized trial of bendamustine-rituximab or R-CHOP/R-CVP in first-line treatment of indolent NHL or MCL: The BRIGHT study". In: *Blood* 123(19), pp. 2944–2952.
- [114] Mondello, Patrizia et al. (2016). "Bendamustine plus rituximab versus R-CHOP as first-line treatment for patients with indolent non-Hodgkin's lymphoma: evidence from a multicenter, retrospective study". In: *Ann Hematol* 95(7), pp. 1107–1114.
- [115] Eberlein, Uta, Marta Cremonesi, and Michael Lassmann (2017). "Individualized Dosimetry for Theranostics: Necessary, Nice to Have, or Counterproductive?" In: *J Nucl Med* 58(Suppl 2), 97S–103S.
- [116] Cremonesi, Marta et al. (2018). "Correlation of dose with toxicity and tumour response to  $^{90}\text{Y}$ - and  $^{177}\text{Lu}$ -PRRT provides the basis for optimization through individualized treatment planning". In: *Eur J Nucl Med Mol Imaging* 45(13), pp. 2426–2441.
- [117] Lassmann, Michael et al. (2008). "EANM Dosimetry Committee series on standard operational procedures for pre-therapeutic dosimetry I: blood and bone marrow dosimetry in differentiated thyroid cancer therapy". In: *Eur J Nucl Med Mol Imaging* 35(7), pp. 1405–1412.

- [118] Benua R, S et al. (1962). “The relation of radioiodine dosimetry to results and complications in the treatment of metastatic thyroid cancer.” In: *Am J Roentgenol Radium Ther Nucl Med* 87, pp. 171–82.
- [119] Garske-Román, Ulrike et al. (2018). “Prospective observational study of  $^{177}\text{Lu}$ -DOTA-octreotate therapy in 200 patients with advanced metastasized neuroendocrine tumours (NETs): feasibility and impact of a dosimetry-guided study protocol on outcome and toxicity”. In: *Eur J Nucl Med Mol Imaging* 45(6), pp. 970–988.
- [120] Wong, Jeffrey Y.C. et al. (2018). “Total Body Irradiation: Guidelines from the International Lymphoma Radiation Oncology Group (ILROG)”. In: *Int J Radiat Oncol Biol Phys* 101(3), pp. 521–529.
- [121] Dorn, Robert et al. (2003). “Dosimetry-guided radioactive iodine treatment in patients with metastatic differentiated thyroid cancer: largest safe dose using a risk-adapted approach.” In: *J Nucl Med* 44(3), pp. 451–456.
- [122] Kairemo, Kalevi and Kangasma Aki (2013). *4D SPECT/CT Acquisition for 3D Dose Calculation and Dose Planning in  $^{177}\text{Lu}$ -Peptide Receptor Radionuclide Therapy: Applications for Clinical Routine*. Ed. by Richard P. Baum and Frank Rösch. Vol. 194. Recent Results in Cancer Research 1. Berlin, Heidelberg: Springer Berlin Heidelberg, pp. 537–550.
- [123] Baum, Richard P (2014). *Therapeutic Nuclear Medicine*. Springer-Verlag Berlin Heidelberg.
- [124] Huizing, Daphne Merel Valerie et al. (2018). “Dosimetry methods and clinical applications in peptide receptor radionuclide therapy for neuroendocrine tumours: a literature review”. In: *EJNMMI Res* 8(1), p. 89.
- [125] Vaughan, Emily et al. (2018). “Retreatment with peptide receptor radionuclide therapy in patients with progressing neuroendocrine tumours: efficacy and prognostic factors for response”. In: *Br J Radiol* 91(1091), p. 20180041.
- [126] DeNardo, Gerald L. et al. (2002). “Rationales, evidence, and design considerations for fractionated radioimmunotherapy”. In: *Cancer* 94(Suppl 4), pp. 1332–1348.
- [127] Illidge, Tim M. et al. (2014). “Fractionated  $^{90}\text{Y}$ -ibritumomab tiuxetan radioimmunotherapy as an initial therapy of follicular lymphoma: An international phase II study in patients requiring treatment according to GELF/BNLI criteria”. In: *J Clin Oncol* 32(3), pp. 212–218.
- [128] Kang, Hye Jin et al. (2013). “Repeated radioimmunotherapy with  $^{131}\text{I}$ -rituximab for patients with low-grade and aggressive relapsed or refractory B cell non-Hodgkin lymphoma”. In: *Cancer Chemother Pharmacol* 71(4), pp. 945–953.

- [129] Heyerdahl, Helen, Ada H.V. Repetto-Llamazares, and Jostein Dahle (2018). “Administration of Beta-Emitting Anti-CD37 Radioimmunoconjugate Lutetium (177Lu) Lilotomab Satetraxetan as Weekly Multiple Injections Increases Maximum Tolerated Activity in Nude Mice with Non-Hodgkin Lymphoma Xenografts”. In: *J Cancer Biol Ther* 4(1), pp. 181–190.
- [130] Repetto-Llamazares, Ada et al. (2014). “Advantage of lutetium-177 versus radioiodine immunoconjugate in targeted radionuclide therapy of B-cell tumors”. In: *Anticancer Res* 34(7), pp. 3263–3269.
- [131] Repetto-Llamazares, Ada et al. (2013). “Biodistribution and Dosimetry of 177Lu-tetulumab, a New Radioimmunoconjugate for Treatment of Non-Hodgkin Lymphoma”. In: *Curr Radiopharm* 6(1), pp. 20–27.
- [132] Eary, J. F. et al. (1990). “Imaging and treatment of B-cell lymphoma”. In: *J Nucl Med* 31(8), pp. 1257–1268.
- [133] Sandström, Mattias et al. (2013). “Individualized dosimetry of kidney and bone marrow in patients undergoing 177Lu-DOTA-octreotate treatment”. In: *J Nucl Med* 54(1), pp. 33–41.
- [134] Ljungberg, Michael and Katarina Sjögreen-Gleisner (2011). “The accuracy of absorbed dose estimates in tumours determined by Quantitative SPECT: A Monte Carlo study”. In: *Acta Oncol* 50(6), pp. 981–989.
- [135] Kaminski, Mark S. et al. (1993). “Radioimmunotherapy of B-Cell Lymphoma with [ 131 I]Anti-B1 (Anti-CD20) Antibody”. In: *N Engl J Med* 329(7), pp. 459–465.
- [136] Kolstad, A. et al. (2017). “A Higher Amount of Lilotomab Pre-Dosing Increases the Activity-Adjusted AUC and has a Protective Effect Against Myelosuppression of Lutetium (177Lu)-Lilotomab Satetraxetan in Indolent NHL Patients (abstract)”. In: *Haematologica* 102(S2), pp. 468–469.
- [137] Hicks, Stuart W. et al. (2017). “The Antitumor Activity of IMG529, a CD37-Targeting Antibody-Drug Conjugate, Is Potentiated by Rituximab in Non-Hodgkin Lymphoma Models”. In: *Neoplasia* 19(9), pp. 661–671.
- [138] Oostindie, Simone C. et al. (2019). “CD20 and CD37 antibodies synergize to activate complement by Fc-mediated clustering”. In: *Haematologica* 104(9), pp. 1841–1852.
- [139] Boross, Peter and Jeanette H W Leusen (2012). “Mechanisms of action of CD20 antibodies.” In: *Am J Cancer Res* 2(6), pp. 676–90.
- [140] Løndalen, Ayca et al. (2021). “FDG PET/CT parameters and correlations with tumor-absorbed doses in a phase 1 trial of 177Lu-lilotomab satetraxetan for treatment of relapsed non-Hodgkin lymphoma”. In: *Eur J Nucl Med Mol Imaging* 48 (6), pp. 1902–1914.

## Bibliography

---

- [141] Schultz, M. K. (2013). *Theranostics, Gallium-68, and Other Radionuclides: A Pathway to Personalized Diagnosis and Treatment*. Vol. 54. 4. Springer, pp. 659–660.
- [142] Svensson, Johanna et al. (2016). “Radiation exposure of the spleen during  $^{177}\text{Lu}$ -DOTATATE treatment and its correlation with haematological toxicity and spleen volume”. In: *EJNMMI Phys* 3(1).
- [143] Ryden, Tobias et al. (2021). “ Deep learning generation of synthetic intermediate projections improves  $^{177}\text{Lu}$  SPECT images reconstructed with sparsely acquired projections ”. In: *J Nucl Med* 62(4), pp. 528–535.
- [144] Kletting, Peter et al. (2011). “Optimal preloading in radioimmunotherapy with anti-CD45 antibody”. In: *Med Phys* 38(5), pp. 2572–2578.

# Papers




## **Paper III**







# Pre-dosing with lilotomab prior to therapy with $^{177}\text{Lu}$ -lilotomab satetraxetan significantly increases the ratio of tumor to red marrow absorbed dose in non-Hodgkin lymphoma patients

Caroline Stokke<sup>1,2</sup>  · Johan Blakkisrud<sup>1</sup> · Ayca Løndalen<sup>3</sup> · Jostein Dahle<sup>4</sup> · Anne C. T. Martinsen<sup>1,5</sup> · Harald Holte<sup>6</sup> · Arne Kolstad<sup>6</sup>

Received: 2 October 2017 / Accepted: 24 January 2018 / Published online: 22 February 2018  
© The Author(s) 2018. This article is an open access publication

## Abstract

**Purpose**  $^{177}\text{Lu}$ -lilotomab satetraxetan is a novel anti-CD37 antibody radionuclide conjugate for the treatment of non-Hodgkin lymphoma (NHL). Four arms with different combinations of pre-dosing and pre-treatment have been investigated in a first-in-human phase 1/2a study for relapsed CD37+ indolent NHL. The aim of this work was to determine the tumor and normal tissue absorbed doses for all four arms, and investigate possible variations in the ratios of tumor to organs-at-risk absorbed doses.

**Methods** Two of the phase 1 arms included cold lilotomab pre-dosing (arm 1 and 4; 40 mg fixed and 100 mg/m<sup>2</sup> BSA dosage, respectively) and two did not (arms 2 and 3). All patients were pre-treated with different regimens of rituximab. The patients received either 10, 15, or 20 MBq  $^{177}\text{Lu}$ -lilotomab satetraxetan per kg body weight. Nineteen patients were included for dosimetry, and a total of 47 lesions were included. The absorbed doses were calculated from multiple SPECT/CT-images and normalized by administered activity for each patient. Two-sided Student's *t* tests were used for all statistical analyses.

**Results** Organs with distinct uptake of  $^{177}\text{Lu}$ -lilotomab satetraxetan, in addition to tumors, were red marrow (RM), liver, spleen, and kidneys. The mean RM absorbed doses were 0.94, 1.55, 1.44, and 0.89 mGy/MBq for arms 1–4, respectively. For the patients not pre-dosed with lilotomab (arms 2 and 3 combined) the mean RM absorbed dose was 1.48 mGy/MBq, which was significantly higher than for both arm 1 ( $p = 0.04$ ) and arm 4 ( $p = 0.02$ ). Of the other organs, the highest uptake was found in the spleen, and there was a significantly lower spleen absorbed dose for arm-4 patients than for the patient group without lilotomab pre-dosing (1.13 vs. 3.20 mGy/MBq;  $p < 0.01$ ).

Mean tumor absorbed doses were 2.15, 2.31, 1.33, and 2.67 mGy/MBq for arms 1–4, respectively. After averaging the tumor absorbed dose for each patient, the patient mean tumor absorbed dose to RM absorbed dose ratios were obtained, given mean values of 1.07 for the patient group not pre-dosed with lilotomab, of 2.16 for arm 1, and of 4.62 for arm 4. The ratios were significantly higher in both arms 1 and 4 compared to the group without pre-dosing ( $p = 0.05$  and  $p = 0.02$ ). No statistically significant difference between arms 1 and 4 was found.

**Conclusions** RM is the primary dose-limiting organ for  $^{177}\text{Lu}$ -lilotomab satetraxetan treatment, and pre-dosing with lilotomab has a mitigating effect on RM absorbed dose. Increasing the amount of lilotomab from 40 mg to 100 mg/m<sup>2</sup> was found to slightly decrease the RM absorbed dose and increase the ratio of tumor to RM absorbed dose. Still, both pre-dosing amounts resulted in significantly higher tumor to RM absorbed dose ratios. The findings encourage continued use of pre-dosing with lilotomab.

**Electronic supplementary material** The online version of this article (<https://doi.org/10.1007/s00259-018-3964-9>) contains supplementary material, which is available to authorized users.

✉ Caroline Stokke  
carsto@ous-hf.no

<sup>1</sup> Department of Diagnostic Physics, Division of Radiology and Nuclear Medicine, Oslo University Hospital, Oslo, Norway

<sup>2</sup> Department of Life Sciences and Health, Oslo Metropolitan University, Oslo, Norway

<sup>3</sup> Division of Radiology and Nuclear Medicine, Oslo University Hospital, Oslo, Norway

<sup>4</sup> Nordic Nanovector ASA, Oslo, Norway

<sup>5</sup> The Department of Physics, University of Oslo, Oslo, Norway

<sup>6</sup> Department of Oncology, Radiumhospitalet, Oslo University Hospital, Oslo, Norway

**Keywords** Non-Hodgkin lymphoma · Antibody radionuclide conjugate therapy · Radioimmunotherapy · Molecular radiotherapy · Dosimetry ·  $^{177}\text{Lu}$ -lilotomab satetraxetan

## Introduction

Antibody-radionuclide-conjugates (ARCs) based on CD20 antibodies have been used routinely for the treatment of non-Hodgkin lymphoma (NHL), and two ARCs are currently FDA-approved;  $^{131}\text{I}$ -iodine-tositumomab (Bexxar) and  $^{90}\text{Y}$ -yttrium-ibritumomab tiuxetan (Zevalin) [1].  $^{177}\text{Lu}$ -lilotomab satetraxetan or Betalutin® (Nordic Nanovector ASA, Oslo, Norway) is a novel ARC that targets the internalizing CD37 antigen, which is expressed on normal and malignant B-cells [2, 3]. During B-cell development, the CD37 antigen is found on mature B-cells, but it is absent on plasma cells and normal stem cells [4, 5]. The ARC therapy is currently under investigation in the phase 1/2a LYMRIT-37-01 trial for patients with relapsed CD37+ B-cell NHL. Four different combinations of pre-dosing and pre-treatment have been investigated in the phase 1 study. Two arms with “cold” lilotomab antibody pre-dosing of 40 mg fixed dosage (arm 1) and 100 mg/m<sup>2</sup> body surface area (BSA) dosage (arm 4), and two without (arms 2 and 3). In addition, all patients were pre-treated with different regimens of rituximab, which targets the CD20 antigen, before the  $^{177}\text{Lu}$ -lilotomab satetraxetan injection. Investigating arms 1 and 2, we have previously shown that red bone marrow (RM) is the primary dose-limiting organ for the treatment, and that hematological toxicity was more severe for patients receiving higher RM doses [6]. RM absorbed doses were lower in arm 1 vs. arm 2. Tumor absorbed doses have been previously reported for  $^{177}\text{Lu}$ -lilotomab satetraxetan patients, without revealing any significant differences between the first two arms [7]. Theoretically, the absorbed dose for a given tissue can be increased or decreased by adjusting the amount of radioactivity prescribed to a patient; however, the absorbed doses

for all other tissues will be shifted by the same factor. The ratio of tumor to organs-at-risk absorbed doses is therefore a parameter of vital interest when determining the pre-dosage and pre-treatment regimen that optimizes the biodistribution.

The aim of this work was to use the SPECT/CT data to determine tumor and normal tissue absorbed doses for  $^{177}\text{Lu}$ -lilotomab satetraxetan patients in all four arms of the phase 1 trial. Furthermore, potential variations in biodistribution and ratios of tumor to RM absorbed doses were to be determined.

## Materials and methods

### Patient characteristics

A total of 19 patients with relapsed indolent B-cell non-Hodgkin lymphoma treated at Oslo University Hospital were included in the dosimetry study. Of these 19 patients, subtypes included follicular grades I–II (16 patients), mantle cell (two patients), and marginal zone (one patient). The CD37 status of the patients was histologically confirmed. The phase 1/2a trial was approved by the regional ethical committee and all patients gave written consent. In the phase 1 trial, patients received a fixed amount of  $^{177}\text{Lu}$ -lilotomab satetraxetan radioactivity per total body mass; 10, 15, or 20 MBq/kg (Table 1). Approximately 4–10 mg of radiolabeled antibody is injected in a typical patient (75 kg body mass, 15 MBq/kg), and the mean amount was 8 mg for the patients included here. The specific activity ranged from 94 to 347 MBq/mg (mean, 186 MBq/mg). Individual patient characteristics can be found in Suppl. Table 1. Four treatment arms were investigated (Fig. 1). The infusion of lilotomab took approximately 1 h

**Table 1** Patient characteristics. Median values (minimum to maximum) are indicated for continuous parameters

	Arm 1	Arm 2	Arm 3	Arm 4
10 MBq/kg dosage level ( <i>n</i> )	2	1	1	0
15 MBq/kg dosage level ( <i>n</i> )	3	2	3	1
20 MBq/kg dosage level ( <i>n</i> )	2	0	0	4
Administered activity (MBq)	1435 (747–1982)	1137 (1013–1416)	1077.5 (891–1366)	1434 (1147–2189)
Sex ( <i>n</i> , females)	1	1	3	0
Age (years)	53 (41–70)	71 (69–72)	75 (59–88)	72 (63–74)
Pre-dosage, lilotomab (mg)	40	0	0	199 (169–224)
Included for tumor dosimetry ( <i>n</i> )	6	3	4	4
Included for RM dosimetry ( <i>n</i> )	4	3	4	4
Included for biodistribution ( <i>n</i> )	3	3	3	3

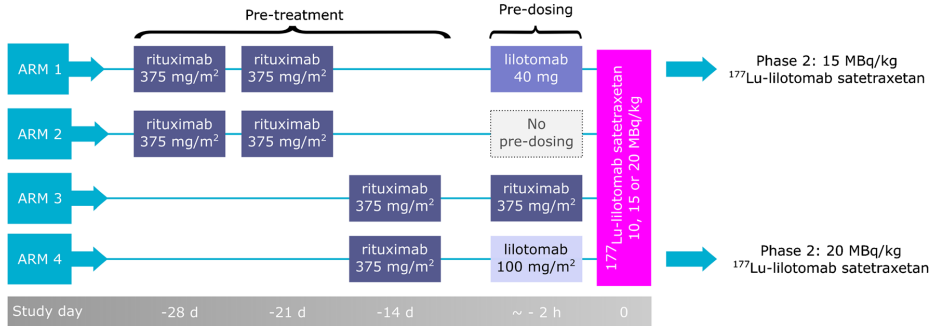


**Fig. 1** Study design of the four arms in the phase 1/2a trial. Different pre-dosing (given approximately 1–3 h before <sup>177</sup>Lu-lilotomab satetraxetan injection) and pre-treatment regimens are shown in parallel. The anti-CD20 antibody rituximab was given to all patients, while only arms 1

and 4 patients received cold lilotomab (anti-CD37 antibody). The zero-hour timepoint of the grey timeline is set according to the administration of <sup>177</sup>Lu-lilotomab satetraxetan. Two of the arms, 1 and 4, are continued in phase 2 as indicated

for the patients, and the indicated lilotomab pre-dosing injection was finished on average 1.7 h (range, 0.9–2.8 h) before <sup>177</sup>Lu-lilotomab satetraxetan injection.

## Image acquisition

In brief, attenuation and scatter-corrected SPECT/CT images were acquired with a Siemens Symbia T16 scanner (Siemens Healthineers, Erlangen, Germany) at 96 and 168 h post injection (p.i.) of <sup>177</sup>Lu-lilotomab satetraxetan. As from arm 2, an additional scan 24 h p.i. was performed. The acquisition covered areas of known lesions, and for at least three patients in each arm, the thorax and abdomen areas were also covered. Planar scintigraphy scans were acquired approximately 2, 24, 96, and 168 h p.i. The acquisition parameters and the methodological considerations have been described previously [8].

## Dosimetry

All patients with available imaging data were included for dosimetry. Absorbed doses to the tumors were calculated from SPECT/CT-images as described previously [7]. In brief, radioactivity in the lesions was obtained from the SPECT images at 96 and 168 h p.i. and time integrated activity coefficients were calculated using mono-exponential curve fitting. The SPECT/CT images obtained at 24 h p.i. were used to calculate time-activity curves from three time points for the lesions, however, to avoid systematic deviations, these results were only used for internal comparisons and not reported (as arm 1 patients were not imaged by SPECT/CT at 24 h p.i.). The volumes were found from the CT images, and a distinct mass of minimum 1.5 ml volume was set as required for dosimetry to be performed. Patient mean tumor doses were found by averaging all available tumor absorbed doses for each patient.

RM absorbed dose was calculated with a SPECT/CT imaging-based approach using the activity in lumbar vertebrae

2–4 [6]. An imaging based method is here needed, as the assumption of equal radioactivity concentrations in blood samples and RM will underestimate the absorbed dose because of specific RM binding of the ARC [6, 9]. For two patients, one of the lumbar vertebrae was not covered. Homogenous uptake and equal mass of the three vertebrae were assumed and both activity and mass were multiplied with a correction factor of 1.5 for these two patients. Patients that had received prior external beam radiation therapy to the lumbar vertebrae were excluded.

Normal tissue absorbed doses for the remaining organs were calculated as previously described, defining spleen, liver, and kidneys as source organs [8]. The activities in these organs at different time points were primarily SPECT-derived. For time points where only planar imaging had been performed, the planar-derived organ counts were adjusted according to the ratio between the planar counts and SPECT activity values day 4. Individual masses were obtained from the CT images. For all other organs, the absorbed doses were calculated using OLINDA/EXM (version 1.1, Vanderbilt University, Nashville, TN, USA).

## Statistics

The patient mean tumor absorbed dose derived for each patient was divided by the RM self-dose for the patient to yield the tumor to RM ratio. Normal tissue absorbed doses, tumor absorbed dose, and the tumor to RM ratio were compared using a two-sided Student's *t* test with a significance level of 0.05. In addition to the separate calculations, arms 2 and 3 were also combined and compared to arm 1 and 4 individually. The values for the combined group are hence obtained by averaging all absorbed dose values in the two arms (not by computing the mean value of the two arms' mean values). The Shapiro–Wilks test and visual inspection of the quantile-quantile-plots showed

that none of the data sets deviated substantially from a normal distribution. Thus, the parametric *t* test was used. The box plots show median values, interquartile ranges, the range of data indicated by whiskers, where points lower or higher than 1.5 times the lower or upper quartile displayed as outliers. All statistical calculations were conducted using Python version 2.7 (Python Software Foundation) with the SciPy (version 0.18) statistics library.

## Results

For  $^{177}\text{Lu}$ -lilotomab satetrexetan patients, the uptake was visually assessed to be most prominent in tumors, spleen, liver, and red marrow (Fig. 2). Also, radioactivity was seen in the blood (including heart cavities) at early time points.

**Tumor absorbed doses on a lesion level** Seventeen of the 19 patients had one or more tumors eligible for dosimetry, and the number of lesions included per patient ranged from 1 to 5 (mode 3). A total of 47 tumor lesions were investigated, and tumor absorbed doses ranged from 33 to 859 cGy. For arms 1–4 the mean tumor absorbed doses per administered activity were 2.15, 2.31, 1.33, and 2.67 mGy/MBq, respectively. Combining arms 2 and 3, the mean tumor absorbed dose per administered activity for patients not pre-dosed with lilotomab was 1.79 mGy/MBq. No significant differences between tumor absorbed doses in this group and the individual arms with lilotomab pre-dosing (arm 1 and 4) were found. However, large variations in tumor absorbed dose were observed (Fig. 3a), and there were also found intra-patient variations

with a range of up to 710 cGy (patient 019, arm 4) (Suppl. Table 1).

**Tumor absorbed doses on the patient level** Patient mean tumor absorbed doses per administered activity for each patient were calculated, and mean values for each arm were found to be 2.08, 2.10, 0.83, and 2.46 mGy/MBq for arms 1–4, respectively. Combining arms 2 and 3, the average patient mean tumor absorbed dose per administered activity was 1.37 mGy/MBq for the patient group not pre-dosed with lilotomab. Note that these values will differ slightly from the overall mean value per arm or group (given in the previous paragraph) since the absorbed doses are here averaged per patient before the mean is obtained. There was a slightly higher patient mean tumor absorbed dose in arm 4 patients compared to the non-pre-dosed group, but the difference was not significant ( $p = 0.13$ ).

**RM absorbed doses** Fifteen patients were included for RM dosimetry, as two of the patients had received prior external beam radiation therapy to the lumbar vertebrae and two of the patients lacked imaging data of the area. The RM absorbed doses ranged from 69 to 204 cGy. Mean RM absorbed doses for the different arms were 0.94, 1.55, 1.44, and 0.89 mGy/MBq for arms 1–4, respectively. Mean absorbed dose for the arms that were not pre-dosed with lilotomab was 1.48 mGy/MBq. There was a significantly higher RM absorbed dose in this non-pre-dosed group compared to arm 1 ( $p = 0.04$ ) and arm 4 ( $p = 0.02$ ) (Fig. 3b).

**Absorbed doses for the rest of normal tissues** The mean spleen absorbed doses were 2.81, 3.12, 3.27, and 1.13 mGy/MBq for arms 1–4, respectively. Combining

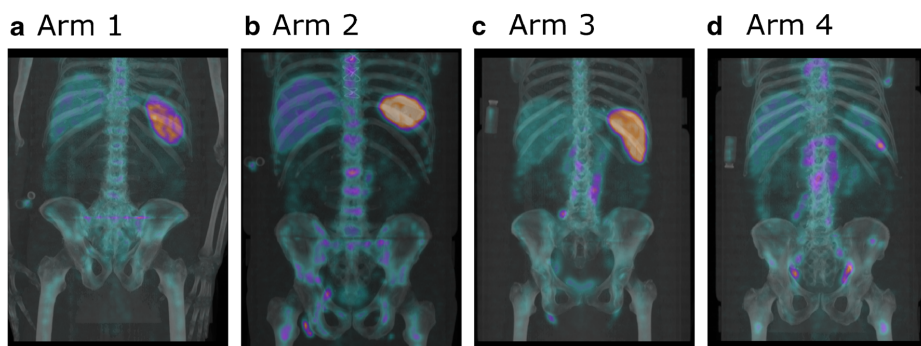


**Fig. 2** Fused SPECT/CT maximum intensity projection images at 96 h after injection of  $^{177}\text{Lu}$ -lilotomab satetrexetan. **a–d** Patients 009 (arm 1; 40 mg lilotomab), 013 (arm 2; no lilotomab), 017 (arm 3; no lilotomab), and 019 (arm 4; 100 mg lilotomab per  $\text{m}^2$  BSA) are shown. After 96 h, most of the ARC has been washed out of the blood, and  $^{177}\text{Lu}$ -lilotomab satetrexetan uptake is observed in tumors, liver, spleen, and bone marrow.

A shift in uptake for the spleen can be observed when an increased amount of pre-dosing with lilotomab is given. Abdominal and inguinal lesions are visible, and the arm 4 patient also had a focal lesion in the spleen. All four patients had received 15 MBq/kg body weight of  $^{177}\text{Lu}$ -lilotomab satetrexetan, and the same intensity scale is used for all images

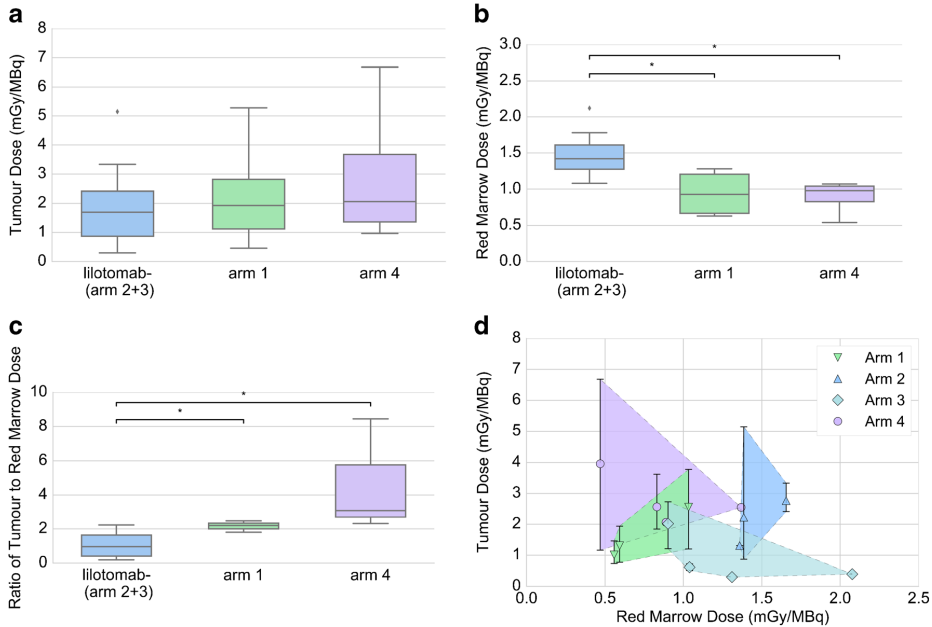


**Fig. 3** **a** The upper left boxplot displays tumor absorbed doses when different amounts of lilotomab are given as pre-dosing before <sup>177</sup>Lu-lilotomab satetraxetan treatment. The three groups are obtained from patients that did not receive lilotomab (arms 2 and 3), patients that received 40 mg lilotomab (arm 1), and patients that received 100 mg lilotomab per m<sup>2</sup> BSA (arm 4). The tumor absorbed doses are normalized by the amount of radioactivity given each patient. For all box plots, significant differences are annotated by asterisks. **b** Similar measures of the RM absorbed doses are also shown for the groups. Both arms 1 and 4 patients had received a significant lower RM absorbed dose than patients not pre-dosed with lilotomab. **c** The boxplot illustrates the ratios between patient mean tumor absorbed doses to RM absorbed doses. Here, the mean tumor absorbed dose is

calculated for each patient before the patient ratios are obtained. Suppl. Fig. 1 displays the same box plots (a–c) separated for each of the four arms, as the rituximab timing differed between arms 2 and 3. **d** To illustrate the correlations between tumor and RM absorbed doses, the values are plotted against each other. The color coding separates the four arms. Each patient is represented by a symbol, and the patient mean tumor absorbed dose values are used (as in c). However, to show the variation in tumor absorbed doses, the intra-patient ranges are also displayed by a line interval between the maximum and minimum tumor absorbed doses for each patient. Some patients had only one lesion eligible for dosimetry, and therefore lack range indicators in panel **d**. The shaded areas are drawn using the extreme values from each arm

arm 2 and 3, the mean dose was 3.20 mGy/MBq for the group not pre-dosed with lilotomab. There was a significantly lower spleen dose in arm 4 patients compared to this group. No significant differences in absorbed doses between each arm were found for the rest of the normal tissues (Table 2). Individual masses, time-integrated activity coefficients, and absorbed doses for all patients can found in supplementary Table 1.

**Ratios between tumor and RM absorbed dose** The tumor to RM absorbed dose ratios were calculated using the patient mean tumor absorbed doses, and the mean ratios were 1.07, 2.16, and 4.62 for patients not pre-dosed with lilotomab, arm 1, and arm 4, respectively (Fig. 3c). There was a significantly higher tumor to RM absorbed dose in both arm 1 ( $p=0.05$ ) and arm 4 ( $p=0.02$ ) compared to the non-pre-dosed group. The ratios calculated separately for arms 2 and 3 gave values of 1.41 and 0.81 (Suppl. Fig. 1).

**Discussion**

In this study, we have investigated normal tissue and tumor absorbed doses for <sup>177</sup>Lu-lilotomab satetraxetan therapy following four different pre-treatment and pre-dosing regimens. For all four arms, RM was found the primary dose-limiting organ, and both pre-dosing amounts with lilotomab investigated had a mitigating effect on RM absorbed dose. Increasing the amount of lilotomab did reduce the RM and spleen absorbed doses, however, the decrease was not significant. The ratio of tumor to RM absorbed dose was found to significantly increase for both the patient group given 40 mg of lilotomab and the group given 100 mg/m<sup>2</sup> of lilotomab compared to patients not pre-dosed with lilotomab.

In our previous work, we have shown that the RM absorbed dose decreased when 40 mg of lilotomab was given as pre-dosing before <sup>177</sup>Lu-lilotomab satetraxetan therapy [6]. In the current study, the approximately fivefold increase in the

**Table 2** Absorbed doses to all organs for the different pre-dosing and pre-treatment regimens

	Arm 1 Mean (range) mGy/MBq	Arm 2 Mean (range) mGy/MBq	Arm 3 Mean (range) mGy/MBq	Arm 4 Mean (range) mGy/MBq
Adrenals	0.12 (0.10–0.14)	0.10 (0.07–0.12)	0.11 (0.07–0.17)	0.12 (0.11–0.13)
Brain	0.10 (0.08–0.13)	0.08 (0.05–0.10)	0.09 (0.05–0.15)	0.10 (0.10–0.11)
Breasts	0.10 (0.08–0.12)	0.08 (0.05–0.10)	0.09 (0.05–0.15)	0.10 (0.09–0.11)
Gallbladder wall	0.12 (0.10–0.14)	0.10 (0.07–0.12)	0.11 (0.07–0.17)	0.12 (0.12–0.14)
LLI wall	0.11 (0.09–0.13)	0.09 (0.06–0.11)	0.09 (0.06–0.16)	0.11 (0.10–0.12)
Small intestine	0.11 (0.09–0.13)	0.09 (0.06–0.11)	0.10 (0.06–0.16)	0.11 (0.10–0.12)
Stomach wall	0.11 (0.09–0.13)	0.09 (0.06–0.11)	0.10 (0.07–0.16)	0.11 (0.10–0.12)
ULI wall	0.11 (0.09–0.14)	0.09 (0.06–0.11)	0.10 (0.06–0.16)	0.11 (0.10–0.12)
Heart wall	0.11 (0.09–0.13)	0.09 (0.06–0.11)	0.10 (0.06–0.16)	0.11 (0.10–0.12)
Kidneys	0.46 (0.28–0.79)	0.25 (0.16–0.30)	0.38 (0.30–0.47)	0.49 (0.34–0.71)
Liver	0.97 (0.74–1.15)	0.95 (0.78–1.05)	1.02 (0.70–1.43)	0.96 (0.69–1.30)
Lungs	0.11 (0.09–0.13)	0.09 (0.06–0.11)	0.09 (0.06–0.16)	0.11 (0.10–0.12)
Muscle	0.10 (0.08–0.13)	0.08 (0.06–0.10)	0.09 (0.06–0.15)	0.10 (0.10–0.11)
Ovaries	0.11 (0.09–0.13)	0.09 (0.06–0.11)	0.09 (0.06–0.16)	0.11 (0.10–0.12)
Pancreas	0.12 (0.1–0.14)	0.10 (0.07–0.12)	0.11 (0.08–0.18)	0.12 (0.11–0.14)
Red marrow	0.94 (0.63–1.28)	1.55 (1.42–1.78)	1.44 (1.08–2.12)	0.89 (0.54–1.07)
Osteogenic cells	0.50 (0.31–0.70)	0.87 (0.73–1.03)	0.80 (0.63–0.91)	0.56 (0.30–0.74)
Skin	0.10 (0.08–0.12)	0.08 (0.05–0.09)	0.08 (0.05–0.14)	0.10 (0.09–0.11)
Spleen	2.81 (1.54–3.60)	3.12 (2.73–3.45)	3.27 (2.65–4.01)	1.13 (0.78–1.43)
Testes	0.10 (0.08–0.13)	0.08 (0.05–0.10)	NA	0.10 (0.10–0.11)
Thymus	0.11 (0.09–0.13)	0.08 (0.06–0.10)	0.09 (0.06–0.15)	0.10 (0.10–0.11)
Thyroid	0.10 (0.08–0.13)	0.08 (0.05–0.10)	0.09 (0.05–0.15)	0.10 (0.10–0.11)
Urinary bladder wall	0.11 (0.09–0.13)	0.08 (0.06–0.10)	0.09 (0.06–0.15)	0.10 (0.10–0.11)
Uterus	0.11 (0.09–0.13)	0.09 (0.06–0.11)	0.09 (0.06–0.16)	0.11 (0.10–0.12)
Total body	0.14 (0.12–0.17)	0.13 (0.11–0.15)	0.14 (0.08–0.20)	0.15 (0.11–0.19)

amount of lilotomab that was given to patients in arm 4 was found to cause a further minor decrease in RM absorbed dose. Only four patients were included from each of the two arms and a larger number of patients is required for statistical verification of this trend. Still, a lower RM absorbed dose is also supported by that a higher radioactivity level could be given to patients in arm 4 (Fig. 1). There is a concern that pre-dosing with cold antibody could block the CD37 antigen on tumor tissues as well, but on a lesion level there was no significant difference in the tumor absorbed dose for arm 1, arm 4, and not pre-dosed patients. However, the overall variation in tumor absorbed doses was highest in arm 4, so we cannot exclude that uptake was influenced by the lilotomab pre-dosing for some lesions (Fig. 3a).

The amount of unlabeled antibody that produced the highest ratio of tumor to whole-body absorbed dose was investigated for individual patients in the first  $^{131}\text{I}$ -tositumomab trials [10]. In the current work, we calculated the ratio of tumor to RM absorbed dose to compare all  $^{177}\text{Lu}$ -lilotomab satetraxetan therapy regimens. The ratio doubled for patients receiving 40 mg lilotomab and doubled again for the patients given 100 mg/m<sup>2</sup> BSA of lilotomab, indicating that the higher

pre-dosing level can optimize the therapeutic effect. It should, however, be noted that the ratio parameter considers the mean tumor absorbed dose across all lesions per patient, and large intra-patient variations in tumor absorbed dose can possibly be obscured. The variation is visualized in Fig. 3d. The limited number of patients in each group with more than two tumors eligible for dosimetry does not allow for statistical comparisons, but for arm 4 the intra-patient tumor absorbed doses variation appears somewhat larger, and the largest intra-patient range (710 cGy) was found in this arm (Suppl. Table 1). Here, we aimed to perform an overall assessment of the different groups rather than effect prediction for individual patients. For such prediction studies, a more suiting parameter could perhaps be the ratio of the patient *minimum* tumor absorbed dose to RM absorbed dose. However, the same trend is shown using this parameter; increasing values for non-pre-dosed patients, arm 1, and arm 4 (data not shown). A larger uncertainty will possibly be introduced by such a parameter, since not all lesions are eligible for dosimetry.

There were some differences in absorbed dose for other normal tissues, but the only significant difference was for the spleen. This absorbed dose was significantly lower for

arm 4 patients than for patients not pre-dosed with lilotomab (Table 2). All organs received absorbed doses within commonly assumed tolerance levels, e.g., the highest spleen absorbed dose across all patients was 6.5 Gy (patient 005), which is lower than the absorbed doses observed to have an effect for other lutetium-177-based treatments [11, 12]. Accordingly, no signs of non-hematological toxicities were observed for the included patients. For the calculation of ratios between tumors and organs-at-risk, we therefore focused on RM as the most important normal tissue.

Pre-dosing with unlabelled antibody as a means of improving biodistribution has been demonstrated effective for ARCs targeting CD20. Treatment with  $^{131}\text{I}$ -tositumomab was described to be preceded by 450 mg cold tositumomab [13] and  $^{90}\text{Y}$ -ibritumomab tiuxetan treatment uses 250 mg/m<sup>2</sup> BSA cold anti-CD20 rituximab as pre-dosing [14]. The theory is that unlabeled antibody will bind the circulating non-malignant B cells expressing target antigens. Administration of pre-dosing therefore prevents rapid ARC sequestration in the spleen and will, as a result, prolong the ARCs' plasma half-life [15]. Reduction of ARC uptake in the spleen is clearly visible, for example  $^{131}\text{I}$ -tositumomab [13], and while the spleen uptake even without lilotomab pre-dosing was lower for  $^{177}\text{Lu}$ -lilotomab satetraxetan, a corresponding reduction can also be observed for this treatment (Fig. 2). We have found that the cumulative activity in blood was higher, and the clearance was lower, for arm 1 patients than for arm 2 patients [6]. The higher amounts of lilotomab given patients in arm 4 increased the cumulative radioactivity in blood even further [16]. This may also explain the somewhat higher mean tumor absorbed dose in arm 4; if the concentration in the blood increases, this may lead to overcoming the binding site barrier and increase diffusion into the tumor [17]. The observed changes in biodistribution may indicate that the same mechanics are applicable for pre-dosing with lilotomab before  $^{177}\text{Lu}$ -lilotomab satetraxetan treatment as for previous ARC pre-dosing regimens. For the patients enrolled so far, the maximum amount of lilotomab pre-dosing has been 224 mg (Table 1). This is lower than the pre-dosing amounts given for  $^{131}\text{I}$ -tositumomab or  $^{90}\text{Y}$ -ibritumomab tiuxetan, but can be considered in relative agreement with that the antigen expression of CD37 has been measured approximately half of the CD20 expression in vitro [5, 18]. It is uncertain whether lilotomab pre-dosing levels above 100 mg/m<sup>2</sup> BSA could prove beneficial. While the increased tumor to RM ratios encourage such investigations, the larger absorbed dose variation for lesions may advise against a continued escalation of pre-dosing amounts. In studies of an iodine-131 labeled anti-CD37 antibody, MB-1, three different protein amounts were investigated, 0.5, 2.5, and 10 mg/kg, which corresponds to

35, 175, and 700 mg for a 70 kg patient [19, 20]. The highest amount yielded the most favorable biodistribution in the majority of patients. Interestingly, the cold antibody was given simultaneously as the ARC (not as pre-dosing), and one should then believe that both cold and radiolabeled antibodies would bind non-malignant B cells and tumors with the same relative effect. This difference in administration does make direct comparisons with the  $^{177}\text{Lu}$ -lilotomab satetraxetan pre-dosing regimens challenging. However, this calls for a closer investigation of the amount of radiolabeled antibody given. For arm 1, the amount of  $^{177}\text{Lu}$ -lilotomab satetraxetan was relatively invariable, and for arm 4 the amount was less than 5% of the amount given as cold lilotomab pre-dosing. A clear deviation was found for one of the patients that did not receive lilotomab pre-dosing, as this patient was given approximately twice the amount of radiolabeled antibody compared to the rest (patient 18, 16.4 mg, supplementary Table 1). While we cannot rule out that variable amounts of radiolabeled antibody will impact the biodistribution, the RM and tumor absorbed doses for patient 18 were within the range of the other arm 3 patients. The absolute amounts of radiolabeled CD37 antibody given are probably too low for any measurable effects of possible differences.

Two arms excluding lilotomab as pre-dosing have been investigated. In the present work, the absorbed doses have been reported separately for these two arms, since the rituximab timing varied between the arms. However, no large differences were observed (Table 2), and the data were combined for some of the analyses and discussion. Pre-dosing with the anti-CD20 targeting rituximab on the same day as  $^{177}\text{Lu}$ -lilotomab satetraxetan was investigated in arm 3 because rituximab will also bind Fcγ receptors [21], and although lilotomab is a mouse antibody, it also binds to subtypes of human Fcγ receptors. Our results show that the rituximab pre-dosing will not introduce the same protective effect for RM as pre-dosing with the same anti-CD37 antibody as is part of the ARC, indicating that the blocking mechanics discussed above are antibody-specific. This is in accordance with that rituximab has been found to block radiolabeled anti-CD20 antibodies, but not radiolabeled anti-CD45 antibodies [22].

In general, biodistribution and dosimetry studies allow for the determination of uptake in organs-at-risk and tumors, and hence the selection of an optimal pre-treatment and pre-dosing regimen. It is an open question as to whether this process should be conducted before activity level escalation (often called dose-escalation) is performed. This could minimize the number of patients in arms that are later judged less effective. While the correlation of RM absorbed dose and hematological toxicity has been demonstrated for the current phase 1/2a trial [6], the observed variation in tumor

absorbed dose prevents fully reliable clinical translation, and further studies are needed to investigate tumor absorbed dose vs. patient outcome. If this issue is resolved, a tumor to RM absorbed dose ratio parameter could prove valuable for predictive purposes.

## Conclusions

For all patient arms, RM was found to be the primary dose-limiting organ for  $^{177}\text{Lu}$ -lilotomab satetraxetan therapy, and pre-dosing with lilotomab had a mitigating effect on RM absorbed dose. Increasing the amount of lilotomab was found to reduce the RM absorbed dose, and the ratio of tumor to RM absorbed dose was found to double. Still, based on the dosimetry data, the variation in tumor absorbed doses leaves the question of the optimal amount of lilotomab somewhat inconclusive. Continued investigations of absorbed dose–effect correlations are therefore needed. However, as both pre-dosage levels investigated significantly increased the tumor to RM absorbed dose ratio, it seems mandatory to include pre-dosing with lilotomab in a treatment regimen with  $^{177}\text{Lu}$ -lilotomab satetraxetan.

**Acknowledgements** We thank the personnel at the Nuclear Medicine section at Oslo University Hospital for technical assistance with the acquisitions. Stine Nygaard, study nurse at the Department of Oncology, is also greatly acknowledged.

**Authors' contributions** All authors contributed to design and draft of the manuscript. All authors read and approved the final manuscript.

**Funding** The LYMRIT37-01 study is sponsored by Nordic Nanovector ASA.

## Compliance with ethical standards

**Conflict of interest** Johan Blakkisrud is supported by a grant (2017/041) from the South-Eastern Norway Regional Health Authority. Harald Holte and Arne Kolstad were both in part supported by grants from the Norwegian Cancer Society. Arne Kolstad is member of the Scientific Advisory Board of Nordic Nanovector ASA. Ayca Løndalen was partly financed by a grant from Nordic Nanovector ASA. Jostein Dahle is an employee and shareholder of Nordic Nanovector ASA.

**Ethical approval and informed consent** All procedures performed were in accordance with the ethical standards of the institutional research committee and with the 1964 Helsinki Declaration and its later amendments or comparable ethical standards. Informed consent was obtained from all individual participants included in the study.

**Open Access** This article is distributed under the terms of the Creative Commons Attribution 4.0 International License (<http://creativecommons.org/licenses/by/4.0/>), which permits unrestricted use, distribution, and reproduction in any medium, provided you give appropriate credit to the original author(s) and the source, provide a link to the Creative Commons license, and indicate if changes were made.

## References

- Jacene HA, Filice R, Kasecamp W, Wahl RL. Comparison of 90Y-ibritumomab tiuxetan and 131I-tositumomab in clinical practice. *J Nucl Med.* 2007;48:1767–76. <https://doi.org/10.2967/jnumed.107.043489>.
- Smeland E, Funderud S, Ruud E, Kiil Blomhoff H, Godal T. Characterization of two murine monoclonal antibodies reactive with human B cells. Their use in a high-yield, high-purity method for isolation of B cells and utilization of such cells in an assay for B-cell stimulating factor. *Scand J Immunol.* 1985;21:205–14.
- Press OW, Howell-Clark J, Anderson S, Bernstein I. Retention of B-cell-specific monoclonal antibodies by human lymphoma cells. *Blood.* 1994;83:1390–7.
- Moldenhauer G. Cd37. *J Biol Regul Homeost Agents.* 2000;14:281–3.
- Dahle J, Repetto-Llamazares AH, Mollatt CS, Melhus KB, Bruland OS, Kolstad A, et al. Evaluating antigen targeting and anti-tumor activity of a new anti-CD37 radioimmunconjugate against non-Hodgkin's lymphoma. *Anticancer Res.* 2013;33:85–95.
- Blakkisrud J, Løndalen A, Dahle J, Turner S, Holte H, Kolstad A, et al. Red marrow-absorbed dose for non-Hodgkin lymphoma patients treated with  $^{177}\text{Lu}$ -lilotomab satetraxetan, a novel anti-CD37 antibody-radiionuclide conjugate. *J Nucl Med.* 2017;58:55–61. <https://doi.org/10.2967/jnumed.116.180471>.
- Blakkisrud J, Løndalen A, Martinsen AC, Dahle J, Holtedahl JE, Bach-Gansmo T, et al. Tumor-absorbed dose for non-Hodgkin lymphoma patients treated with the anti-CD37 antibody radiionuclide conjugate  $^{177}\text{Lu}$ -lilotomab satetraxetan. *J Nucl Med.* 2017;58:48–54. <https://doi.org/10.2967/jnumed.116.173922>.
- Blakkisrud J, Holtedahl JE, Løndalen A, Dahle J, Bach-Gansmo T, Holte H, et al. Biodistribution and dosimetry results from a phase I trial of  $^{177}\text{Lu}$ -lilotomab satetraxetan antibody-radiionuclide conjugate therapy. *J Nucl Med.* 2017; <https://doi.org/10.2967/jnumed.117.195347>.
- Sgouros G. Bone marrow dosimetry for radioimmunotherapy: theoretical considerations. *J Nucl Med.* 1993;34:689–94.
- Kaminski MS, Zasadny KR, Francis IR, Milik AW, Ross CW, Moon SD, et al. Radioimmunotherapy of B-cell lymphoma with [131I]anti-B1 (anti-CD20) antibody. *N Engl J Med.* 1993;329:459–65. <https://doi.org/10.1056/NEJM199308123290703>.
- Kulkarni HR, Prasad V, Schuchardt C, Baum RP. Is there a correlation between peptide receptor radiionuclide therapy-associated hematological toxicity and spleen dose? *Recent Results Cancer Res.* 2013;194:561–6. [https://doi.org/10.1007/978-3-642-27994-2\\_33](https://doi.org/10.1007/978-3-642-27994-2_33).
- Svensson J, Hagmarker L, Magnander T, Wangberg B, Bernhardt P. Radiation exposure of the spleen during ( $^{177}\text{Lu}$ -DOTATATE treatment and its correlation with haematological toxicity and spleen volume. *EJNMMI Phys.* 2016;3:15. <https://doi.org/10.1186/s40658-016-0153-4>.
- Wahl RL. Tositumomab and (131I)I therapy in non-Hodgkin's lymphoma. *J Nucl Med.* 2005;46(Suppl 1):128S–40S.
- Wiseman GA, White CA, Stabin M, Dunn WL, Ervin W, Dahlbom M, et al. Phase I/II 90Y-Zevalin (yttrium-90 ibritumomab tiuxetan, IDEC-Y2B8) radioimmunotherapy dosimetry results in relapsed or refractory non-Hodgkin's lymphoma. *Eur J Nucl Med.* 2000;27:766–77.
- Goldsmith SJ. Radioimmunotherapy of lymphoma: Bexxar and Zevalin. *Semin Nucl Med.* 2010;40:122–35. <https://doi.org/10.1053/j.semnuclmed.2009.11.002>.
- Kolstad A, Madsbu U, Stokke C, Blakkisrud J, Løndalen AM, Dahle J, et al. A higher amount of Lilotomab pre-dosing increases the activity-adjusted AUC and has a protective effect against myelosuppression of lutetium ( $^{177}\text{Lu}$ )-lilotomab satetraxetan in indolent NHL patients. *Haematologica.* 2017;102:468–9.





17. Wittrup KD, Thurber GM, Schmidt MM, Rhoden JJ. Practical theoretic guidance for the design of tumor-targeting agents. *Methods Enzymol.* 2012;503:255–68. <https://doi.org/10.1016/B978-0-12-396962-0.00010-0>.
18. Repetto-Llamazares AH, Larsen RH, Patzke S, Fleten KG, Didierlaurent D, Pichard A, et al. Targeted cancer therapy with a novel anti-CD37 Beta-particle emitting radioimmunoconjugate for treatment of non-Hodgkin lymphoma. *PLoS One.* 2015;10:e0128816. <https://doi.org/10.1371/journal.pone.0128816>.
19. Press OW, Eary JF, Badger CC, Martin PJ, Appelbaum FR, Levy R, et al. Treatment of refractory non-Hodgkin's lymphoma with radiolabeled MB-1 (anti-CD37) antibody. *J Clin Oncol.* 1989;7:1027–38. <https://doi.org/10.1200/JCO.1989.7.8.1027>.
20. Press OW, Eary JF, Appelbaum FR, Martin PJ, Badger CC, Nelp WB, et al. Radiolabeled-antibody therapy of B-cell lymphoma with autologous bone marrow support. *N Engl J Med.* 1993;329:1219–24. <https://doi.org/10.1056/NEJM199310213291702>.
21. Boross P, Leusen JH. Mechanisms of action of CD20 antibodies. *Am J Cancer Res.* 2012;2:676–90.
22. Gopal AK, Press OW, Wilbur SM, Maloney DG, Pagel JM. Rituximab blocks binding of radiolabeled anti-CD20 antibodies (Ab) but not radiolabeled anti-CD45 Ab. *Blood.* 2008;112:830–5. <https://doi.org/10.1182/blood-2008-01-132142>.



## Paper IV



## Myelosuppression in patients treated with <sup>177</sup>Lutetium-lilotomab satetraxetan can be predicted with absorbed dose to the red marrow as the only variable

Johan Blakkisrud<sup>a,b</sup> , Ayca Løndalen<sup>a,c</sup>, Jostein Dahle<sup>d</sup>, Anne Catrine Martinsen<sup>a,e\*</sup>, Arne Kolstad<sup>f</sup> and Caroline Stokke<sup>a,b</sup> 

<sup>a</sup>Division of Radiology and Nuclear Medicine, Oslo University Hospital, Oslo, Norway; <sup>b</sup>Department of Physics, University of Oslo, Oslo, Norway; <sup>c</sup>Faculty of Medicine, University of Oslo, Oslo, Norway; <sup>d</sup>Nordic Nanovector ASA, Oslo, Norway; <sup>e</sup>Faculty of Health Sciences, Oslo Metropolitan University, Oslo, Norway; <sup>f</sup>Department of Oncology, Radiumhospitalet, Oslo University Hospital, Oslo, Norway

### ABSTRACT

**Background:** The aim of this study was to investigate dosimetry data and clinical variables to predict hematological toxicity in non-Hodgkin lymphoma (NHL) patients treated with [<sup>177</sup>Lutetium]Lu-lilotomab satetraxetan.

**Material and methods:** A total of 17 patients treated with [<sup>177</sup>Lu]Lu-lilotomab satetraxetan in a first-in-human phase 1/2a study were included. Absorbed dose to the red marrow was explored using SPECT/CT-imaging of the lumbar vertebrae L2–L4 over multiple time points. Percentage reduction of thrombocytes and neutrophils at nadir compared to baseline (PBN) and time to nadir (TTN) were chosen as indicators of myelosuppression and included as dependent variables. Two models were applied in the analysis, a multivariate linear model and a sigmoidal description of toxicity as a function of absorbed dose. A total of 10 independent patient variables were investigated in the multivariate analysis.

**Results:** Absorbed dose to the red marrow ranged from 1 to 4 Gy. Absorbed dose to the red marrow was found to be the only significant variable for PBN for both thrombocytes and neutrophils. The sigmoid function gave similar results in terms of accuracy when compared to the linear model.

**Conclusion:** Myelosuppression in the form of thrombocytopenia and neutropenia in patients treated with [<sup>177</sup>Lu]Lu-lilotomab satetraxetan can be predicted from the SPECT/CT-derived absorbed dose estimate to the red marrow.

### ARTICLE HISTORY

Received 11 February 2021  
Accepted 20 July 2021

### KEYWORDS

Non-Hodgkin lymphoma;  
internal dosimetry;  
radioimmunotherapy;  
myelosuppression



## Introduction

Radioimmunotherapy (RIT) is a treatment modality where an antibody guides a radioactive nuclide to the tumor cells, delivering a tumoricidal amount of localized radiation [1,2]. The treatment has proven itself a promising part of the cancer therapy armamentarium in the treatment of the radiosensitive NHL [3,4].


Two RIT agents have been granted approval by the U.S. Food and Drug Administration for treatment of refractory or relapsed low-grade, follicular, or transformed B-cell NHL: [<sup>131</sup>Iodine]I-tositumomab (Bexxar<sup>®</sup>) and [<sup>90</sup>Yttrium]Y-ibritumomab tiuxetan (Zevalin<sup>®</sup>) [5]. Both RITs target B-cell NHL by binding to epitopes on the CD20 antigen. The RIT agents carry two different radionuclides, <sup>131</sup>I and <sup>90</sup>Y. <sup>90</sup>Y is a pure β-emitter that deposits 90% of its energy in a sphere with a radius of 5.2 mm while <sup>131</sup>I is a β emitter with shorter penetration (a sphere of 1.0 mm radius) and also emits γ-radiation suitable for medical imaging [6]. Both treatments can also

induce cytotoxic events by binding the antibody itself, besides the treatment mechanism provided by the localized radiation from the beta-emitting nuclides [5].

[<sup>177</sup>Lutetium]Lu-lilotomab satetraxetan (Betalutin<sup>®</sup>) is a RIT targeting the CD37-antigen [7]. CD37 is expressed on mature B-cells and the majority of B-cell NHL, and previous studies of CD37-targeting treatments have shown promising results in both clinical and preclinical studies [8–13]. Targeting CD37 may be an especially promising alternative for relapsed indolent NHL patients, as previous treatment with anti-CD20 drugs can lead to resistance against further anti-CD20 treatment [14]. This RIT is currently being investigated in three trials, including the multi-center, non-randomized, open-label, first in human phase 1/2a-study LYMRIT-37-01 (NCT01796171). The radionuclide carried by [<sup>177</sup>Lu]Lu-lilotomab satetraxetan is <sup>177</sup>Lu. This radionuclide is, similarly to <sup>131</sup>I and <sup>90</sup>Y, also a β-emitter that deposits 90% of its radiation energy in a sphere with a radius of 0.6 mm. It also has γ-emission suitable for medical imaging. These imaging

**CONTACT** Johan Blakkisrud  [johbla@ous-hf.no](mailto:johbla@ous-hf.no)  Division of Radiology and Nuclear Medicine, Oslo University Hospital, P.O. Box 4959, Gaustad sykehus bygg 20, Nydalen, Oslo 0424, Norway

\*Present address: Sunnaas Rehabilitation Hospital, Oslo, Norway.

 Supplemental data for this article can be accessed [here](#).

© 2021 The Author(s). Published by Informa UK Limited, trading as Taylor & Francis Group. This is an Open Access article distributed under the terms of the Creative Commons Attribution-NonCommercial-NoDerivatives License (<http://creativecommons.org/licenses/by-nc-nd/4.0/>), which permits non-commercial re-use, distribution, and reproduction in any medium, provided the original work is properly cited, and is not altered, transformed, or built upon in any way.

capabilities of  $^{177}\text{Lu}$  allow in-depth studies of biodistribution and consequently the absorbed dose to different tissues in each patient post-treatment.

Myelosuppression has been established as the primary dose-limiting toxicity in other RIT treatments [15–17]. Early studies indicated that this toxicity was not dependent on the amount of administered radioactivity, precluding prediction based on administered radioactivity alone [18]. This variation could possibly be explained by two factors. One is patient-specific biodistribution of the RIT, resulting in different absorbed doses to the bone marrow between patients. Red marrow absorbed dose or indirect markers has been shown to correlate with hematological toxicity in various targeted therapies with radionuclides [19–23]. The second factor is interpatient differences in bone marrow reserve. This reserve will vary between patients and can be dependent on previous treatment, for example, external beam radiation therapy or myelotoxic chemotherapy [24]. As RIT is primarily used in relapsed patients, many will have undergone substantial previous treatments.

Myelosuppression has also been identified as the dose-limiting toxicity in [ $^{177}\text{Lu}$ ]Lu-lilotomab satetraxetan, resulting in transient thrombocytopenia and neutropenia [25]. Previously, we have shown for a smaller group of eight patients that the absorbed dose to red marrow, derived by quantitative imaging, is related to this toxicity [26]. Therefore, the aim of the current work was to devise a model to predict myelosuppression in patients treated with [ $^{177}\text{Lu}$ ]Lu-lilotomab satetraxetan considering both patient pretreatment characteristics and individual absorbed dose to red marrow.

## Methods

### Patient population

A total of 17 CD37-positive patients with relapsed indolent NHL treated with [ $^{177}\text{Lu}$ ]Lu-lilotomab satetraxetan at Oslo University Hospital between 2012 and 2017 in the open-label, non-randomized LYMRIT 37-01-study were included. Key inclusion criteria in the LYMRIT-37-01-study were follicular lymphoma grade I-IIIA, marginal zone lymphoma, small lymphocytic lymphoma, and mantle cell lymphoma  $\geq 18$  years with  $<25\%$  tumor infiltration in the bone marrow determined by bone marrow biopsy. Key exclusion criteria were central nervous system involvement of lymphoma, history of human anti-mouse antibodies, previous irradiation of more than 25% of the bone marrow, absolute neutrophil counts below  $1.5 \times 10^9/\text{l}$ , platelet count below  $150 \times 10^9/\text{l}$ , total bilirubin above 30 mmol/l, liver values ALP and ALAT above four times of normal values, and elevated creatinine. The study was approved by the regional ethical committee and all patients participated upon informed consent form.

The majority of the included patients had follicular subtype Grade 1–2 ( $n = 14$ ), two had mantle cell lymphoma and one had marginal zone lymphoma. Patients from four treatment arms with different pretreatment and pre-dosing regimens were included. All patients received a single injection of [ $^{177}\text{Lu}$ ]Lu-lilotomab satetraxetan. This was a phase 1/2a

activity escalation trial, where the amount of activity was based on patient body mass; either 10, 15, or 20 MBq per kilogram. Patients in Arm 1 received pretreatment with 375 mg per  $\text{m}^2$  body surface area of rituximab 28 and 21 days before pre-dosing with 40 mg non-radioactive lilotomab followed by an administration of [ $^{177}\text{Lu}$ ]Lu-lilotomab satetraxetan. Patients in arm 2 received the same pretreatment as those in arm 1, but no pre-dosing. Patients in arm 3 had a single administration of rituximab ( $375 \text{ mg}/\text{m}^2$ ) pretreatment 14 days before the day of administration of [ $^{177}\text{Lu}$ ]Lu-lilotomab satetraxetan, and a pre-dosing with rituximab ( $375 \text{ mg}/\text{m}^2$ ). In arm 4, patients were pretreated with rituximab ( $375 \text{ mg}/\text{m}^2$ ) 14 days before treatment with [ $^{177}\text{Lu}$ ]Lu-lilotomab satetraxetan and received a pre-dosing of  $100 \text{ mg}/\text{m}^2$  body surface area non-radioactive lilotomab.

### Analysis of hematological toxicity and blood pharmacokinetic parameters

Blood samples to monitor thrombocytes and neutrophil counts were collected before treatment, and posttreatment on days 1, 2, 3, 4, and 7, and then weekly from weeks 4 to 12. Additional blood samples were taken if deemed necessary. Hematologic adverse events (thrombocytopenia and neutropenia) were graded by the Common Terminology Criteria for Adverse Events (CTCAE), version 4.0 [27]. The PBN and TTN were used as measures of toxicity.

Pharmacokinetic parameters were calculated as previously described [25]. In brief, total radioactivity in the blood was sampled at several time points and AUC and half-life in blood were calculated by noncompartmental modeling using the 'linear up log down'-method implemented in Phoenix WinNonLin 64 version 8.1 build 8.1.0.3530 (Certera). These parameters were available for 15 of the included patients.

### Bone marrow dosimetry

Image-based quantification of the radioactivity in lumbar vertebrae L2–L4 at multiple time points post-injection was carried out as previously described [26]. In brief, patients were imaged on a dual-headed Symbia T16 SPECT/CT-scanner. Attenuation and scatter-corrected images were acquired nominally (mean, range) 96 (100, 94–122) and 168 (173, 145–193) hours p.i. Images were reconstructed using the vendor's software (Siemens Medical Esoft). A nuclear medicine specialist delineated the volumes of interest in a slice-by-slice manner. Care was taken to not include the activity of adjacent physiological or tumor tissue. The total numbers of disintegrations (time-integrated activity) were found from the resulting mono-exponentially fitted time-activity curves. Factors to convert the total number of disintegrations to absorbed dose were calculated with the cellularity factor proposed by the International Commission on Radiological Protection (ICRP) [28]. In [Supplementary Appendix A](#), a detailed description of the methodology is shown.

**Statistical analysis**

The following ten patient characteristics and variables were considered potential predictors of toxicity and included as independent variables:

1. Age at treatment (years).
2. Baseline cell-counts.
  - i. Baseline cell-count of thrombocytes ( $10^9/l$ ).
  - ii. Baseline cell-count of neutrophils ( $10^9/l$ ).
3. History of prior external beam radiation treatment (yes/no).
4. Total number of previous chemotherapy treatments (including rituximab).
5. Elapsed time since last chemotherapy (months).
6. Absorbed dose to the red marrow (Gy).
7. Activity dosage level (either 10, 15 or 20 MBq/kg body mass).
8. Total administered radioactivity (MBq).
9. Area under the curve for [ $^{177}\text{Lu}$ ]Lu-lilotomab satetraxetan in blood (AUC) (h kBq/ml).
10. Half-life of [ $^{177}\text{Lu}$ ]Lu-lilotomab satetraxetan in blood ( $t_{1/2}$ ) (h).

Multiple linear regression analyses were performed with PBN and TTN as the dependent variables. The model is formed as a linear sum:

$$Y = \sum_i \alpha_i \times X_i + \beta \tag{1}$$

with fitting variables  $\alpha_i$  and  $\beta$  and independent variables  $X_i$ . Thrombocytes and neutrophils were treated separately.

Variable selection was done by choosing the models that had all variables with a significance level ( $p$ ) less than 0.05. Multiple significant models for the same dependent variable were evaluated based on the Akaike Information Criteria (AIC). The variance of inflation factor in model candidates was evaluated to ensure that predictors with multicollinearity were not included. The best model was tested with a leave-1-out analysis where one patient was left out and coefficients were calculated and used to predict the PBN of the patient that had been removed. This was repeated for all patients and the predicted and observed CTCAE grade of myelosuppression was compared.

As the initial multivariate analysis found absorbed dose to the red marrow to be the only significant parameter for PBN, a sigmoid relationship between absorbed dose to red

marrow and PBN was also explored. This was performed with a simple sigmoid function [29]:

$$\text{PBN} = 100 - \frac{100 \cdot D^N}{D^N + D_{50}^N} \tag{2}$$

with  $D$  being the absorbed dose to red marrow and  $D_{50}$  and  $N$  being fitting parameters.  $D_{50}$  is the absorbed dose resulting in a 50% reduction.

To compare the two models, the sums of mean square errors were used. Intra-patient variability for multiple sites was investigated by examining the absolute difference between the maximum and the minimum dose calculated in the same patient.

**Results**

A summary of the patient characteristics and variables for the 17 patients included in the prediction analysis are shown in Table 1. Red marrow absorbed dose was calculated for all patients and ranged from 1.0 to 3.7 Gy. As an illustration, the thrombocyte counts relative to baseline and activity distribution 4 days after treatment for two patients are shown in Figure 1.

**Myelosuppression**

PBN ranged from 4% to 56% and 1% to 53% for thrombocytes and neutrophils respectively. Median PBN values were 21% (thrombocytes) and 26% (neutrophils). The Median and range of TTN were 37 (28–251) and 44 (34–62) days for thrombocytes and neutrophils respectively. All patients experienced thrombocytopenia, grade 4 ( $n = 5$ ), 3 ( $n = 2$ ), 2 ( $n = 4$ ) or 1 ( $n = 6$ ). Fourteen patients experienced neutropenia, grade 4 ( $n = 2$ ), 3 ( $n = 8$ ) or 2 ( $n = 4$ ) whereas three patients did not experience any neutropenia (grade 0).

**Percentage reduction at nadir**

Figure 2 shows the predicted and observed values for the individual predictor candidates. The multivariate linear analysis showed that absorbed dose to red marrow was the only significant predictive parameter of PBN for both thrombocytes ( $F$ -test,  $p = 0.0415$ ,  $\text{AIC} = 138.1$ ,  $r^2 = 0.249$ ) and neutrophils ( $F$ -test,  $p = 0.0178$ ,  $\text{AIC} = 134.3$ ,  $r^2 = 0.321$ ). Figure 3(a,b) shows the PBN as a function of absorbed dose to the red marrow. The root-mean-square error was 12.5 and 11.2

**Table 1.** Patient characteristics and variables of the 17 patients included in the prediction analysis.

Patient characteristics included as potential predictors	Mean	STD	Range min	Range max	<i>n</i>
Age at treatment (years).	68.7	9.7	48.3	87.5	
Baseline cell-count of thrombocytes ( $10^9/l$ )	232	52.3	127	369	
Baseline cell-count of neutrophils ( $10^9/l$ )	4	1.7	1.7	8.1	
History of prior external beam radiation treatment. (yes/no)					5
Total number of previous chemotherapy treatments (including rituximab)	2.1	1.1	1	5	
Elapsed time since last chemotherapy (days)	635.4	508.7	89	1830	
Absorbed dose to the red marrow (Gy)	2.2	0.8	1.0	3.7	
Activity dosage level (either 10, 15 or 20 MBq/kg body mass)	15.3	3.6	10	20	
Total administered activity (MBq)	1238.2	291.2	746	1769	
Area under the curve for [ $^{177}\text{Lu}$ ]Lu-lilotomab satetraxetan in blood (AUC) (h kBq/ml)	9737.3	4972.7	3860	20,200	
Half-life of [ $^{177}\text{Lu}$ ]Lu-lilotomab satetraxetan in blood ( $t_{1/2}$ ) (h)	53.9	12.3	26.3	75.8	

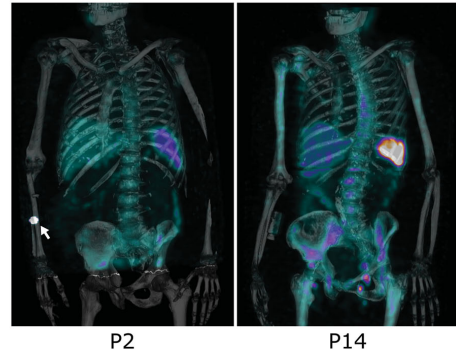
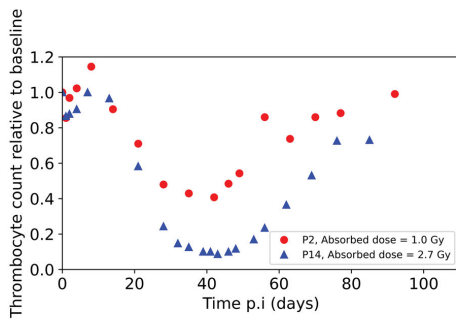


**Figure 1.** Left: The thrombocyte and neutrophil counts in blood, relative to baseline, were used to indicate myelosuppression. The relative thrombocyte count after treatment with [ $^{177}\text{Lu}$ ]Lu-lilotomab satetraxetan is shown for two patients, patient 2 and 14. The absorbed dose of the two patients is indicated in the figure. Right: Volume renderings of the activity distributions of the two patients. The white arrow on patient 2 points to a vial filled with a known amount of  $^{177}\text{Lu}$  activity, included for technical quality assurance. Note that the SPECT-image does not cover the whole CT in patient 2. The image intensities in both images have been scaled to the same range.

for thrombocytes and neutrophils respectively. In the leave-1-out analysis, the exact thrombocytopenia and neutropenia grade was predicted in 3/17 and 6/17 for thrombocytopenia and neutropenia respectively. Haematological toxicity grade  $\pm 1$  was predicted in 12/17 (thrombocytopenia) and 15/17 (neutropenia).

#### Time to nadir

Multivariate analysis of the ten parameters yielded one significant model of TTN of neutrophils: Absorbed dose to red marrow as the single parameter ( $F$ -test,  $p = 0.00753$ ,  $\text{AIC} = 111.0$ ,  $r^2 = 0.388$ ). Figure 3(c,d) shows the TTN plotted against the absorbed dose to red marrow. For thrombocytes, no significant model between the ten parameters and TTN was found (the lowest  $p$  for the linear model was 0.096).

#### Sigmoid fit

The sigmoid function was fitted with coefficients  $D_{50} = 0.59$  and  $N = 0.95$  and  $D_{50} = 0.66$  and  $N = 0.96$  for thrombocytes and neutrophils respectively (Figure 4). The root means squared errors of the sigmoid function were 12.6 and 11.4 for thrombocytes and neutrophils. A similar leave-1-out analysis as for the linear model was performed, resulting in an agreement of 12/17 and 15/17 for thrombocytopenia and neutropenia grade  $\pm 1$ , and 3/17 and 8/17 for exact agreement between predicted and observed toxicity grade.

#### Discussion

Absorbed dose to red marrow was the only variable that predicted hematological toxicity for both thrombocytes and neutrophils in patients treated with [ $^{177}\text{Lu}$ ]Lu-lilotomab satetraxetan. The absorbed dose was also found to be predictive of the TTN of neutrophils.

Correlations between myelosuppression and potential risk factors including absorbed dose to the red marrow have been investigated previously, both for RIT- and other

radionuclide treatments. In a phase III study with [ $^{90}\text{Y}$ ]Y-ibritumomab tiuxitan no correlation was found between absorbed dose and myelosuppression; possibly due to limitations with the absorbed dose calculation [30,31]. In another study with  $^{131}\text{I}$ -labelled anti carcinoembryonic antigen RIT absorbed dose to the red marrow, baseline blood cell counts, multiple bone metastasis, and chemotherapy within the last 3–6 months of treatment were found to be predictors of myelosuppression [32]. In a study with [ $^{131}\text{I}$ ]I-tositumomab ( $n = 14$ ) and [ $^{90}\text{Y}$ ]Y-ibritumomab tiuxitan ( $n = 18$ ), the elapsed time from the last chemotherapy was identified as the only predictive parameter [33]. However, the authors argued, the range of absorbed dose to the red marrow was narrow (mean  $1.6 \pm 0.4$  Gy and  $2.1 \pm 0.4$  Gy for [ $^{131}\text{I}$ ]I-tositumomab and [ $^{90}\text{Y}$ ]Y-ibritumomab tiuxitan, respectively), and therefore not a factor of variability. Using whole-body absorbed dose as a surrogate for absorbed dose to the bone marrow, a relationship between this parameter and myelosuppression was found for patients treated with [ $^{131}\text{I}$ ]I-metaiodobenzylguanidine, whereas no relationship was found for administered radioactivity [20]. In a study with [ $^{90}\text{Y}$ ]Y-DOTATOC, a peptide receptor radionuclide therapy, a correlation was observed between the level of platelets at nadir and absorbed dose to red marrow [19]. Unlike previous studies, we found absorbed dose to red marrow to be the only variable to significantly predict PBN also after having adjusted for other candidate factors. Further, neither activity dosage level (MBq/kg) nor amount of total administered radioactivity were predictive of myelosuppression. Hence other means, that is, image-based dosimetry taking the individual biodistribution into account as we have done in this study, is most likely the best method to predict hematological toxicity for patients receiving [ $^{177}\text{Lu}$ ]Lu-lilotomab satetraxetan. We have previously shown that specific pre-dosing with unlabeled lilotomab resulted in reduced absorbed dose to the red marrow and thus pre-dosing was not included as an independent variable [34]. When we included several parameters in the multivariate analyses, this did not strengthen the prediction models. For the neutrophils there was a model that was borderline



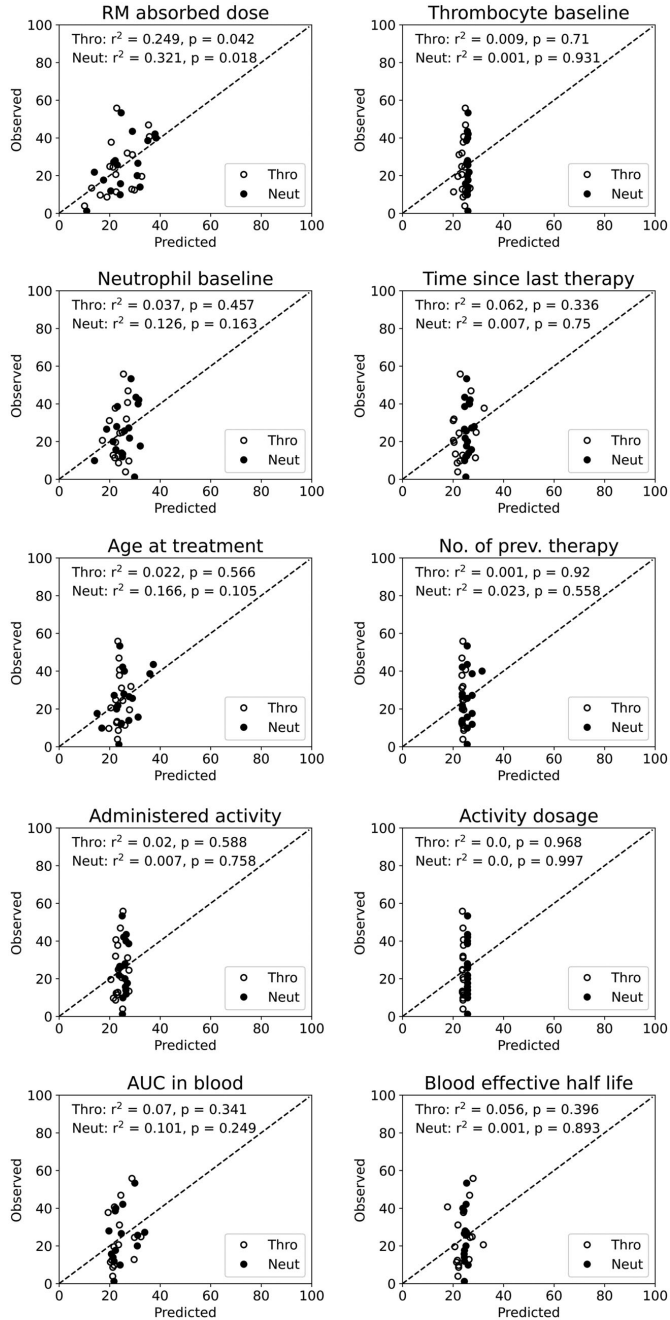


**Figure 2.** Absorbed dose to red marrow (upper left panel) was found as the only significant predictive parameter of PBN. None of the other parameters, shown here with predicted and observed PBN-values, were predictive of PBN. The  $r^2$ - and  $p$ -values are indicated for each parameter. Thrombocytes and neutrophils are shown as unfilled and filled dots respectively.

significant including neutrophils at baseline ( $F$ -test  $p$ -value = 0.01, absorbed dose  $p$ -value = 0.008, baseline neutrophils  $p$ -value = 0.058) while as for the thrombocytes the second

most promising model included absorbed dose, history of previous EBRT-therapy and baseline neutrophil counts ( $F$ -test  $p$ -value = 0.08, absorbed dose  $p$ -value = 0.036, the other  $p$ -

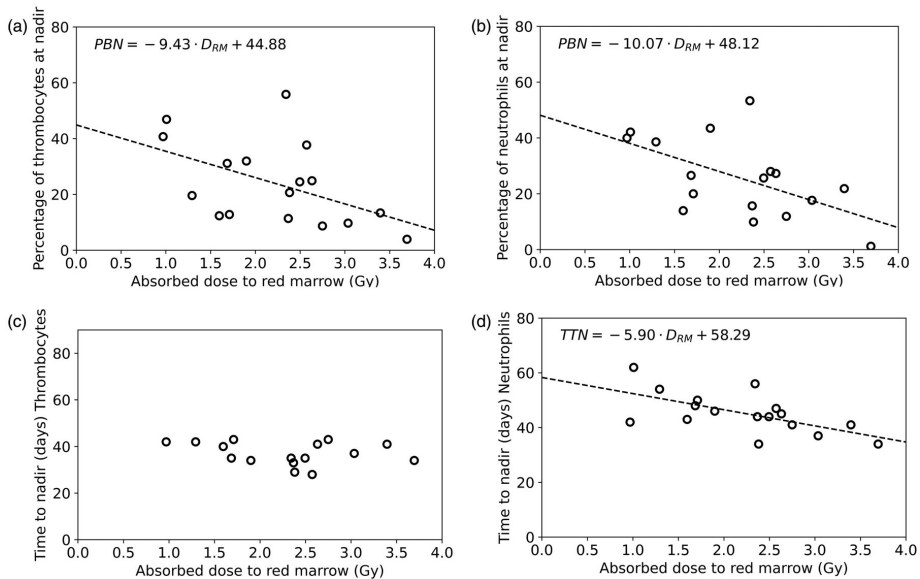


**Figure 3.** The dominating predictor was absorbed dose to the red marrow. The four toxicity indicators are here shown plotted against this predictor: PBN of thrombocytes (a) and neutrophils (b) and TTN for thrombocytes (c) and neutrophils (d). PBN for thrombocytes and neutrophils and TTN for neutrophils were all found to be significantly correlated to red marrow absorbed dose. One patient (P19) had a thrombocyte TTN value of 251 days and is excluded from panel C.

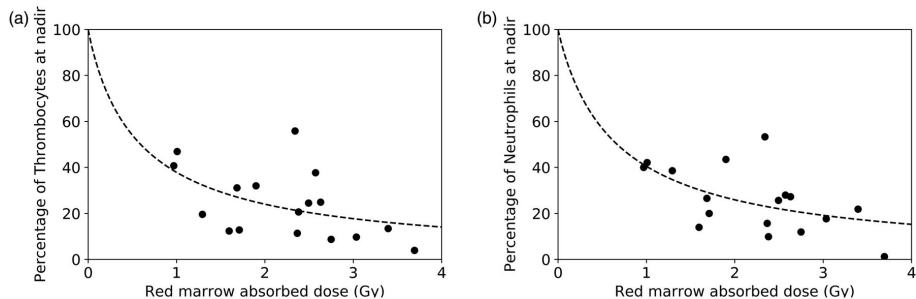


**Figure 4.** A sigmoid relationship between red marrow absorbed dose and PBN was explored. The s-shaped response curve is shown plotted against PBN of thrombocytes (a) and neutrophils (b). The root mean squared errors of the s-curves were almost identical to the linear response curves.

values  $> 0.18$ ). Pharmacokinetic parameters did not yield significant predictors in the linear toxicity model. This could potentially be due to that pharmacokinetics alone is an incomplete description of the distribution of  $[^{177}\text{Lu}]\text{Lu}$ -lilotomab satetaxetan in the red marrow for individual patients.

Absorbed doses to red marrow ranged from approximately 1 to 4 Gy in our study. This is higher than previously reported for a subgroup of patients from the same trial [26], as a correction factor for reference cellularity was here included in the dose calculation. While this has shifted the absolute values, the relative interpatient differences remain unchanged with some differences due to whole-body contribution and patient sex. The upper absorbed doses are somewhat higher than the toxicity limit of 2 Gy used in dosimetry-guided radioiodine treatment of differentiated thyroid cancer protocols [35]. Our absorbed doses are however in the same order of magnitude as those reported for patients treated

with high dose  $[^{131}\text{I}]\text{-metaiodobenzylguanidine}$  therapy for neuroblastoma (range 2.06–5.02 Gy) [22]. With a hybrid, SPECT/CT-imaging technique of patients treated with the RIT  $[^{131}\text{I}]\text{-rituximab}$ , absorbed doses were found to be comparable to ours (range 1.09–1.90 Gy) [23]. Direct comparison of absorbed doses from previous studies of other therapies is however to be done with caution. This is mainly due to differences in biological vectors and radionuclides, which leads to differences in absorbed dose rate and energy deposition, which in turn can result in variations in radiobiological effects. Moreover, while the recent improvements in radioactivity quantification technology have enabled more direct and accurate measurements of radioactivity, there are still methodological differences to be considered [36]. Overall, our findings indicate an upper limit in the same order of magnitude as previous relevant publications, approximately 3 Gy when our methodology is used.

After having established that absorbed dose dominated in the multivariate analyses, we proceeded to further investigate the best model for this predictor. Relationships between absorbed dose and normal tissue complications are usually expected to follow sigmoid functions, of which parameters are found for specific clinical situations [37]. The sigmoid function used in our work has previously been reported to describe the relationship between absorbed dose to red marrow and decrease in thrombocytes in metastatic prostate cancer patients treated with [ $^{186}\text{Re}$ ]Re-HEDP [29]. The value for  $D_{50}$ , the absorbed dose resulting in a 50% reduction of platelets, was there reported to be 2.09 Gy in a group of previously untreated patients, four times the value found in the current work. This difference could be explained by the fact that the patients included in the current study have been heavily pretreated, and thus more radiosensitive. An alternative explanation may be differences between the radiobiological effects of the different radionuclides and carrier molecules. The sigmoid model had a similar root mean square error as the linear model, however, the sigmoid model showed slightly superior predictive abilities in the cross-validation compared to the linear model. The two models seem to overlap in the range of the recorded absorbed doses. Due to the comparable predictive power and the simplicity of the linear description, we recommend that the linear description should be considered the preferred working model except at very high or very low absorbed doses.

Absorbed dose to red marrow enabled identification of high-risk patients for myelotoxicity after therapy with [ $^{177}\text{Lu}$ ]Lu-lilotomab satetraxetan as it could be calculated as early as 7 days post-treatment, before the onset of neutropenia and thrombocytopenia. Severe myelosuppression was uncommon for our patient group [25] who received a single dose of radioimmunotherapy. However, the prediction of hematologic toxicity might become particularly interesting for repeated administrations. Dosimetry after the first treatment cycle can then, in a multi-cycle treatment protocol, be used to predict the toxicity of future cycles, and thus be used to tailor the number and size of the cycles. Such an approach has been explored in peptide receptor radionuclide therapy [38]. Results in a murine model have suggested that fractionated therapy is a possible treatment strategy for [ $^{177}\text{Lu}$ ]Lu-lilotomab satetraxetan [39]. In such a treatment setting, patients could benefit from being stratified into groups that can allow for more intensive treatment for those that have a more favorable therapeutic index.

## Conclusion

It is possible to predict levels of thrombocytopenia and neutropenia by applying absorbed dose to red marrow as the only predictor. No other investigated patient characteristics or variables strengthened this correlation in this study.

## Acknowledgments

We thank the personnel at the Nuclear Medicine section at Oslo University Hospital for technical assistance with the acquisitions.

## Disclosure statement

Arne Kolstad is a member of the Scientific Advisory Board of Nordic Nanovector ASA. Jostein Dahle is an employee and shareholder of Nordic Nanovector ASA. The authors have no further conflicts of interest to disclose.

## Funding

The present work was financially supported by the South-Eastern Norway Regional Health Authority.

## ORCID

Johan Blakkisrud  <http://orcid.org/0000-0002-0046-7327>  
Caroline Stokke  <http://orcid.org/0000-0003-4465-9635>

## References

- [1] Larson SM, Carrasquillo JA, Cheung NKV, et al. Radioimmunotherapy of human tumours. *Nat Rev Cancer*. 2015; 15(6):347–360.
- [2] Steiner M, Neri D. Antibody-radionuclide conjugates for cancer therapy: Historical considerations and new trends. *Clin Cancer Res*. 2011;17(20):6406–6416.
- [3] Witzig TE, Gordon LI, Cabanillas F, et al. Randomized controlled trial of yttrium-90-labeled ibritumomab tiuxetan radioimmunotherapy versus rituximab immunotherapy for patients with relapsed or refractory low-grade, follicular, or transformed B-cell non-Hodgkin's lymphoma. *J Clin Oncol*. 2021;81(10):1229–2463.
- [4] Kaminski MS, Tuck M, Estes J, et al. 131I-tositumomab therapy as initial treatment for follicular lymphoma. *N Engl J Med*. 2005; 352(5):441–449.
- [5] Jacene HA, Filice R, Kasecamp W, et al. Comparison of 90Y-ibritumomab tiuxetan and 131I-tositumomab in clinical practice. *J Nucl Med*. 2007;48(11):1767–1776.
- [6] Papadimitroulas P, Loudos G, Nikiforidis GC, et al. A dose point kernel database using GATE Monte Carlo simulation toolkit for nuclear medicine applications: comparison with other Monte Carlo codes. *Med Phys*. 2012;39(8):5238–5247.
- [7] Dahle J, Repetto-Llamazares AHV, Mollatt CS, et al. Evaluating antigen targeting and anti-tumor activity of a new anti-cd37 radioimmunconjugate against non-hodgkin's lymphoma. *Anticancer Res*. 2013;33(1):85–96.
- [8] Zhao X, Tridandapani S, Lehman A, et al. Targeting CD37-positive lymphoid malignancies with a novel engineered small modular immunopharmaceutical. *Blood*. 2007;110(7):2569–2577.
- [9] Schwartz-Albiez R, Dörken B, Hofmann W, et al. The B cell-associated CD37 antigen (gp40-52). Structure and subcellular expression of an extensively glycosylated glycoprotein. *J Immunol*. 1988;140:905–914.
- [10] Heider K-h, Kiefer K, Zenz T, et al. LYMPHOID NEOPLASIA A novel Fc-engineered monoclonal antibody to CD37 with enhanced ADCC and high proapoptotic activity for treatment of B-cell malignancies. *Blood*. 2011;118(15):4159–4169.
- [11] Deckert J, Park PU, Chicklas S, et al. A novel anti-CD37 antibody-drug conjugate with multiple anti-tumor mechanisms for the treatment of B-cell malignancies. *Blood*. 2013;122(20):3500–3510.
- [12] Bertoni F, Stathis A. Staining the target: CD37 expression in lymphomas. *Blood*. 2016;128(26):3022–3023.
- [13] Kaminski MS, Zasadny KR, Francis IR, et al. Iodine-131-anti-B1 radioimmunotherapy for B-cell lymphoma. *J Clin Oncol*. 1996; 14(7):1974–1981.
- [14] Hiraga J, Tomita A, Sugimoto T, et al. Down-regulation of CD20 expression in B-cell lymphoma cells after treatment with

- rituximab-containing combination chemotherapies: its prevalence and clinical significance. *Blood*. 2009;113(20):4885–4893.
- [15] Kaminski MS, Fig LM, Zasadny KR, et al. Imaging, dosimetry, and radioimmunotherapy with iodine 131-labeled anti-CD37 antibody in B-cell lymphoma. *J Clin Oncol*. 1992;10(11):1696–1711.
- [16] Hindorf C, Glatting G, Chiesa C, et al. EANM dosimetry committee guidelines for bone marrow and whole-body dosimetry. *Eur J Nucl Med Mol Imaging*. 2010;37(6):1238–1250.
- [17] Puvvada SD, Guillén-Rodríguez JM, Yan J, et al. Yttrium-90-ibritumomab tiuxetan (Zevalin<sup>®</sup>) radioimmunotherapy after cytoreduction with ESHAP chemotherapy in patients with relapsed follicular non-Hodgkin lymphoma: final results of a phase II study. *Oncology*. 2018;94(5):274–280.
- [18] Wahl RL. The clinical importance of dosimetry in radioimmunotherapy with tositumomab and iodine I 131 tositumomab. *Semin Oncol*. 2003;30(2 Suppl 4):31–38.
- [19] Walrand S, Barone R, Pauwels S, et al. Experimental facts supporting a red marrow uptake due to radiometal transchelation in 90Y-DOTATOC therapy and relationship to the decrease of platelet counts. *Eur J Nucl Med Mol Imaging*. 2011;38(7):1270–1280.
- [20] Buckley SE, Chittenden SJ, Saran FH, et al. Whole-body dosimetry for individualized treatment planning of 131I-MIBG radionuclide therapy for neuroblastoma. *J Nucl Med*. 2009;50(9):1518–1524.
- [21] Matthay KK, Panina C, Huberty J, et al. Correlation of tumor and whole-body dosimetry with tumor response and toxicity in refractory neuroblastoma treated with (131I)-MIBG. *J Nucl Med*. 2001;42:1713–1721.
- [22] DuBois SG, Messina J, Maris JM, et al. Hematologic toxicity of high-dose iodine-131-metaiodobenzylguanidine therapy for advanced neuroblastoma. *J Clin Oncol*. 2004;22(12):2452–2460.
- [23] Boucek JA, Turner JH. Validation of prospective whole-body bone marrow dosimetry by SPECT/CT multimodality imaging in 131I-anti-CD20 rituximab radioimmunotherapy of non-Hodgkin's lymphoma. *Eur J Nucl Med Mol Imaging*. 2005;32(4):458–469.
- [24] Aksejtijevich I, Flinn I. Chemotherapy and bone marrow reserve: lessons learned from autologous stem cell transplantation. *Cancer Biother Radiopharm*. 2002;17(4):399–403.
- [25] Kolstad A, Illidge T, Bolstad N, et al. Phase 1/2a study of 177Lu-lilotomab satetraxetan in relapsed/refractory indolent non-Hodgkin lymphoma. *Blood Adv*. 2020;4(17):4091–4101.
- [26] Blakkisrud J, Løndalen A, Dahle J, et al. Red marrow-absorbed dose for non-Hodgkin lymphoma patients treated with 177Lu-lilotomab satetraxetan, a novel anti-CD37 antibody-radionuclide conjugate. *J Nucl Med*. 2017;58(1):55–61.
- [27] CTCAE4. Common terminology criteria for adverse events. 4th ed. Bethesda (MD): US National Cancer Institute; 2009.
- [28] ICRP. Basic anatomical and physiological data for use in radiological protection – the skeleton. ICRP Publication 70. Ann ICRP. 1995;25(2):1–80.
- [29] de Klerk JM, van Dieren EB, van Het Schip AD, et al. Bone marrow absorbed dose of rhenium-186-HEDP and the relationship with decreased platelet counts. *J Nucl Med*. 1996;37(1):38–41.
- [30] Wiseman GA, White CA, Sparks RB, et al. Biodistribution and dosimetry results from a phase III prospectively randomized controlled trial of Zevalin<sup>™</sup> radioimmunotherapy for low-grade, follicular, or transformed B-cell non-Hodgkin's lymphoma. *Crit Rev Oncol Hematol*. 2001;39(1-2):181–194.
- [31] Wiseman G, Kornmehl E, Leigh B, et al. Radiation dosimetry results and safety correlations from 90Y-ibritumomab tiuxetan radioimmunotherapy for relapsed or refractory non-Hodgkin's lymphoma: Combined data from 4 clinical trials. *J Nucl Med*. 2003;44:465–474.
- [32] Juweid ME, Zhang CH, Blumenthal RD, et al. Prediction of hematologic toxicity after radioimmunotherapy with 131-I-labeled anti-carcinoembryonic antigen monoclonal antibodies. *J Nucl Med*. 1999;40(10):1609–1616.
- [33] Baechler S, Hobbs RF, Jacene HA, et al. Predicting hematologic toxicity in patients undergoing radioimmunotherapy with 90Y-ibritumomab tiuxetan or 131I-tositumomab. *J Nucl Med*. 2010;51(12):1878–1884.
- [34] Stokke C, Blakkisrud J, Løndalen A, et al. Pre-dosing with lilotomab prior to therapy with 177Lu-lilotomab satetraxetan significantly increases the ratio of tumor to red marrow absorbed dose in non-Hodgkin lymphoma patients. *Eur J Nucl Med Mol Imaging*. 2018;45(7):1233–1241.
- [35] Lassmann M, Flux G, Hindorf C, et al. EANM Dosimetry Committee series on standard operational procedures for pre-therapeutic dosimetry I: blood and bone marrow dosimetry in differentiated thyroid cancer therapy. *Eur J Nucl Med Mol Imaging*. 2008;35(7):1405–1412.
- [36] Lassmann M, Eberlein U. The relevance of dosimetry in precision medicine. *J Nucl Med*. 2018;59(10):1494–1499.
- [37] Yorke ED. Modeling the effects of inhomogeneous dose distributions in normal tissues. *Semin Radiat Oncol*. 2001;11(3):197–209.
- [38] Sundlöf A, Sjögreen-Gleisner K, Svensson J, et al. Individualised 177Lu-DOTATATE treatment of neuroendocrine tumours based on kidney dosimetry. *Eur J Nucl Med Mol Imaging*. 2017;44(9):1480–1489.
- [39] Heyerdahl H, Repetto-Llamazares AHV, Dahle J. Administration of beta-emitting anti-CD37 radioimmunconjugate lutetium (177Lu) lilotomab satetraxetan as weekly multiple injections increases maximum tolerated activity in nude mice with non-Hodgkin lymphoma xenografts. *GJCT*. 2018;4(1):181–190.

# Appendices

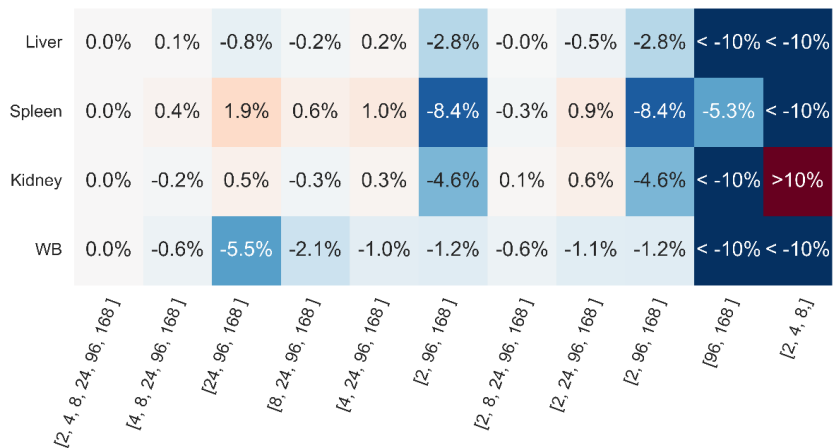


# Paper 1 Appendix





**Supplemental Fig 1.** Percentage errors of the TIACs introduced for protocols with a reduced number of imaging time points (indicated as hours p.i) compared to the original six time point protocol (2, 4, 8, 24, 96 and 168 hours p.i.). The numbers in brackets are the included time points in units of hours p.i. The integral is calculated as described in the article. Largest errors across patient 1-5 are shown. The color scale reflects the magnitude of the error from -10 to 10 %. Error above 10 % or undefined integrals are written as “>10 %” Protocol (2, 24, 96 and 168 hours p.i.) was chosen for arm 2. An interactive figure can be found as Supplementary file 2.





## **Paper 3 Appendix**



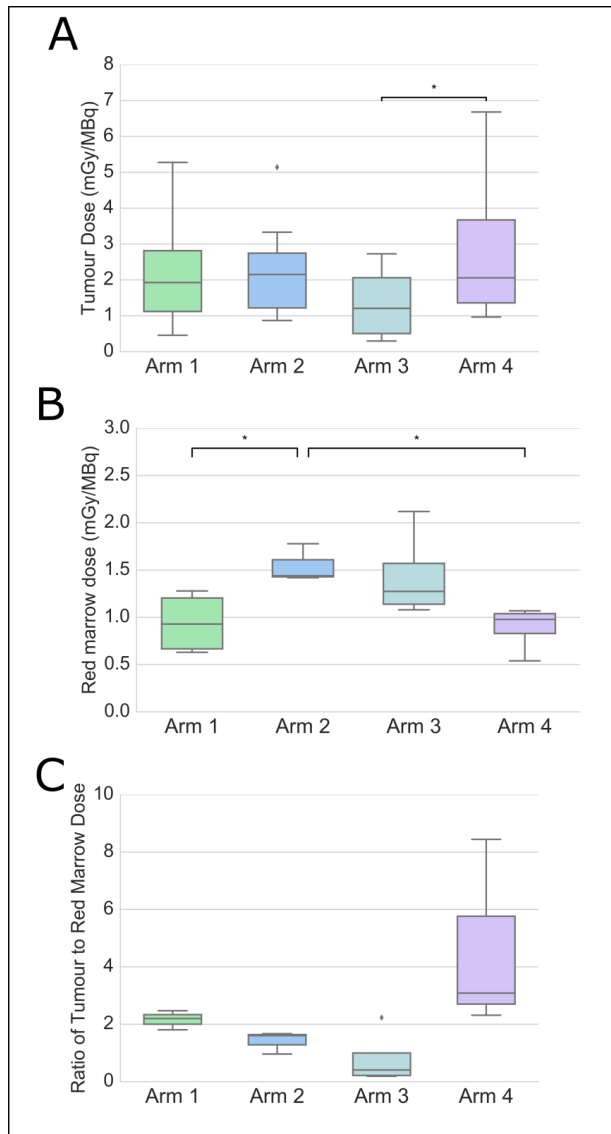
SUPPLEMENTARY TABLE 1.

Individual patient characteristics, as well as absorbed doses, masses and time-integrated activity coefficients (TIACs) for the target organs.

“N.A.” indicates that insufficient imaging data are available, that the red bone marrow (RM) has been treated by external beam radiation previously, or that no tumours were eligible for dosimetry.

Patient number	Sex	Arm	Prescription level [MBq/kg]	Body weight [kg]	Injected activity [MBq]	Amount of labelled lilotomab [mg]	Amount of lilotomab pre-dosing [mg]	Liver			Spleen			Kidney			RM Dose (Gy)	Tumours Mean (range) (Gy)
								Mass (g)	TIAC (h)	Dose (Gy)	Mass (g)	TIAC (h)	Dose (Gy)	Mass (g)	TIAC (h)	Dose (Gy)		
1	F	3	10,0	118,0	1102,0	N.A.	0,0	1876,0	14,6	0,8	262,0	8,0	2,9	204,0	0,7	0,3	1,5	0.33 (0.33-0.33)
2	M	1	10,0	103,0	1036,0	7,9	40,0	2405,0	19,8	0,8	406,0	7,2	1,6	233,0	0,7	0,3	0,7	1.04 (0.76-1.51)
3	M	1	10,0	73,0	746,0	7,9	40,0	1295,0	16,7	0,9	100,0	4,2	2,7	117,0	1,1	0,6	0,9	1.91 (0.89-2.82)
5	M	1	20,0	98,0	1982,0	8,3	40,0	1705,0	19,4	2,0	194,0	7,3	6,5	270,0	0,9	0,6	N.A.	2.09 (0.91-3.28)
7	M	1	20,0	74,0	1505,0	8,1	40,0	N.A.	N.A.	N.A.	N.A.	N.A.	N.A.	N.A.	N.A.	N.A.	N.A.	5.06 (3.19-7.94)
9	M	1	15,0	110,0	1696,0	7,8	40,0	N.A.	N.A.	N.A.	N.A.	N.A.	N.A.	N.A.	N.A.	N.A.	1,2	2.21 (1.31-3.28)
11	M	1	15,0	97,0	1435,0	8,9	40,0	N.A.	N.A.	N.A.	N.A.	N.A.	N.A.	N.A.	N.A.	N.A.	N.A.	4.57 (2.77-6.72)
12	F	1	15,0	67,0	1015,0	8,9	40,0	N.A.	N.A.	N.A.	N.A.	N.A.	N.A.	N.A.	N.A.	N.A.	1,3	N.A.
13	M	2	15,0	94,0	1416,0	9,5	0,0	1690,0	20,0	1,5	170,0	6,8	4,9	211,0	0,7	0,4	2,0	3.15 (1.23-7.28)
14	F	2	15,0	65,0	1013,0	9,1	0,0	1687,0	19,1	1,0	152,0	5,6	3,2	147,0	0,5	0,3	1,8	2.80 (2.45-3.38)
15	M	2	10,0	112,0	1137,0	8,8	0,0	2030,0	17,6	0,9	187,0	5,9	3,1	282,0	0,5	0,2	1,6	1.48 (1.48-1.48)

16	F	3	15,0	59,0	891,0	8,2	0,0	1290,6	20,8	1,3	214,9	10,0	3,6	120,1	0,6	0,4	1,9	0.35 (0.35-0.35)
17	F	3	15,0	69,0	1053,0	8,3	0,0	1644,2	16,9	1,0	260,4	9,4	3,3	171,7	0,7	0,4	1,1	2.12 (1.27-2.87)
18	M	3	15,0	92,0	1366,0	16,4	0,0	N.A.	N.A.	N.A.	N.A.	N.A.	N.A.	N.A.	N.A.	N.A.	1,6	0.84 (0.69-0.98)
19	M	4	15,0	85,0	1286,0	8,6	199	N.A.	N.A.	N.A.	N.A.	N.A.	N.A.	N.A.	N.A.	N.A.	0,7	5.09 (1.49-8.59)
21	M	4	20,0	91,0	1769,0	5,4	207	2818,8	21,6	1,2	398,7	3,5	1,4	161,9	0,8	0,7	1,6	4.59 (3.30-6.49)
22	M	4	20,0	59,0	1147,0	3,4	169	N.A.	N.A.	N.A.	N.A.	N.A.	N.A.	N.A.	N.A.	N.A.	1,2	2.36 (2.36-2.36)
23	M	4	20,0	72,0	1434,0	4,3	191	2105,4	30,6	1,9	566,6	9,3	2,1	153,6	1,3	1,0	1,5	N.A
25	M	4	20,0	109,0	2189,0	6,3	224	1790,4	17,7	1,9	198,7	2,7	2,6	219,6	0,8	0,8	N.A.	2.67 (2.12-3.43)



**Supplementary Figure 1.** (A) The upper boxplot displays tumour absorbed doses when different amounts of lilotomab are given as pre-dosing before  $^{177}\text{Lu}$ -lilotomab satetraxetan treatment. The four patient arms are shown. Arms 2 and 3 did not receive lilotomab, arm 1 patients received 40 mg lilotomab and arm 4 patients received 100 mg lilotomab per  $\text{m}^2$  BSA. The tumour absorbed doses are corrected by the amount of radioactivity given each patient. For all box plots, significant differences are annotated by asterisks. (B) Similar measures of the RM absorbed doses are also shown for the groups. (C) The boxplot illustrates the ratios between patient mean tumour doses to RM absorbed doses. Here, the mean tumour absorbed dose is calculated for each patient before the patient ratios are obtained. Fig. 1 displays the same box plots when arms 2 and 3 are grouped.





## **Paper 4 Appendix**



## Appendix A: Calculation of the skeletal-specific S-values

Absorbed dose was calculated using the MIRD-formalism. The time integrated activity of each site,  $\tilde{A}$  and site volume  $V$  were determined from volumes of interest drawn with PMOD vs 3.8 (PMOD industries, Zurich). The volume was corrected with the ICRP-cellularity factor (70 %) and a correction for trabecular volume fractions taken from table 4 in (O'Reilly et al. 2016) and table 1 from (Hough et al. 2011) for female (0.1260) and male (0.1025) patients, respectively. A mass density of 1.03 g/ml was also used in accordance with both look-up-tables to form the mass of the red marrow:

$$m_{AM} = V(1 - f_{TBM}) \cdot CF \quad (A1)$$

CF- specific absorbed energy fractions were calculated by the specific uptake fractions found in the tables A1-A13 of the appendices of (O'Reilly et al. 2016) and (Hough et al. 2011) multiplied by the red marrow masses. The reference masses were calculated using tables 4 and 1 from (O'Reilly et al. 2016) and (Hough et al. 2011) respectively, and equations (2) and (4) from (Hough et al. 2011).

$$\phi(\text{AM} \leftarrow \text{AM}, CF, E) = \Phi(\text{AM} \leftarrow \text{AM}, CF, E) \cdot m_{AM\text{-ref}} \quad (A2)$$

The final  $S$ -factor was found by summation of the mean energy,  $\Delta_i$  and corresponding  $\phi$  for all  $\beta^-$ , internal conversion and auger-electron-emission ( $i$ ) of  $^{177}\text{Lu}$ . These were extracted

from the software program DECDATA version 2.7, which contains the data of ICRP-publication 107 (International Commission on Radiological Protection 2008).

$$S(\text{AM} \leftarrow \text{AM}, CF) = \sum_i \Delta_i \phi(\text{AM} \leftarrow \text{AM}, CF, E_i) \quad (\text{A3})$$

$$D(\text{AM}, CF) = \frac{\tilde{A} \cdot S(\text{AM} \leftarrow \text{AM}, CF)}{m_{\text{AM}}} \quad (\text{A4})$$

The required values to do the dose calculations were implemented as a python-class object to create a phantom from specific absorption fractions and energy spectrum from DECDATA, together with associated class-methods to do dosimetry calculation based on input in the form of time integrated activity and volume measurements (python version 3.7.6). The software with included documentation is freely available on github:

<https://github.com/blakkisrud/RedMarrowSFactor>.

### Appendix references

- I) Matthew Hough et al *An image-based skeletal dosimetry model for the ICRP reference adult male—internal electron sources*. 2011 Phys. Med. Biol. 56 2309
- II) Shannon E O'Reilly et al *An image-based skeletal dosimetry model for the ICRP reference adult female—internal electron sources*. 2016 Phys. Med. Biol. 61 8794
- III) ICRP. *Nuclear Decay Data for Dosimetric Calculations*. ICRP Publication 107. 2008 Ann. ICRP 38

